Fall 2019

Propagation of uncertainty through coning, sculling, and scrolling corrections for inertial navigation

James Daniel Alan Brouk

PROPAGATION OF UNCERTAINTY THROUGH CONING, SCULLING, AND

SCROLLING CORRECTIONS FOR INERTIAL NAVIGATION

by

JAMES DANIEL ALAN BROUK

A THESIS

Presented to the Graduate Faculty of the

MISSOURI UNIVERSITY OF SCIENCE AND TECHNOLOGY

In Partial Fulfillment of the Requirements for the Degree

MASTER OF SCIENCE

in

AEROSPACE ENGINEERING

2019

Approved by

Kyle J. DeMars, Advisor
Henry Pernicka
Serhat Hosder

ABSTRACT

This thesis investigates the propagation of estimation errors through generalized coning, sculling, and scrolling algorithms used in modern day inertial navigation systems, in order to accurately quantify the uncertainty in the estimation of position, velocity, and attitude. The corrections for coning, sculling, and scrolling algorithms have an often unaccounted for effect on documented and empirically derived error statistics for measurements used to predict the uncertainty in a vehicle's position, velocity, and attitude estimates. Through the development of an error analysis for these generalized algorithms, mappings of the measurement and estimation errors through the correction term are generated. Using the developed mappings, an efficient and consistent propagation of state uncertainty with the multiplicative extended Kalman filter is achieved. A simulation environment is developed to investigate the performance of the algorithms within a descent-to-landing scenario. Monte Carlo analysis is used to analyze the effects of the developed error propagation and the accompanying algorithms to compare them with commonly used discrete dead-reckoning approaches.

ACKNOWLEDGMENTS

First and foremost, I would like to thank my graduate advisor, Dr. Kyle DeMars. Throughout my time as a graduate student in the AREUS lab, you have offered the support and guidance that I required for success in both research and coursework. Under your advising, I have been constantly inspired by your devotion to your students and craft. Without your aid in directing my curiosity and the invaluable skills that I have gained under your direction, I would not be where I am today.

I would also like to express my gratitude to Dr. Henry Pernicka and Dr. Serhat Hosder, my committee members. Dr. Pernicka, your courses on orbital mechanics were the first taste I had of astrodynamics; through your teaching and passion for your subject, you inspired me to pursue a career in space technologies, like so many other undergraduates in aerospace engineering. Dr. Hosder, your coursework was some of the most difficult that I've had the pleasure of taking, but the skills that I honed throughout have been invaluable to me in my own research and I'm certain will be applicable throughout my career.

To my family, thank you for your continued love and support throughout my childhood and college career. Without your persistent encouragement, driving me toward achievement and success, I would never have made it this far.

Last but not least, I would like to thank the members of the AREUS and SSE labs who have served as companions throughout this journey in my life. Listed in no particular order, I would like to thank Kari Ward, Matt Gualdoni, Christine Schmidt, Gunner Fritch, Cameron Helmuth, Bruce Morrison, Donna Jennings, Jill Davis, and Daniel Newberry. Without the support and friendship of each of you, the third floor of Toomey Hall would not be the home it is to me today.

TABLE OF CONTENTS

Page

LIST OF ILLUSTRATIONS

LIST OF TABLES

1. INTRODUCTION

Exploration and utilization of the space environment is continually testing the capabilities of modern space systems and technnology, often inventing those that do not yet exist. The increased interest coming from commercial industry has only reinforced the need for accelerated technological evolution by pushing these boundaries with refreshed perspectives and ideologies. The development of vehicles and technology that enable the investigation of another celestial body are a crucial component for an ever increasing planetary footprint of human exploration and knowledge. The capability to maintain accurate estimates for a vehicle's states – often described by position, velocity, and attitude – is required to enable the increasing complexity of spacecraft mission objectives. However, along with an estimate of the vehicle's state, a measure for the accuracy, or uncertainty, in that estimate is also maintained and may significantly impact the decision making process. When deliberating upon mission-critical decisions, it is desirable to have an estimate that is trustworthy to maximize the likelihood of mission success; to determine whether or not the estimate is trustworthy, precise quantification of the uncertainty is necessary. By incorporating additional information, usually in the form of external measurements, the levels of uncertainty can be significantly reduced, though the reduction is dependent upon an accurate accounting of that uncertainty.

During the first crewed lunar descent, Astronaut Neil Armstrong assumed manual control when it became clear that the automatic descent would land in a boulder field and could endanger the crew [21]. Peering out the window of the Apollo 11 Lunar Module, he selected and guided the Eagle to a safe and successful landing. For the next generation of spacecraft navigating in the lunar vicinity, much of the vehicle navigation process will be enhanced by the incorporation of state-of-the-art technology, just as it was in 1969. New systems integrated into the landing portfolio will leverage advancements made in the

decades since the pivotal moon landing to maximize the probability of mission success[1]. Recently, additional emphasis on *precision* landing has been made and is reinforced by the advent of the NASA SPLICE (Safe & Precise Landing – Integrated Capabilities Evolution) project. The SPLICE project aims to advance technologies for precise and safe landing that are critical to the success of future robotic science and exploration missions [4]. As defined by the SPLICE project, the goal of a precision landing is to safely land within close proximity, or within 100 meters, of a desired surface target.

Though much of the technology that these spacecraft depend upon has seen tremendous strides developmentally, some have fallen behind. One such technology is that of the coning, sculling, and scrolling algorithms often used within inertial navigation to improve vehicle state estimates. These algorithms, while correcting for nonlinear effects unrecognized by the sensing systems, have a small contribution to the overall state uncertainty and, before now, have not been a topic of concern within the literature. This thesis seeks to understand the effects of incorporating the coning, sculling, and scrolling algorithms used for inertial navigation on the state uncertainty within a scenario that desires and requires a significant level of precision. By providing an accounting of the uncertainty contribution of these algorithms, the goals of increased precision and safety are supported.

1.1. BACKGROUND

Inertial navigation describes the integration of inertial acceleration and angular rate measurements to estimate the non-gravitational changes in position, velocity, and attitude. Gimbaled inertial navigation systems (INSs) use platforms that mechanically isolate accelerometers and gyroscopes mounted to the platform from the rotation of the vehicle and any present vibration; because of this mechanization, gimbaled INSs are often referred to as "stable-table" INSs. Some examples of gimbaled INSs include the Apollo

---

[1]https://www.nasa.gov/directorates/spacetech/flightopportunities/One_Giant_Leap_for_Lunar_Landing_Navigation

PGNCS [9], which served on both the command module and lunar module, and those developed for the Minuteman III and Peacekeeper intercontinental ballistic missiles [29]. The onboard navigation computer then maintains the navigation frame which describes the orientation of the gimbal and the sensors in relation to some reference. However, gimbaled platforms have since been widely replaced by strapdown systems, where the sensors are instead attached or "strapped-down" directly to the structure of the vehicle, which couples the measurements to the dynamics of the vehicle. Though strapdown INSs are commonly used in modern navigation architectures, one of the earliest adoptions on a high-profile mission was the backup system for the Apollo Abort Guidance System in 1969 [7]. While gimballed systems are still sometimes used for ballistic missiles, strapdown sensors have been adopted for most modern aircraft, guided missile, ship, and underwater vehicle navigation applications [26]. The combination of ring laser gyros and advancements in computing technology initiated and solidified the conversion from gimballed to strapdown systems. Finally, their adoption is well aligned with the continued reduction of size, weight and power (SWaP) requirements for space technology, as their introduction significantly reduced the weight and complexity of the necessary navigation architecture by removing the auxiliary components required for the housing and stabilization of the gimbaled platform [27]. The continued advancement in circuitry and computer technologies has further reduced the size and weight required for strapdown sensors, solidifying their prominence in the field of navigation.

Several obstacles were met and overcome with the incorporation of strapdown sensors, including the need to computationally, as opposed to mechanically, maintain the vehicle's navigation frame. The measurements obtained from gimbaled INSs are defined within context of the frame controlled by the platform, decreasing the computational complexity of the vehicle's position and velocity integration. However, with the adoption of strapdown sensors, the navigation frame is no longer fixed but linked to the attitude of the vehicle, resulting in the need for its computational maintenance. In the transition to

strapdown systems and the computational maintenance of the navigation frame, the ability to account for errors in the state estimates due to coning, sculling, and scrolling motion also became apparent.

Coning motion is defined as the condition where the angular velocity vector of the vehicle is itself rotating, sculling motion describes the combined effects of underlying rotation of the attitude and velocity vectors on the integration of the vehicle's non-gravitational change in velocity, and scrolling details the effects of the attitude and velocity rotation on the position integration. Coning motion is commonly seen in vibrational environments where out-of-phase sinusoidal motion in two axes causes a constant drift in the third axis' attitude estimate [19]. When a vehicle is undergoing pure coning motion, the angular velocity vector magnitude stays constant, while the direction changes such that the vector appears to move on the surface of a cone; hence the name *coning* motion. Sculling and scrolling effects can be present in a variety of scenarios, such as maneuvers for braking or accelerating. Coning, sculling, and scrolling algorithms are now used to detect and generate a correction to the obtained measurements by processing a batch of measurements obtained at a frequency greater than the on-board navigation filter computer cycle. Algorithms designed to approximate errors introduced by the presence of coning, sculling, and scrolling motion, and their application to precision navigation systems, are of primary interest within this thesis.

1.2. MOTIVATION

The modern INS is typically comprised of three orthogonal linear accelerometers and gyroscopes that are used to measure the non-gravitational acceleration and angular velocity of the vehicle, while a navigation computer is employed to integrate these measurements and predict the vehicle states. Additionally, state-of-the-art INSs operating at a high frequency generally apply some combination of the coning, sculling, and scrolling corrections. The extended Kalman filter (EKF) is a tried and true architecture that serves as the backbone for many modern navigation systems [14]. The EKF requires a model

for the dynamics and a statistical representation for the uncertainty in the measurements and dynamics. An equivalent measurement produced by the coning, sculling, and scrolling algorithms is often used in place of the raw measurements to account for the drift incurred by the constant angular velocity assumption. Unfortunately, in the application of common coning, sculling, and scrolling algorithms, there is often an unaccounted-for contribution to the uncertainty, generated by the use of measurements which contain errors due to a variety of factors. Therefore, the known measurement error statistics are no longer representative of the true dynamics. By developing and implementing an error mapping through the algorithms used for coning, sculling, and scrolling corrections, a rigorous treatment of these errors and their effect on the state uncertainty can be realized.

1.3. OVERVIEW

In order to discuss the contributions to and development of the error propagation for the coning, sculling and scrolling algorithms, this thesis is composed of two primary components, the first of which contains preliminary and background information and encompasses Sections 2 – 4. Mathematical notation and attitude representations are reviewed in Section 2. Section 3 introduces the extended and multiplicative extended Kalman filters and the derivation of each. the continuous and discretized equations of motion for a spacecraft are presented in Sections 4.1 and 4.2, while a model for the strapdown inertial measurement unit (IMU) commonly used for inertial navigation is presented within Section 4.3. A summary of the coning, sculling, and scrolling algorithms and their importance is provided in Section 4.4 and incorporated into the discretized equations of motion in Section 4.5.

The second primary component presents the contributions from this thesis and analyzes their application within a lunar descent-to-landing scenario. Within Section 5, the methods for error propagation development, the standard error propagation for the IMU measurement errors, and the propagation of those errors through the coning, sculling, and

scrolling algorithms are derived. The propagation of these measurement errors through the coning, sculling, and scrolling algorithms is then incorporated into the derivation for the propagation of uncertainty using the traditional form of the discrete dead-reckoning equations. Section 6 presents the simulation implementation and analyzes the impact of including the coning, sculling, and scrolling algorithms and the error propagation within the navigation filter. Finally, Section 7 summarizes the results and contributions of this thesis, describing the benefits of including the error propagation for the coning, sculling, and scrolling algorithms within the lunar descent-to-landing scenario.

2. PRELIMINARIES

Throughout this thesis, assumptions are made pertaining to the reader's background in mathematics, engineering, and estimation. To facilitate clarity and continuity throughout the thesis, a few preliminary topics are discussed in order to provide a baseline upon which to expand. Section 2.1 outlines the underlying mathematical notation, discussing standards for quantities such as scalar, vector, and matrix representations. Frame definitions are presented within Section 2.2, describing the frames relevant for a lunar descent-to-landing trajectory. Finally, common attitude representations present throughout the work are discussed in Section 2.3.

2.1. MATHEMATICAL NOTATION AND DEFINITIONS

The mathematical notation within this thesis attempts to align itself with common techniques seen throughout the estimation and engineering community. In general, the spaces explored within this thesis rely upon the space of all real numbers represented by $\mathbb{R}$, with the n-dimensional space expressed as $\mathbb{R}^n$. A scalar variable is represented as a non-bold character, such as x or X, while a vector quantity of length n is given by a bold lowercase character, such as $\boldsymbol{x}$. The vector $\boldsymbol{x}$ is then composed of scalar elements from the set $\{x_1, x_2, \ldots x_n\}$ and ordered such that

$$\boldsymbol{x} = \begin{bmatrix} x_1 \\ x_2 \\ \vdots \\ x_n \end{bmatrix}.$$

A matrix is represented as a bold, capital character, such as X, with elements from the set $\{x_{1,1}, x_{1,2}, x_{2,1}, \ldots x_{n,m}\}$ and ordered such that

$$X = \begin{bmatrix} x_{1,1} & x_{1,2} & \cdots & x_{1,m} \\ x_{2,1} & \ddots & \ddots & \vdots \\ \vdots & \ddots & \ddots & \vdots \\ x_{n,1} & \cdots & \cdots & x_{n,m} \end{bmatrix}.$$

The inverse of a matrix is expressed using the "-1" superscript, while the transpose of a matrix or vector is given by the "T" superscript. The $n \times n$ identity matrix is represented by $I_{n \times n}$. The cross product between two vectors a, $b \in \mathbb{R}^3$ is denoted by $a \times b$; the same operation can be represented by a matrix multiplication such that $a \times b = [a\times]b$, where

$$[a\times] = \begin{bmatrix} 0 & -a_3 & a_2 \\ a_3 & 0 & -a_1 \\ -a_2 & a_1 & 0 \end{bmatrix}$$

is the skew-symmetric cross product matrix. Similar matrices composed with vectors can also be defined such as the diagonal matrix $[a\searrow]$, with elements of the vector appearing on the diagonal of the matrix, and a matrix similar to the cross product matrix $[a*]$, but lacks the sign changes seen for the cross product. It is worth acknowledging that the diagonal matrix is not limited to being 3×3, while the others are; for $a \in \mathbb{R}^3$, the matrices are expressed as

$$[a\searrow] = \begin{bmatrix} a_1 & 0 & 0 \\ 0 & a_2 & 0 \\ 0 & 0 & a_3 \end{bmatrix} \quad \text{and} \quad [a*] = \begin{bmatrix} 0 & a_3 & a_2 \\ a_3 & 0 & a_1 \\ a_2 & a_1 & 0 \end{bmatrix}.$$

Quaternions, which are often used for representing the rotation between frames, are denoted by a bold lowercase character with an overbar, i.e. $\bar{\boldsymbol{q}}$. Additionally, as discussed further in Section 2.3.2, quaternions are composed of scalar and vector elements; in general, the ordering of the two is arbitrary. As such, the right-handed vector-first, scalar-second construction is used. The vector part of the quaternion is denoted by the same bold and lowercase character, though it lacks the overbar. The scalar part is then taken to be the same lowercase character, non-bold, and without the overbar. These definitions allow the expression of the quaternion and its magnitude as

$$\bar{\boldsymbol{q}} = \begin{bmatrix} \boldsymbol{q} \\ q \end{bmatrix} \quad \text{and} \quad \bar{q} = \|\bar{\boldsymbol{q}}\|,$$

where $\| \cdot \|$ is used to express the matrix or, in this case, vector ℓ_2−norm. Additionally, the quaternion multiplication operator is denoted as $\otimes$ and defines the multiplication of the quaternions $\bar{\boldsymbol{p}}$ and $\bar{\boldsymbol{q}}$, expressed as

$$\bar{\boldsymbol{p}} \otimes \bar{\boldsymbol{q}} = \begin{bmatrix} \boldsymbol{p} \\ p \end{bmatrix} \otimes \begin{bmatrix} \boldsymbol{q} \\ q \end{bmatrix} = \begin{bmatrix} q\boldsymbol{p} + p\boldsymbol{q} - \boldsymbol{p} \times \boldsymbol{q} \\ pq - \boldsymbol{p} \cdot \boldsymbol{q} \end{bmatrix},$$

which defines the quaternion multiplication such that they are multiplied in the same order as the equivalent transformation matrices. Finally, the quaternion inverse is simply given by the negative of the vector component and expressed with the " -1 " superscript, or

$$\bar{\boldsymbol{q}}^{-1} = \begin{bmatrix} -\boldsymbol{q} \\ q \end{bmatrix}.$$

The operator $\mathrm{E}\{\cdot\}$ denotes the expected value of a variable. An estimated quantity, or estimate, is denoted by a hat (ˆ) accented variable, while the time-derivative of a given variable is recognized by the dot (˙) accent. Finally, the Kronecker delta is denoted by δ_{ij}

and defined to be 1 when the $i = j$ and 0 otherwise, i.e.

$$
\delta_{ij} = \begin{cases} 1 & i = j \\ 0 & i \neq j \end{cases}.
$$

2.2. FRAME DEFINITIONS

For the discussion within this thesis, three reference frames must be considered for a basic lunar descent trajectory. These three reference frames are the moon-centered inertially fixed frame, the spacecraft navigation or body frame, and the IMU case frame. Each is defined by a set of three mutually orthogonal unit vectors, located at a specific point in space. The definition of these frames allows for the declaration of translation and rotation between points and directions in space. First, the moon-centered and inertially-fixed or non-accelerating frame is located at the center of mass for the moon, depicted by the i subscript or superscript, and defined by the J2000 reference frame. The J2000 coordinate frame has a standard epoch of 2000 January 1.5 with a reference time scale of Barycentric Dynamical Time (TDB), or Julian Date 2451545.0 [1].

The spacecraft body frame is defined to be co-aligned with the IMU case frame, where each also has a common origin. Additionally, the common origin is colocated with the center of gravity for the spacecraft. For the general strapdown IMU, a triad of three orthogonal linear accelerometers and gyroscopes is contained within the case and directed away from their common center, defined to be the origin of the case frame. Therefore, the measurements obtained from the IMU's accelerometers and gyroscopes will be a vector of three values, directed along the axes and defined within the IMU case frame, denoted by a subscript or superscript c. It is worth acknowledging that the spacecraft body frame and IMU case frame are interchangeable within this thesis, though effort will be made to discuss the frames within general circumstances where this may not be the case.

2.3. ATTITUDE REPRESENTATIONS

As previously discussed in Section 1, the computationally maintained estimate of the vehicle attitude became more important with the advent of strapdown technology. Unfortunately, the expression of a vehicle's attitude, defining the orthogonal transformation from an inertially-fixed reference frame to a body-fixed frame, is not as easy as position and velocity. Several representations for the rotation are available, where each has its own quirks, meaning that certain approaches can be better applied to different problems. Two common expressions include the Euler axis/angle and quaternion representations. In-depth reviews of attitude representations are available in Reference [28], though the following sections will briefly discuss some common attitude representations.

2.3.1. Euler Axis and Angle. Each rotation from one frame to another can be expressed as a transformation of one vector to another such that

$$x^B = T_A^B x^A$$

where T_A^B defines the transformation from the A frame to the B frame. Euler's Theorem states that this same rotation can be represented by a rotation vector ϕ, described by a magnitude of rotation ϕ about a fixed axis e; these are known as the Euler angle and Euler axis [18]. Using this definition and decomposing the rotation into orthogonal and parallel projections of one basis onto another, the attitude matrix can be expressed as

$$T_A^B = I_{3\times3} - \sin\phi\,[e\times] + (1 - \cos\phi)\,[e\times]^2\,. \tag{2.1}$$

Recognize that should the angle of rotation be zero, meaning that the A and B frames must be the same, Equation (2.1) gives the expected $T_A^B = I_{3\times3}$. The attitude matrix must represent the transformation through an orthonormal bases, i.e. T_A^B must satisfy

$$T_A^B T_B^A = T_A^B (T_A^B)^T = I_{3\times3},$$

which yields six constraints. Despite the need to satisfy six constraints, the attitude matrix is useful as it allows the mapping of vectors defined within one frame to another related by T_A^B, a common practice within inertial navigation systems.

2.3.2. Quaternion. The quaternion representation is related to that of the Euler angle and Euler axis representation by the identity

$$\bar{q} = \begin{bmatrix} \sin(\phi/2)e \\ \cos(\phi/2) \end{bmatrix},$$

which also allows the definition of the attitude matrix as

$$T_A^B = \left(q^2 - ||\boldsymbol{q}||^2\right) I_{3\times3} - 2q\left[\boldsymbol{q}\times\right] + 2\boldsymbol{q}\boldsymbol{q}^T.$$

The vector and scalar part, $\boldsymbol{q}$ and q respectively, of the quaternion are known as the Euler-Rodrigues parameters or the Euler symmetric parameters primarily because of the dual contributions of Euler and Rodgrigues to their development [18]. Quaternions describing a rotation are subject to a unit-norm constraint and defined such that

$$||\bar{q}|| = 1.$$

The reduction to four parameters from the nine used for the attitude matrix is computationally desirable and the reduced number of constraints makes the quaternion a useful description of attitude commonly seen in spacecraft navigation systems. It is worth noting that the quaternion representation is not a minimal representation, making it difficult to directly interpret, though it is globally non-singular unlike those posed by minimal three-parameter representations, allowing the avoidance of gimbal-lock.

3. KALMAN FILTERING

The Kalman filter is a widely used instrument for the optimal estimation of uncertain linear systems [13]. The structure of the Kalman filter can be separated into two parts, commonly referred to as the predictor and the corrector. Given some state estimate, the uncertainty in the estimate, and knowledge of the dynamics governing the system, future estimates, or predictions, for the state and uncertainty may be determined. Measurements may then be processed to incorporate new information, which allows the state estimate and the uncertainty to be refined, or corrected, as additional information is acquired. It is important to note that the correction stage of the Kalman filter, sometimes referred to as the update, is not developed in this section. The absense of the update development is primarily due to the lack of external measurements being processed within this work; the inertial measurements provided by an IMU are instead used to make state predictions. Through its application, the Kalman filter is used to minimize the mean square estimation error, a desirable attribute for many engineering applications.

Within this thesis, estimation of position, velocity, and attitude states for a spacecraft on a lunar approach and descent trajectory is the primary topic of interest. Unfortunately, the assumption of linearity in the Kalman filter is far from reality for most engineering applications, including the dynamics that govern the motion of a spacecraft navigating the lunar approach and descent. To apply the Kalman filter to the proposed scenario, the framework must be augmented and extended for use within a general nonlinear regime. This augmentation is done through the linearization of the dynamics about the mean which results in the ubiquitous extended Kalman filter [14]. Throughout the following sections, the extended Kalman filter and multiplicative extended Kalman filter are presented and discussed, alongside their application to the aforementioned spacecraft navigation scenario.

3.1. EXTENDED KALMAN FILTER

Consider the discrete, nonlinear dynamical system model described by the stochastic difference equation

$$\boldsymbol{x}_k = \boldsymbol{f}(\boldsymbol{x}_{k-1}) + \boldsymbol{M}_{k-1}\boldsymbol{w}_{k-1}, \tag{3.1}$$

where $\boldsymbol{f}(\cdot)$ describes the nonlinear dynamics governing the state evolution of $\boldsymbol{x}_{k-1}$ at t_{k-1} to $\boldsymbol{x}_k$ at t_k and $\boldsymbol{w}_{k-1}$ describes the random process noise mapped into the state by the deterministic mapping $\boldsymbol{M}_{k-1}$. The random noise is taken to be zero-mean, i.e. $\mathrm{E}\{\boldsymbol{w}_{k-1}\} = \boldsymbol{0}$, with covariance defined by

$$\mathrm{E}\left\{\boldsymbol{w}_i\boldsymbol{w}_j^T\right\} = \boldsymbol{Q}_i\delta_{ij}, \tag{3.2}$$

where δ_{ij} is the Kronecker delta that enforces the definition for time-wise uncorrelated process noise. To formulate the extended Kalman filter, consider the expected value of Equation (3.1),

$$\mathrm{E}\{\boldsymbol{x}_k\} = \mathrm{E}\{\boldsymbol{f}(\boldsymbol{x}_{k-1}) + \boldsymbol{M}_{k-1}\boldsymbol{w}_{k-1}\}, \tag{3.3}$$

which can then be distributed to produce

$$\mathrm{E}\{\boldsymbol{x}_k\} = \mathrm{E}\{\boldsymbol{f}(\boldsymbol{x}_{k-1})\} + \mathrm{E}\{\boldsymbol{M}_{k-1}\boldsymbol{w}_{k-1}\}, \tag{3.4}$$

since the expected value operator is a linear operator. Because $\boldsymbol{M}_{k-1}$ is deterministic and the expected value of a randomly distributed variable is the mean, i.e. $\mathrm{E}\{\boldsymbol{x}_k\} = \hat{\boldsymbol{x}}_k$, Equation (3.4) is restated such that

$$\hat{\boldsymbol{x}}_k = \mathrm{E}\left\{\boldsymbol{f}(\boldsymbol{x}_{k-1})\right\} + \boldsymbol{M}_{k-1}\mathrm{E}\left\{\boldsymbol{w}_{k-1}\right\}$$

$$= \mathrm{E}\left\{\boldsymbol{f}(\boldsymbol{x}_{k-1})\right\}. \tag{3.5}$$

The dynamics may be approximated by a first order Taylor series expansion about the mean, given by

$$\boldsymbol{f}(\boldsymbol{x}_{k-1}) \cong \boldsymbol{f}(\hat{\boldsymbol{x}}_{k-1}) + \boldsymbol{F}(\hat{\boldsymbol{x}}_{k-1})(\boldsymbol{x}_{k-1} - \hat{\boldsymbol{x}}_{k-1}), \tag{3.6}$$

where the dynamics Jacobian $\boldsymbol{F}(\hat{\boldsymbol{x}}_{k-1})$ is defined to be

$$\boldsymbol{F}(\hat{\boldsymbol{x}}_{k-1}) = \left[\frac{\partial \boldsymbol{f}(\boldsymbol{x}_{k-1})}{\partial \boldsymbol{x}_{k-1}}\bigg|_{\boldsymbol{x}_{k-1}=\hat{\boldsymbol{x}}_{k-1}}\right]. \tag{3.7}$$

Substituting, Equation (3.6) into Equation (3.5), the evolution of the state estimate is then expressed as

$$\hat{\boldsymbol{x}}_k = \mathrm{E}\left\{\boldsymbol{f}(\hat{\boldsymbol{x}}_{k-1}) + \boldsymbol{F}_{k-1}(\boldsymbol{x}_{k-1} - \hat{\boldsymbol{x}}_{k-1})\right\}, \tag{3.8}$$

where $\boldsymbol{F}_{k-1} = \boldsymbol{F}(\hat{\boldsymbol{x}}_{k-1})$ for notational simplification. Assuming that $\boldsymbol{F}_{k-1}$ and $\boldsymbol{f}(\hat{\boldsymbol{x}}_{k-1})$ are deterministic yields

$$\hat{\boldsymbol{x}}_k = \boldsymbol{f}(\hat{\boldsymbol{x}}_{k-1}) + \boldsymbol{F}_{k-1}\mathrm{E}\left\{\boldsymbol{x}_{k-1} - \hat{\boldsymbol{x}}_{k-1}\right\}. \tag{3.9}$$

Define the error between the state and mean to be $\boldsymbol{e}_{k-1} = \boldsymbol{x}_{k-1} - \hat{\boldsymbol{x}}_{k-1}$, allowing the simplification of Equation (3.9) to

$$\hat{\boldsymbol{x}}_k = \boldsymbol{f}(\hat{\boldsymbol{x}}_{k-1}) + \boldsymbol{F}_{k-1}\mathrm{E}\left\{\boldsymbol{e}_{k-1}\right\}. \tag{3.10}$$

Finally, taking the noise and error be unbiased, or zero-mean, the expression for the propagation of the mean becomes

$$\hat{\boldsymbol{x}}_k = \boldsymbol{f}(\hat{\boldsymbol{x}}_{k-1}), \tag{3.11}$$

which is the well-known state propagation for the extended Kalman filter with initial condition $\hat{\boldsymbol{x}}_0$.

To propagate the covariance, consider the error between the true and estimated state at time t_k, i.e.

$$\boldsymbol{e}_k = \boldsymbol{x}_k - \hat{\boldsymbol{x}}_k. \tag{3.12}$$

Substituting for each of the right-hand side terms, using Equations (3.1) and (3.11), the error can be expressed as

$$\boldsymbol{e}_k = \boldsymbol{f}(\boldsymbol{x}_{k-1}) + \boldsymbol{M}_{k-1}\boldsymbol{w}_{k-1} - \boldsymbol{f}(\hat{\boldsymbol{x}}_{k-1}). \tag{3.13}$$

Substituting the first order Taylor series expansion of $\boldsymbol{f}(\boldsymbol{x}_{k-1})$ in Equation (3.6), the error dynamics for the extended Kalman filter can be simplified to

$$\begin{aligned} \boldsymbol{e}_k &= \boldsymbol{f}(\hat{\boldsymbol{x}}_{k-1}) + \boldsymbol{F}_{k-1}(\boldsymbol{x}_{k-1} - \hat{\boldsymbol{x}}_{k-1}) + \boldsymbol{M}_{k-1}\boldsymbol{w}_{k-1} - \boldsymbol{f}(\hat{\boldsymbol{x}}_{k-1}) \\ &= \boldsymbol{F}_{k-1}\boldsymbol{e}_{k-1} + \boldsymbol{M}_{k-1}\boldsymbol{w}_{k-1}. \end{aligned} \tag{3.14}$$

It is worth noting that $\mathrm{E}\{\boldsymbol{e}_k\} = \boldsymbol{0}$ if $\mathrm{E}\{\boldsymbol{e}_{k-1}\} = \boldsymbol{0}$, by the zero-mean noise assumption. The estimation error covariance is defined as

$$\boldsymbol{P}_k = \mathrm{E}\left\{\boldsymbol{e}_k\boldsymbol{e}_k^T\right\}, \tag{3.15}$$

and through the substitution of the error dynamics in Equation (3.14) into Equation (3.15), the covariance can be expanded to

$$
\begin{aligned}
\boldsymbol{P}_k =& \mathrm{E}\left\{\left[\boldsymbol{F}_{k-1}\boldsymbol{e}_{k-1} + \boldsymbol{M}_{k-1}\boldsymbol{w}_{k-1}\right]\left[\boldsymbol{F}_{k-1}\boldsymbol{e}_{k-1} + \boldsymbol{M}_{k-1}\boldsymbol{w}_{k-1}\right]^T\right\} \\
=& \mathrm{E}\left\{\boldsymbol{F}_{k-1}\boldsymbol{e}_{k-1}\boldsymbol{e}_{k-1}^T\boldsymbol{F}_{k-1}^T\right\} + \mathrm{E}\left\{\boldsymbol{F}_{k-1}\boldsymbol{e}_{k-1}\boldsymbol{w}_{k-1}^T\boldsymbol{M}_{k-1}^T\right\} \\
& + \mathrm{E}\left\{\boldsymbol{M}_{k-1}\boldsymbol{w}_{k-1}\boldsymbol{e}_{k-1}^T\boldsymbol{F}_{k-1}^T\right\} + \mathrm{E}\left\{\boldsymbol{M}_{k-1}\boldsymbol{w}_{k-1}\boldsymbol{w}_{k-1}^T\boldsymbol{M}_{k-1}^T\right\},
\end{aligned}
\tag{3.16}
$$

where it is again noted that the expected value operator is a linear operator and distributable. Assuming that the error in the state and noise are uncorrelated, and recalling that $\boldsymbol{M}_{k-1}$ and $\boldsymbol{F}_{k-1}$ are assumed to be deterministic, Equation (3.16) is

$$
\boldsymbol{P}_k = \boldsymbol{F}_{k-1}\mathrm{E}\left\{\boldsymbol{e}_{k-1}\boldsymbol{e}_{k-1}^T\right\}\boldsymbol{F}_{k-1}^T + \boldsymbol{M}_{k-1}\mathrm{E}\left\{\boldsymbol{w}_{k-1}\boldsymbol{w}_{k-1}^T\right\}\boldsymbol{M}_{k-1}^T.
\tag{3.17}
$$

Notice here that $\mathrm{E}\left\{\boldsymbol{e}_{k-1}\boldsymbol{e}_{k-1}^T\right\}$ is simply the estimation error covariance at t_{k-1}, $\boldsymbol{P}_{k-1}$. The propagation of the state covariance can then finally be stated as

$$
\boldsymbol{P}_k = \boldsymbol{F}_{k-1}\boldsymbol{P}_{k-1}\boldsymbol{F}_{k-1}^T + \boldsymbol{M}_{k-1}\boldsymbol{Q}_{k-1}\boldsymbol{M}_{k-1}^T,
\tag{3.18}
$$

which is the well-known propagation for the state uncertainty for the extended Kalman filter with initial condition $\boldsymbol{P}_0$.

3.2. MULTIPLICATIVE EXTENDED KALMAN FILTER

When considering the estimation of attitude, an expression for the direction and magnitude of rotation from one frame to another, quaternions are often used to avoid the singularities that exist in common three-parameter attitude representations. Their ability to avoid singularities and linearly represent the attitude dynamics, while also allowing the easy computation of the attitude matrix, makes the rotation quaternion a useful parameterization

for attitude [15]. However, the estimation of attitude within the EKF poses an issue because rotations are not additive, meaning that the EKF cannot be directly applied. A formulation of the extended Kalman filter developed to specifically handle the quaternion representation of attitude is called the multiplicative extended Kalman filter (MEKF)[5], which applies a small angle approximation for the attitude error and reduces its dimension by one. This alteration still allows the attitude to be represented by a quaternion.

The multiplicative quaternion propagation is defined such that

$$\bar{q}_k = \bar{q}(\Delta\theta_k) \otimes \bar{q}_{k-1} \tag{3.19}$$

where $\bar{q}(\Delta\theta_k)$ is the quaternion representation for the rotation $\Delta\theta_k$ between t_{k-1} and t_k. The error quaternion $\delta\bar{q}_k$, representing the error between the true attitude $\bar{q}_k$ and estimated attitude $\hat{\bar{q}}_k$ at t_k, is defined such that

$$\delta\bar{q}_k = \bar{q}_k \otimes \hat{\bar{q}}_k^{-1}. \tag{3.20}$$

The quaternion error is analogous to the error in rotation matrices – the post-multiplication with the inverse transformation yields the error between them. If the two quaternions represent the same rotation, there will be no error, i.e. Equation (3.20) will yield the identity quaternion $\bar{\imath}$ with vector-part $\mathbf{0}$ and scalar-part 1. Substituting Equation (3.19) into Equation (3.20) for the estimated and true attitude quaternions, the error can be expressed as

$$
\begin{aligned}
\delta\bar{q}_k &= (\bar{q}(\Delta\theta_k) \otimes \bar{q}_{k-1}) \otimes \left(\bar{q}(\Delta\hat{\theta}_k) \otimes \hat{\bar{q}}_{k-1}\right)^{-1} \\
&= \bar{q}(\Delta\theta_k) \otimes \bar{q}_{k-1} \otimes \hat{\bar{q}}_{k-1}^{-1} \otimes \bar{q}(\Delta\hat{\theta}_k)^{-1} \\
&= \bar{q}(\Delta\theta_k) \otimes \delta\bar{q}_{k-1} \otimes \bar{q}(\Delta\hat{\theta}_k)^{-1} \\
&= \bar{q}(\Delta\theta_k) \otimes \bar{q}(\Delta\hat{\theta}_k)^{-1} \otimes \bar{q}(\Delta\hat{\theta}_k) \otimes \delta\bar{q}_{k-1} \otimes \bar{q}(\Delta\hat{\theta}_k)^{-1}, \tag{3.21}
\end{aligned}
$$

where $\Delta\hat{\boldsymbol{\theta}}_k = \mathrm{E}\{\Delta\theta_k\}$ is the estimated rotation between t_{k-1} and t_k. After expanding the quaternion multiplication, it can be shown that [32]

$$\bar{\boldsymbol{q}}(\Delta\hat{\boldsymbol{\theta}}_k) \otimes \delta\bar{\boldsymbol{q}}_{k-1} \otimes \bar{\boldsymbol{q}}(\Delta\hat{\boldsymbol{\theta}}_k)^{-1} = \begin{bmatrix} \boldsymbol{T}(\Delta\hat{\boldsymbol{\theta}}_k)\delta\boldsymbol{q}_{k-1} \\ \delta q_{k-1} \end{bmatrix}, \tag{3.22}$$

given the transformation defined in Equation (2.1). This result allows the expression of $\delta\bar{\boldsymbol{q}}_k$ to be written as

$$\delta\bar{\boldsymbol{q}}_k = \bar{\boldsymbol{q}}(\Delta\boldsymbol{\theta}_k) \otimes \bar{\boldsymbol{q}}(\Delta\hat{\boldsymbol{\theta}}_k)^{-1} \otimes \begin{bmatrix} \boldsymbol{T}(\Delta\hat{\boldsymbol{\theta}}_k)\delta\boldsymbol{q}_{k-1} \\ \delta q_{k-1} \end{bmatrix}. \tag{3.23}$$

A small angle assumption well approximates $\bar{\boldsymbol{q}}(\Delta\boldsymbol{\theta}_k) \otimes \bar{\boldsymbol{q}}(\Delta\hat{\boldsymbol{\theta}}_k)^{-1}$, i.e.

$$\bar{\boldsymbol{q}}(\Delta\boldsymbol{\theta}_k) \otimes \bar{\boldsymbol{q}}(\Delta\hat{\boldsymbol{\theta}}_k)^{-1} \approx \begin{bmatrix} \frac{1}{2}\boldsymbol{e}_{\Delta\theta,k} \\ 1 \end{bmatrix}, \tag{3.24}$$

where $\boldsymbol{e}_{\Delta\theta,k} = \Delta\boldsymbol{\theta}_k - \Delta\hat{\boldsymbol{\theta}}_k$ is the error in the rotation between t_{k-1} and t_k. Therefore, $\delta\bar{\boldsymbol{q}}_k$ is given by

$$\delta\bar{\boldsymbol{q}}_k = \begin{bmatrix} \frac{1}{2}\boldsymbol{e}_{\Delta\theta,k} \\ 1 \end{bmatrix} \otimes \begin{bmatrix} \boldsymbol{T}(\Delta\hat{\boldsymbol{\theta}}_k)\delta\boldsymbol{q}_{k-1} \\ \delta q_{k-1} \end{bmatrix}. \tag{3.25}$$

Assuming that the error is small, the vector component of the error quaternion fully represents the attitude error [15] and allows the approximation of Equation (3.25) to first-order, such that

$$\delta\boldsymbol{q}_k = \boldsymbol{T}(\Delta\hat{\boldsymbol{\theta}}_k)\delta\boldsymbol{q}_{k-1} + \frac{1}{2}\boldsymbol{e}_{\Delta\theta,k}. \tag{3.26}$$

Recognizing that the rotation vector $\Delta\boldsymbol{\theta}_k$ is approximately twice the vector-part of the quaternion for small angles, i.e. $\boldsymbol{e}_{A,k} = 2\bar{\boldsymbol{q}}_k$, the error propagation for the attitude error covariance can then be expressed as

$$\boldsymbol{e}_{A,k} = \boldsymbol{T}(\Delta\hat{\boldsymbol{\theta}}_k)\boldsymbol{e}_{A,k-1} + \boldsymbol{e}_{\Delta\theta,k}. \tag{3.27}$$

The attitude covariance is defined such that

$$\boldsymbol{P}_{A,k} = \mathrm{E}\left\{\boldsymbol{e}_{A,k}\boldsymbol{e}_{A,k}^T\right\}, \tag{3.28}$$

or, substituting Equation (3.27) and expanding,

$$
\begin{aligned}
\boldsymbol{P}_{A,k} =& \mathrm{E}\left\{\left[\boldsymbol{T}(\Delta\hat{\boldsymbol{\theta}}_k)\boldsymbol{e}_{A,k-1} + \boldsymbol{e}_{\Delta\theta,k}\right]\left[\boldsymbol{T}(\Delta\hat{\boldsymbol{\theta}}_k)\boldsymbol{e}_{A,k-1} + \boldsymbol{e}_{\Delta\theta,k}\right]^T\right\} \\
=& \mathrm{E}\left\{\boldsymbol{T}(\Delta\hat{\boldsymbol{\theta}}_k)\boldsymbol{e}_{A,k-1}\boldsymbol{e}_{A,k-1}^T\boldsymbol{T}^T(\Delta\hat{\boldsymbol{\theta}}_k)\right\} + \mathrm{E}\left\{\boldsymbol{e}_{\Delta\theta,k}\boldsymbol{e}_{\Delta\theta,k}^T\right\} \\
&+ \mathrm{E}\left\{\boldsymbol{e}_{\Delta\theta,k}\boldsymbol{e}_{A,k-1}^T\boldsymbol{T}^T(\Delta\hat{\boldsymbol{\theta}}_k)\right\} + \mathrm{E}\left\{\boldsymbol{T}(\Delta\hat{\boldsymbol{\theta}}_k)\boldsymbol{e}_{A,k-1}\boldsymbol{e}_{\Delta\theta,k}^T\right\}.
\end{aligned}
\tag{3.29}
$$

Assuming that $\boldsymbol{T}(\Delta\hat{\boldsymbol{\theta}}_k)$ is deterministic and that error in the rotation vector is uncorrelated to the error in the attitude, the expression in Equation (3.29) simplifies to

$$\boldsymbol{P}_{A,k} = \boldsymbol{T}(\Delta\hat{\boldsymbol{\theta}}_k)\mathrm{E}\left\{\boldsymbol{e}_{A,k-1}\boldsymbol{e}_{A,k-1}^T\right\}\boldsymbol{T}^T(\Delta\hat{\boldsymbol{\theta}}_k) + \mathrm{E}\left\{\boldsymbol{e}_{\Delta\theta,k}\boldsymbol{e}_{\Delta\theta,k}^T\right\}. \tag{3.30}$$

Equation (3.30) simplifies one step further by recognizing $\mathrm{E}\left\{\boldsymbol{e}_{A,k-1}\boldsymbol{e}_{A,k-1}^T\right\}$ as the attitude covariance $\boldsymbol{P}_{A,k-1}$ and $\mathrm{E}\left\{\boldsymbol{e}_{\Delta\theta,k}\boldsymbol{e}_{\Delta\theta,k}^T\right\}$ as the rotation error covariance $\boldsymbol{Q}_{\Delta\theta,k}$, yielding the propagation for the attitude covariance for the MEKF,

$$\boldsymbol{P}_{A,k} = \boldsymbol{T}(\Delta\hat{\boldsymbol{\theta}}_k)\boldsymbol{P}_{A,k-1}\boldsymbol{T}^T(\Delta\hat{\boldsymbol{\theta}}_k) + \boldsymbol{Q}_{\Delta\theta,k}. \tag{3.31}$$

In summary, the MEKF uses a globally non-singular attitude representation, here taken to be the right-handed vector-first quaternion, to estimate attitude. A small angle assumption is applied within the formulation to produce the attitude covariance through a three-component representation of the attitude error in the body-fixed navigation frame. When estimating attitude as a subset of the state, the MEKF is applied only to the attitude component, while the aforementioned EKF formulation is used for the remaining states. Because of the small angle assumption in the formulation of the MEKF, correlations between the attitude estimation error and non-attitude states will also be reliant upon the small angle assumption. Finally, it is worth noting that the resulting covariance will be dimension $(n-1) \times (n-1)$, where n is the number of states being estimated because the attitude error is represented as a rotation vector instead of an attitude quaternion.

4. TECHNIQUES FOR INERTIAL NAVIGATION

The INS requires a complete description of a vehicle's dynamics to successfully predict the evolution of its translational and rotational states. To accurately describe these dynamics, a model for the effects of known forces on the vehicle must be utilized. While a sufficiently accurate model can be generated for the effects of gravitational forces on the body, non-gravitational forces and torques are often more difficult to model. Using measurements from inertial sensors, usually housed within the INS, effects of external non-gravitational forces and torques acting on the vehicle need not be modeled. The equations of motion used to describe the state evolution are provided in their continuous form in Section 4.1.

Unfortunately, inertial measurements are obtained at a certain frequency within the navigation computer, requiring an adaptation of the continuous dynamics to process these discrete measurements. To incorporate the non-gravitational acceleration and rotation of the vehicle, a discretized form of the dynamics is generally used and is shown in Section 4.2. Measurements from the strapdown inertial sensor systems are affected by many known error sources that a navigation filter can typically estimate. As such, a model for a strapdown IMU with a triad of accelerometers and gyroscopes is developed within Section 4.3. Coning, sculling, and scrolling algorithms are often used to downsample the measurements and generate a correction for the errors introduced by underlying vibrational or unmodeled effects of a time-varying acceleration or angular velocity vector; a set of second-order coning, sculling, and scrolling algorithms is provided in Section 4.4, which describes methods for using the inertial measurements to provide corrected quantities for the same interval. Finally, the results from the coning, sculling, and scrolling equations must be incorporated into the discretized dynamics, and this is illustrated in Section 4.5.

4.1. CONTINUOUS VEHICLE DYNAMICS

The continuous equations of motion for a vehicle utilizing strapdown inertial sensors are given by [6]

$$\dot{\boldsymbol{r}}_c^i(t) = \boldsymbol{v}_c^i(t) \tag{4.1a}$$

$$\dot{\boldsymbol{v}}_c^i(t) = \boldsymbol{a}_g^i \left(\boldsymbol{r}_c^i(t) + \boldsymbol{T}_c^i(t)\boldsymbol{r}_{cg/c}^c(t) \right) + \boldsymbol{T}_c^i(t)\boldsymbol{a}_{ng}^c(t) \tag{4.1b}$$

$$\dot{\bar{\boldsymbol{q}}}_i^c(t) = \frac{1}{2}\bar{\omega}_{c/i}^c(t) \otimes \bar{\boldsymbol{q}}_i^c(t), \tag{4.1c}$$

where the temporal derivatives for position and velocity are $\dot{\boldsymbol{r}}$ and $\dot{\boldsymbol{v}}$, respectively, and $\dot{\bar{\boldsymbol{q}}}_i^c$ describes the attitude evolution, i.e. the time-rate of change for the rotation from the inertial frame to the IMU case frame. The vector superscript i denotes a quantity expressed in the inertial frame, while the superscript c denotes a quantity expressed in the case frame of the IMU. The direction cosine matrix defining the rotation from IMU case frame to the inertial frame is given by $\boldsymbol{T}_c^i$, while $\boldsymbol{r}_c^i$ is the position of the IMU case frame origin, $\boldsymbol{a}_g^i(\cdot)$ is the gravitational acceleration evaluated at the center of gravity of the vehicle, $\boldsymbol{a}_{ng}^c$ is the non-gravitational specific force experienced by the vehicle, $\boldsymbol{r}_{cg/c}^c$ defines the position of the case frame origin with respect to the vehicle's center of gravity, and $\bar{\omega}_{c/i}^c$ is the angular velocity of the case frame with respect to the inertial frame and expressed as a pure quaternion.

4.2. DISCRETIZED VEHICLE DYNAMICS

The continuous dynamics shown in Equations (4.1) govern the motion of a spacecraft aided by strapdown inertial sensors. Unfortunately, inertial measurements are not available continuously but discretely at a given sample frequency. However, given that the measurement time interval is small, the non-gravitational incremental angle and velocity sensed by the inertial sensors are assumed to be constant from t_{k-1} to t_k. Under this assumption, the incremental angle $\Delta\boldsymbol{\theta}_k^c$ and velocity $\Delta\boldsymbol{v}_{ng,k}^c$ are then related to the vehicle angular

velocity and acceleration such that

$$\Delta\boldsymbol{\theta}_k^c = \boldsymbol{\omega}_{c/i}^c \Delta t_k \quad \text{and} \quad \Delta\boldsymbol{v}_{ng,k}^c = \boldsymbol{a}_{ng,k}^c \Delta t_k. \tag{4.2}$$

Discretizing Equations (4.1) via analytical integration and using the definitions in Equation (4.2), the dynamics are expressed by [32]

$$\boldsymbol{r}_{c,k}^i = \boldsymbol{r}_{c,k-1}^i + \boldsymbol{v}_{c,k-1}^i \Delta t_k + \boldsymbol{T}_{c,k-1}^i \Delta \boldsymbol{r}_{ng,k}^c \tag{4.3a}$$
$$+ \frac{1}{2}\left(\boldsymbol{g}_{k-1} - \frac{1}{3}\boldsymbol{G}_{k-1}\boldsymbol{T}_{c,k-1}^i \left[\boldsymbol{r}_{cg/c,k-1}^c \times\right]\Delta\boldsymbol{\theta}_k^c\right)\Delta t_k^2$$

$$\boldsymbol{v}_{c,k}^i = \boldsymbol{v}_{c,k-1}^i + \boldsymbol{T}_{c,k-1}^i \Delta \boldsymbol{v}_{ng,k}^c + \left(\boldsymbol{g}_{k-1} - \frac{1}{2}\boldsymbol{G}_{k-1}\boldsymbol{T}_{c,k-1}^i \left[\boldsymbol{r}_{cg/c,k-1}^c \times\right]\Delta\boldsymbol{\theta}_k^c\right)\Delta t_k \tag{4.3b}$$

$$\bar{\boldsymbol{q}}_{i,k}^c = \bar{\boldsymbol{q}}(\Delta\boldsymbol{\theta}_k^c) \otimes \bar{\boldsymbol{q}}_{i,k-1}^c, \tag{4.3c}$$

where $\Delta t_k = t_k - t_{k-1}$ is the time between navigation cycles which is, in this case, equivalent to the frequency of measurements from the inertial sensors. The subscripts k and $k-1$ denote a quantity available to the navigation computer at t_k and t_{k-1}, respectively. Additionally, the specific force acting on the vehicle due to gravity is denoted by $\boldsymbol{g}_{k-1} = \boldsymbol{a}_g^i\left(\boldsymbol{r}_{cg,k-1}^i\right)$ and $\boldsymbol{G}_{k-1}$ is the Jacobian of $\boldsymbol{g}_{k-1}$, which must be evaluted at the vehicle's center of gravity $\boldsymbol{r}_{cg,k-1}^i$. Note that the position of the center of gravity is defined to be the vector addition of the IMU position and position of the center of gravity with respect to the IMU, i.e. $\boldsymbol{r}_{cg,k-1}^i = \boldsymbol{r}_{c,k-1}^i + \boldsymbol{T}_{c,k-1}^i \boldsymbol{r}_{cg/c,k-1}^c$. Finally, the non-gravitational changes in the position and velocity are described by

$$\Delta\boldsymbol{r}_{ng,k}^c = \frac{1}{2}\left(\boldsymbol{I}_{3\times3} + \frac{1}{3}\left[\Delta\boldsymbol{\theta}_k^c \times\right]\right)\Delta\boldsymbol{v}_k^c \Delta t_k \tag{4.4a}$$

$$\Delta\boldsymbol{v}_{ng,k}^c = \left(\boldsymbol{I}_{3\times3} + \frac{1}{2}\left[\Delta\boldsymbol{\theta}_k^c \times\right]\right)\Delta\boldsymbol{v}_k^c, \tag{4.4b}$$

which includes a correction for the vector rotation from t_{k-1} to t_k.

4.3. STRAPDOWN SENSOR MODEL

Measurements of non-gravitational accleration and total angular velocity with an IMU are corrupted by several error sources resulting from imperfections in the manufacturing process, circuitry, and errors introduced by installing the unit. The incremental angle and velocity measurements provided by a strapdown IMU, can be expressed as

$$\Delta\boldsymbol{\theta}_{m,k}^c = (\boldsymbol{I}_{3\times3} + [\boldsymbol{s}_{g,k}\searrow])(\boldsymbol{I}_{3\times3} + [\boldsymbol{m}_{g,k}\times] + [\boldsymbol{n}_{g,k}*])(\Delta\boldsymbol{\theta}_k^c + \boldsymbol{b}_{g,k} + \boldsymbol{w}_{g,k}) \qquad (4.5a)$$

$$\Delta\boldsymbol{v}_{m,k}^c = (\boldsymbol{I}_{3\times3} + [\boldsymbol{s}_{a,k}\searrow])(\boldsymbol{I}_{3\times3} + [\boldsymbol{m}_{a,k}\times] + [\boldsymbol{n}_{a,k}*])(\Delta\boldsymbol{v}_k^c + \boldsymbol{b}_{a,k} + \boldsymbol{w}_{a,k}), \qquad (4.5b)$$

where $\boldsymbol{b}_{g,k}$, $\boldsymbol{s}_{g,k}$, $\boldsymbol{n}_{g,k}$, $\boldsymbol{m}_{g,k}$, and $\boldsymbol{w}_{g,k}$ are the bias, scale factor, nonorthogonality, misalignment, and zero-mean, time-wise uncorrelated process noise error vectors in the gyroscope measurement at t_k, respectively, while $\Delta\boldsymbol{\theta}_k$ is the true incremental angle, and $\Delta\boldsymbol{\theta}_{m,k}$ is the measured incremental angle at t_k. Similarly, $\boldsymbol{b}_{a,k}$, $\boldsymbol{s}_{a,k}$, $\boldsymbol{n}_{a,k}$, $\boldsymbol{m}_{a,k}$, and $\boldsymbol{w}_{a,k}$ are the bias, scale factor, nonorthogonality, misalignment, and zero-mean, time-wise uncorrelated process noise error vectors in the accelerometer measurement at t_k, respectively, $\Delta\boldsymbol{v}_k^c$ is the true incremental angle, and $\Delta\boldsymbol{v}_{m,k}^c$ is the measured incremental angle at t_k. From hereon, the case frame superscript will be neglected for the expression of the true and measured incremental angle and velocity, allowing them to be expressed as

$$\Delta\boldsymbol{\theta}_k^c \rightarrow \Delta\boldsymbol{\theta}_k, \quad \Delta\boldsymbol{\theta}_{m,k}^c \rightarrow \Delta\boldsymbol{\theta}_{m,k}, \quad \Delta\boldsymbol{v}_k^c \rightarrow \Delta\boldsymbol{v}_k, \quad \text{and} \quad \Delta\boldsymbol{v}_{m,k}^c \rightarrow \Delta\boldsymbol{v}_{m,k}.$$

Applying the models given in Equations (4.5), the true incremental angle and incremental velocity can be obtained from the measured quantities such that

$$\Delta\boldsymbol{\theta}_k = (\boldsymbol{I}_{3\times3} + [\boldsymbol{m}_{g,k}\times] + [\boldsymbol{n}_{g,k}*])^{-1}(\boldsymbol{I}_{3\times3} + [\boldsymbol{s}_{g,k}\searrow])^{-1}\Delta\boldsymbol{\theta}_{m,k} - \boldsymbol{b}_{g,k} - \boldsymbol{w}_{g,k} \qquad (4.6a)$$

$$\Delta\boldsymbol{v}_k = (\boldsymbol{I}_{3\times3} + [\boldsymbol{m}_{a,k}\times] + [\boldsymbol{n}_{a,k}*])^{-1}(\boldsymbol{I}_{3\times3} + [\boldsymbol{s}_{a,k}\searrow])^{-1}\Delta\boldsymbol{v}_{m,k} - \boldsymbol{b}_{a,k} - \boldsymbol{w}_{a,k}. \qquad (4.6b)$$

Equations (4.6) can be simplified to

$$\Delta\boldsymbol{\theta}_k = (\boldsymbol{I}_{3\times3} + \boldsymbol{\Lambda}_g)^{-1}\Delta\boldsymbol{\theta}_{m,k} - \boldsymbol{b}_{g,k} - \boldsymbol{w}_{g,k} \tag{4.7a}$$

$$\Delta\boldsymbol{v}_k = (\boldsymbol{I}_{3\times3} + \boldsymbol{\Lambda}_a)^{-1}\Delta\boldsymbol{v}_{m,k} - \boldsymbol{b}_{a,k} - \boldsymbol{w}_{a,k} \tag{4.7b}$$

where $\boldsymbol{\Lambda}_g = [\boldsymbol{s}_{g,k}\searrow] + [\boldsymbol{m}_{g,k}\times] + [\boldsymbol{n}_{g,k}*]$ and $\boldsymbol{\Lambda}_a = [\boldsymbol{s}_{a,k}\searrow] + [\boldsymbol{m}_{a,k}\times] + [\boldsymbol{n}_{a,k}*]$ by neglecting second-order terms. Applying the matrix inversion lemma [8],

$$(\boldsymbol{I}_{3\times3} + \boldsymbol{\Lambda})^{-1} = \boldsymbol{I}_{3\times3} - \boldsymbol{\Lambda}(\boldsymbol{I}_{3\times3} + \boldsymbol{\Lambda})^{-1},$$

and iteratively applying the result, the combined mapping for the scale factor, misalignment, and nonorthogonality can be written to first-order in $\boldsymbol{\Lambda}$ as

$$(\boldsymbol{I}_{3\times3} + \boldsymbol{\Lambda})^{-1} \approx \boldsymbol{I}_{3\times3} - \boldsymbol{\Lambda}. \tag{4.8}$$

Applying Equation (4.8) to Equations (4.7), the true incremental angle and non-gravitational velocity may then be expressed as

$$\Delta\boldsymbol{\theta}_k = (\boldsymbol{I}_{3\times3} - [\boldsymbol{s}_{g,k}\searrow] - [\boldsymbol{m}_{g,k}\times] - [\boldsymbol{n}_{g,k}*])\Delta\boldsymbol{\theta}_{m,k} - \boldsymbol{b}_{g,k} - \boldsymbol{w}_{g,k}$$

$$\Delta\boldsymbol{v}_k = (\boldsymbol{I}_{3\times3} - [\boldsymbol{s}_{a,k}\searrow] - [\boldsymbol{m}_{a,k}\times] - [\boldsymbol{n}_{a,k}*])\Delta\boldsymbol{v}_{m,k} - \boldsymbol{b}_{a,k} - \boldsymbol{w}_{a,k}.$$

or, after distributing and rearranging,

$$\Delta\boldsymbol{\theta}_k = \Delta\boldsymbol{\theta}_{m,k} - [\Delta\boldsymbol{\theta}_{m,k}\searrow]\boldsymbol{s}_{g,k} + [\Delta\boldsymbol{\theta}_{m,k}\times]\boldsymbol{m}_{g,k} - [\Delta\boldsymbol{\theta}_{m,k}*]\boldsymbol{n}_{g,k} - \boldsymbol{b}_{g,k} - \boldsymbol{w}_{g,k} \tag{4.10a}$$

$$\Delta\boldsymbol{v}_k = \Delta\boldsymbol{v}_{m,k} - [\Delta\boldsymbol{v}_{m,k}\searrow]\boldsymbol{s}_{a,k} + [\Delta\boldsymbol{v}_{m,k}\times]\boldsymbol{m}_{a,k} - [\Delta\boldsymbol{v}_{m,k}*]\boldsymbol{n}_{a,k} - \boldsymbol{b}_{a,k} - \boldsymbol{w}_{a,k}. \tag{4.10b}$$

Using the models given in Equations (4.10), the propagation of estimation errors can be quantified for implementation within the navigation system architecture.

4.4. CORRECTIONS FOR CONING, SCULLING, AND SCROLLING MOTION

The coning, sculling, and scrolling algorithms inspected within this thesis generate second-order corrections for coning, sculling, and scrolling motion and are based upon the methods discussed by Savage in References [24, 25, 26]. These algorithms, along with many other coning, sculling, and scrolling algorithms, were developed after Bortz presented a differential equation for the integration of the orientation vector, given by [3]

$$\dot{\boldsymbol{\phi}} = \boldsymbol{\omega} + \frac{1}{2}\boldsymbol{\phi} \times \boldsymbol{\omega} + \frac{1}{\phi^2}\left(1 - \frac{\phi \sin \phi}{2(1 - \cos \phi)}\right)\boldsymbol{\phi} \times \boldsymbol{\phi} \times \boldsymbol{\omega}, \tag{4.11}$$

where $\boldsymbol{\phi}$ is the orientation vector and describes the rotation of one frame to another through an angle, $\phi = \|\boldsymbol{\phi}\|$, about an axis pointing in the direction of $\boldsymbol{\phi}$, and $\boldsymbol{\omega}$ is the angular rotation of the body that is inertially measurable by strapdown angular-rate sensors. Equation (4.11) is commonly referred to as the Bortz equation and allows for the exact integration of the orientation vector using measurements from strapdown sensors. Many of the coning algorithms originate from the isolation and approximation of the non-commutative rate vector $\dot{\boldsymbol{\phi}}_{nc}$ in the Bortz equation,

$$\dot{\boldsymbol{\phi}}_{nc} = \frac{1}{2}\boldsymbol{\phi} \times \boldsymbol{\omega} + \frac{1}{\phi^2}\left(1 - \frac{\phi \sin \phi}{2(1 - \cos \phi)}\right)\boldsymbol{\phi} \times \boldsymbol{\phi} \times \boldsymbol{\omega}. \tag{4.12}$$

A common approximation for Equation (4.12) is given by considering the power series expansion for the coefficient of the second term in the non-commutative rate vector, such that

$$\frac{1}{\phi^2}\left(1 - \frac{\phi \sin \phi}{2(1 - \cos \phi)}\right) = \frac{1}{12}\left(1 + \frac{1}{60}\phi^2 + \cdots\right) \approx \frac{1}{12}. \tag{4.13}$$

With the approximation in Equation (4.13), the Bortz equation is approximated as

$$\dot{\boldsymbol{\phi}} \approx \boldsymbol{\omega} + \frac{1}{2}\boldsymbol{\phi} \times \boldsymbol{\omega} + \frac{1}{12}\boldsymbol{\phi} \times (\boldsymbol{\phi} \times \boldsymbol{\omega}). \tag{4.14}$$

The use of Equation (4.14) as an approximation for Equation (4.11) to compensate for coning motion in a two-stage algorithm, which generates the correction at a higher frequency than the state propagation, by Bortz [3] and Jordan [12] laid the foundation for modern coning algorithms. These two-stage approaches perform high frequency, low complexity corrections to the measurements, the results of which are fed into a lower frequency algorithm that produces the state estimates. One of the original two-stage algorithms was proposed by Savage in 1966, which utilizes a first-order equation at a higher frequency to recognize high-frequency vibrations and a second-order attitude update at a lower frequency, providing an efficient and accurate attitude estimate based upon the output of the first-order algorithm [22]. While the two-stage approach was originally introduced because of limited computer capabilities, modern computing capabilities have prompted the desire to return to a single cycle algorithm [24]. However, the algorithms described for most of the two-stage algorithms can also be expanded instead to process a batch of sequential measurements to produce an equivalent, coned measurement at a lower-frequency.

Modern coning, sculling, and scrolling algorithms utilize a mixture of major, minor, and subminor time intervals, as illustrated in Figure 4.1. The subminor interval $[t_{m-1}, t_m]$ describes the time over which discrete inertial measurement unit measurements from a triad of linear accelerometers and gyroscopes are integrated and available, the minor interval $[t_{\ell-1}, t_\ell]$ defines where the high-speed correction algorithms are applied, and the major interval $[t_{k-1}, t_k]$ defines the navigation rate, or the rate at which the state propagation is performed. For the algorithms considered throughout this thesis, the assumption is made that $[t_{m-1}, t_m] = [t_{\ell-1}, t_\ell] \subseteq [t_{k-1}, t_k]$, such that the minor and subminor intervals are equivalent. Therefore, each minor interval within the major interval uses only a single new measurement for subsequent corrections.

The algorithms considered within this thesis perform a generalized form of the corrections, assuming that the quantities vary linearly over the minor interval. Many modern coning correction algorithms have been optimized for error minimization, dependent upon
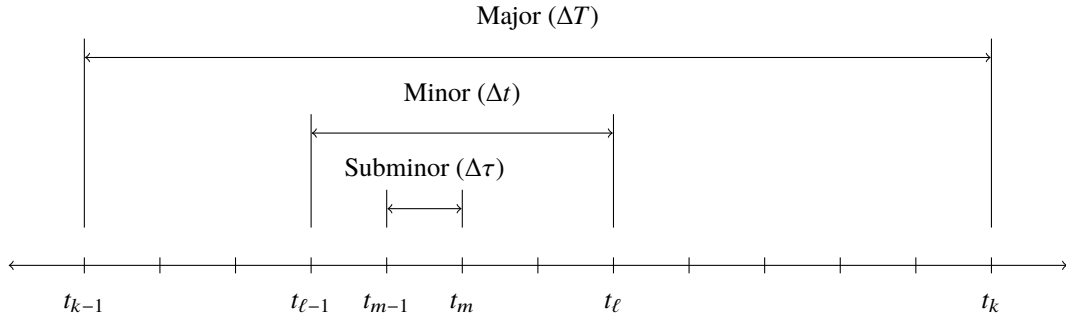
Figure 4.1. Major, minor, and subminor time intervals considered within the INS

the expected environment or intended number of measurements [10, 11, 20, 23]. It is also important to realize that sculling and scrolling algorithm design has seen much less research and development, leading to a significantly smaller body of literature examining their use. By performing an analysis of the error propagation through unoptimized and more simple algorithms, the foundation for analyzing and developing an error propagation architecture for other coning, sculling, and scrolling algorithms used for inertial navigation is established. A detailed derivation of the algorithms is provided by Savage in [24, 25, 26]; as such, the not explicitly derived within this thesis.

4.4.1. A Second-Order Coning Algorithm. Given that the IMU gyroscope measurements are

$$\Delta \boldsymbol{\theta}_n^c = \int_{t_{n-1}}^{t_n} \boldsymbol{\omega}_{c/i}^c(\tau) \mathrm{d}\tau \,,$$

where $\omega_{c/i}^c(\tau)$ is the angular rate of the IMU case frame with respect to the inertial frame, the coning algorithm generates a second-order approximation for the coning motion. Note that the superscript c denotes that the angular velocity is expressed in the case frame of the IMU; this superscript will be implied for the coning elements from hereon, as the frames will be consistent throughout the remainder of the thesis. The coning algorithm can be split into two separate accumulations for the interval $[t_{\ell-1}, t_\ell]$: the measurement and coning

correction accumulations. The measurement accumulation is

$$\boldsymbol{\theta}_\ell = \boldsymbol{\theta}_{\ell-1} + \Delta\boldsymbol{\theta}_\ell = \sum_{i=1}^{\ell} \Delta\boldsymbol{\theta}_i , \qquad (4.15)$$

where $\boldsymbol{\theta}_\ell$ is the accumulation of the measurements; the accumulation of the coning correc-

tions are expressed similarly to Equation (4.15), as

$$\boldsymbol{\beta}_\ell = \boldsymbol{\beta}_{\ell-1} + \Delta\boldsymbol{\beta}_\ell = \sum_{i=1}^{\ell} \Delta\boldsymbol{\beta}_i , \qquad (4.16)$$

where $\Delta\boldsymbol{\beta}_i$ is the coning correction generated at t_i under the assumption of a linearly varying

angular velocity, i.e.

$$\Delta\boldsymbol{\beta}_i = \frac{1}{2}\left[\boldsymbol{\theta}_{i-1} + \frac{1}{6}\Delta\boldsymbol{\theta}_{i-1}\right] \times \Delta\boldsymbol{\theta}_i. \qquad (4.17)$$

Given the accumulations in Equations (4.15) and (4.16), the coned rotation vector, $\Delta\boldsymbol{\phi}_k$, is

the sum of two accumulations, such that

$$\Delta\boldsymbol{\phi}_k = \boldsymbol{\theta}_k + \boldsymbol{\beta}_k , \qquad (4.18)$$

where $\boldsymbol{\theta}_k$ describes the sensed inertial change in the attitude over the $[t_{k-1}, t_k]$ interval and

$\boldsymbol{\beta}_k$ accounts for the non-commutative or unmeasured component due to the coning motion.

At the initialization of the algorithm for any given major interval, the terms from the

previous time-step must be zero ($\Delta\boldsymbol{\theta}_i = \mathbf{0}$ and $\Delta\boldsymbol{\beta}_i = \mathbf{0}$ at $t_i = t_{k-1}$) because no information

is available for the correction on the current attitude-update interval. Additionally, this

algorithm can be used to process any number of measurements, but when $[t_{\ell-1}, t_\ell] = [t_{k-1}, t_k]$

or just a single measurement is processed, the algorithm becomes identical to traditional

methods of dead-reckoning, where only a single IMU measurement is processed for the

attitude update at each step; this statement can be proven by recognizing that with the

initialization of the accumulation variables to zero, $\Delta \boldsymbol{\beta} = \mathbf{0}$. Finally, if the angular velocity vector is constant in direction, there is no coning motion, and the coning correction in each measurement will be zero.

4.4.2. A Second-Order Sculling Algorithm. The velocity integration algorithms correct for errors incurred by the rotation of the IMU frame and the rotation of the velocity vector during the measurement interval $[t_{n-1}, t_n]$. The algorithm uses the incremental velocity measurement from the IMU, a quantification of the non-gravitational specific forces acting on the vehicle given by

$$\Delta \boldsymbol{v}_n^c = \int_{t_{n-1}}^{t_n} \boldsymbol{a}_{ng}^c(\tau) \mathrm{d}\tau.$$

Note that the superscript c denotes the expression of the incremental velocity in the case frame of the IMU; this subscript will also be implied for the sculling elements for the remainder of the thesis. Similar to the accumulation of the measurements in Equation (4.15), the incremental velocity measurements must also be accumulated, such that

$$\boldsymbol{v}_\ell = \boldsymbol{v}_{\ell-1} + \Delta \boldsymbol{v}_\ell = \sum_{i=1}^{\ell} \Delta \boldsymbol{v}_i. \tag{4.19}$$

The non-gravitational incremental velocity can then be separated into three components as

$$\Delta \boldsymbol{v}_{ng,\ell} = \boldsymbol{v}_\ell + \Delta \boldsymbol{v}_{scul,\ell} + \Delta \boldsymbol{v}_{rot,\ell}, \tag{4.20}$$

where $\Delta \boldsymbol{v}_{scul,\ell}$ is the sculling correction and $\Delta \boldsymbol{v}_{rot,\ell}$ is the compensation for the rotation of the velocity vector. The sculling correction is accumulated, such that

$$\Delta \boldsymbol{v}_{scul,\ell} = \Delta \boldsymbol{v}_{scul,\ell-1} + \delta \boldsymbol{v}_{scul,\ell} = \sum_{i=1}^{\ell} \delta \boldsymbol{v}_{scul,i}, \tag{4.21}$$

where the incremental sculling correction is given by

$$\delta v_{scul,i} = \frac{1}{2} \left[\left(\boldsymbol{\theta}_{i-1} + \frac{1}{6} \Delta \boldsymbol{\theta}_{i-1} \right) \times \Delta v_i + \left(v_{i-1} + \frac{1}{6} \Delta v_{i-1} \right) \times \Delta \boldsymbol{\theta}_i \right]. \tag{4.22}$$

The correction due to the rotation of the velocity vector on the interval is given by

$$\Delta v_{rot,\ell} = \frac{1}{2} \left(\boldsymbol{\theta}_\ell \times v_\ell \right), \tag{4.23}$$

where $\boldsymbol{\theta}_\ell$ is the accumulation of the incremental angle measurements as discussed in Section 4.4.1. Equation (4.20) then describes the change in velocity contributed to non-gravitational effects on the body including the rotation of the body and nonlinear contributions of coning and sculling motion.

At the initialization of the algorithm, for any given major interval, the terms from the previous time-step must be zero ($v_i = \mathbf{0}$ and $\Delta v_{scul,i} = \mathbf{0}$ at $t_i = t_{k-1}$) because no information is available for the correction on the current interval. Similarly to the coning algorithm, this algorithm can be used to process any number of measurements, and when $[t_{\ell-1}, t_\ell] = [t_{k-1}, t_k]$, or just a single measurement is processed, the algorithm becomes identical to dead-reckoning at the rate of the IMU; this statement can be proven by recognizing that with the initialization of the accumulation variables to zero, $\Delta v_{scul} = \mathbf{0}$.

4.4.3. A Second-Order Scrolling Algorithm. No additional measurement source is used for the position integration algorithm; the integrated specific force is again integrated to provide the position increment, while the scrolling algorithm corrects for the effects of varying angular rate and specific forces upon the integration. The effects of scrolling can be accounted for in the non-gravitational specific force integration, given by

$$\Delta r_{ng,k} = s_{v,\ell} + \Delta r_{rot,k} + \Delta r_{scrl,\ell}. \tag{4.24}$$

The accumulation of the integrated incremental velocity is defined to be

$$s_{v,\ell} = s_{v,\ell-1} + \Delta s_{v,\ell} = \sum_{i=1}^{\ell} \Delta s_{v,i}, \qquad (4.25)$$

where

$$\Delta s_{v,i} = v_{i-1}\Delta t_{\ell} + \frac{1}{12}\left(5\Delta v_i + \Delta v_{i-1}\right)\Delta t_{\ell} \qquad (4.26)$$

describes the trapezoidal integration of the incremental velocity with $\Delta t_{\ell} = t_{\ell} - t_{\ell-1}$. The rotational component of the scrolling correction is given by

$$\Delta r_{rot,k} = \frac{1}{6}\left(s_{\theta,k} \times v_k + \theta_k \times s_{v,k}\right), \qquad (4.27)$$

with the integrated incremental angle accumulating as

$$s_{\theta,\ell} = s_{\theta,\ell-1} + \Delta s_{\theta,\ell} = \sum_{i=1}^{\ell} \Delta s_{\theta,i},$$

where

$$\Delta s_{\theta,i} = \theta_{i-1}\Delta t_{\ell} + \frac{1}{12}\left(5\Delta\theta_i + \Delta\theta_{i-1}\right)\Delta t_{\ell}.$$

The scrolling correction can be broken can be broken into a component accounting for the effects due to sculling and a component accounting for other higher-order effects. The accumulation of these effects is therefore given by

$$\Delta r_{scrl,i} = \Delta r_{scrl,i-1} + \delta r_{scrl/scul,i} + \delta r_{scrl/other,i}, \qquad (4.28)$$

where the scrolling correction contributed by sculling is

$$\delta \boldsymbol{r}_{scrl/scul,i} = \Delta \boldsymbol{v}_{scul,i-1} \Delta t_\ell + \frac{1}{2} \left[\boldsymbol{\theta}_{i-1} - \frac{1}{12} (\Delta \boldsymbol{\theta}_i - \Delta \boldsymbol{\theta}_{i-1}) \right] \times \left(\Delta \boldsymbol{s}_{v,i} - \boldsymbol{v}_{i-1} \Delta t_\ell \right) \tag{4.29}$$

$$+ \frac{1}{2} \left[\boldsymbol{v}_{i-1} - \frac{1}{12} (\Delta \boldsymbol{v}_i - \Delta \boldsymbol{v}_{i-1}) \right] \times \left(\Delta \boldsymbol{s}_{\theta,i} - \boldsymbol{\theta}_{i-1} \Delta t_\ell \right) \tag{4.30}$$

and the correction for the other higher-order effects is

$$\delta \boldsymbol{r}_{scrl/other,i} = \frac{1}{6} \left[\boldsymbol{s}_{v,i-1} + \frac{\Delta t_\ell}{24} (\Delta \boldsymbol{v}_i - \Delta \boldsymbol{v}_{i-1}) \right] \times \Delta \boldsymbol{\theta}_i - \frac{1}{6} \left[\boldsymbol{s}_{\theta,i-1} + \frac{\Delta t_\ell}{24} (\Delta \boldsymbol{\theta}_i - \Delta \boldsymbol{\theta}_{i-1}) \right] \times \Delta \boldsymbol{v}_i$$

$$+ \frac{\Delta t_\ell}{6} \left[\boldsymbol{\theta}_{i-1} - \frac{1}{6} (\Delta \boldsymbol{\theta}_i - \Delta \boldsymbol{\theta}_{i-1}) \right] \times \left[\boldsymbol{v}_{i-1} - \frac{1}{6} (\Delta \boldsymbol{v}_i - \Delta \boldsymbol{v}_{i-1}) \right]$$

$$- \frac{\Delta t_\ell}{2160} (\Delta \boldsymbol{\theta}_i - \Delta \boldsymbol{\theta}_{i-1}) \times (\Delta \boldsymbol{v}_i - \Delta \boldsymbol{v}_{i-1}). \tag{4.31}$$

Similar to the coning and sculling algorithms, each term from the previous cycle must be initialized to zero ($\boldsymbol{s}_{\theta,i} = \boldsymbol{0}$, $\boldsymbol{s}_{v,i} = \boldsymbol{0}$, $\boldsymbol{\theta}_i = \boldsymbol{0}$, $\Delta \boldsymbol{\theta}_i = \boldsymbol{0}$, $\boldsymbol{v}_i = \boldsymbol{0}$ and $\Delta \boldsymbol{v}_i = \boldsymbol{0}$ at $t_i = t_{k-1}$) because no information is available for the correction on the current interval. Additionally, this algorithm can be used to process any number of measurements. When just a single measurement is processed, i.e. $[t_{\ell-1}, t_\ell] = [t_{k-1}, t_k]$, the algorithm becomes identical to traditional dead-reckoning at the rate of the IMU; this statement can be proven by recognizing that with the initialization of the accumulation variables to zero, $\Delta \boldsymbol{r}_{scrl} = \boldsymbol{0}$.

4.5. INTEGRATING THE CONING, SCULLING, AND SCROLLING CORREC-TIONS

Through the application of coning, sculling, and scrolling algorithms within an inertial navigation system, non-gravitational increments for the vehicle's position, velocity, and total rotation for the vehicle are generated using ℓ measurements obtained between t_{k-1} and t_k. The corrections generated for the assumed linearly time-varying rotation and velocity are incorporated to correct for the assumptions made within the development of the discretized dynamics in Equations (4.3), i.e. that the vehicle's angular velocity and velocity

vectors are approximately constant with a small time step. Incorporating the corrected quantities, propagation of the vehicle's position, velocity, and attitude can be restated as

$$
\begin{aligned}
\boldsymbol{r}^i_{c,k} =&\, \boldsymbol{r}^i_{c,k-1} + \boldsymbol{v}^i_{c,k-1}\Delta t_k + \boldsymbol{T}^i_{c,k-1}\Delta \boldsymbol{r}_{ng,k} \\
&+ \frac{1}{2}\left(\boldsymbol{g}_{k-1} - \frac{1}{3}\boldsymbol{G}_{k-1}\boldsymbol{T}^i_{c,k-1}\left[\boldsymbol{r}^c_{cg/c,k-1}\times\right]\Delta \boldsymbol{\phi}_k\right)\Delta t_k^2 \\
\boldsymbol{v}^i_{c,k} =&\, \boldsymbol{v}^i_{c,k-1} + \left(\boldsymbol{g}_{k-1} - \frac{1}{2}\boldsymbol{G}_{k-1}\boldsymbol{T}^i_{c,k-1}\left[\boldsymbol{r}^c_{cg/c,k-1}\times\right]\Delta \boldsymbol{\phi}_k\right)\Delta t_k + \boldsymbol{T}^i_{c,k-1}\Delta \boldsymbol{v}_{ng,k} \\
\bar{\boldsymbol{q}}^c_{i,k} =&\, \bar{\boldsymbol{q}}(\Delta \boldsymbol{\phi}_k) \otimes \bar{\boldsymbol{q}}^c_{i,k-1},
\end{aligned}
$$

where the non-gravitational changes in position $\Delta \boldsymbol{r}_{ng,k}$ and velocity $\Delta \boldsymbol{v}_{ng,k}$ are described by Equations (4.24) and Equations (4.20), respectively, while the coned rotational increment $\boldsymbol{\phi}_k$ is described by Equation (4.18). Additionally, to simplify the notation, vectors described the case frame and expressed within the inertial frame will no longer contain an i superscript or i subscript; while the transformation matrix $\boldsymbol{T}^i_{c,k-1}$ is then expressed as $\boldsymbol{T}^T_{k-1}$, such that $\boldsymbol{T}_{k-1}$ describes the transformation from the inertial to the case frame. The discretized dynamics for a vehicle aided by a strapdown sensor and employing coning, sculling, and scrolling corrections, are given by

$$
\boldsymbol{r}_k = \boldsymbol{r}_{k-1} + \boldsymbol{v}_{k-1}\Delta t_k + \boldsymbol{T}^T_{k-1}\Delta \boldsymbol{r}_{ng,k} + \frac{1}{2}\left(\boldsymbol{g}_{k-1} - \frac{1}{3}\boldsymbol{G}_{k-1}\boldsymbol{T}^T_{k-1}\left[\boldsymbol{r}_{cg/c,k-1}\times\right]\Delta \boldsymbol{\phi}_k\right)\Delta t_k^2 \tag{4.33a}
$$

$$
\boldsymbol{v}_k = \boldsymbol{v}_{k-1} + \boldsymbol{T}^T_{k-1}\Delta \boldsymbol{v}_{ng,k} + \left(\boldsymbol{g}_{k-1} - \frac{1}{2}\boldsymbol{G}_{k-1}\boldsymbol{T}^T_{k-1}\left[\boldsymbol{r}_{cg/c,k-1}\times\right]\Delta \boldsymbol{\phi}_k\right)\Delta t_k \tag{4.33b}
$$

$$
\bar{\boldsymbol{q}}_k = \bar{\boldsymbol{q}}(\Delta \boldsymbol{\phi}_k) \otimes \bar{\boldsymbol{q}}_{k-1}. \tag{4.33c}
$$

5. PROPAGATION OF ERRORS THROUGH INERTIAL NAVIGATION CORRECTIONS

Predictions of position, velocity, and attitude often rely upon incremental angle and velocity measurements to describe the effects of non-gravitational forces and rotations on the vehicle's state evolution, as observed in Section 4.2. However, if these measurements are corrupted by error sources, the state estimate will incur an associated error. Unfortunately, inertial measurements are often susceptible to a multitude of error sources resulting from a variety of manufacturing defects and complications due to hardware or software interactions. In general, a distribution and time-evolution for each possible error source is empirically derived and provided by sensor manufacturers. Given the manufacturer specifications and a model that describes the effect of common strapdown sensor error sources on the measurement, an expression for the uncertainty propagated into the measurement, from each error source, and thus into the state estimate, can be determined. Additionally, if these error sources or parameters are known to exist and an estimate for their manifestation is available, the associated error contributions can be rectified. However, even if an estimate is available, a level of uncertainty is likely to exist. Using the expression describing the propagation of errors into the state estimate from the measurements, contributions to the state uncertainty by the uncertainty in the estimated parameters can also be described.

Through the application of the coning, sculling, and scrolling algorithms presented in Section 4.4, incremental angle and velocity measurements obtained at a high frequency are used to generate corrections for higher-order effects not directly realized in the measurements. These corrections, in conjunction with the accumulated incremental angle and velocity, are used for state propagation, as seen in Equations (4.33). If the incremental angle and velocity measurements are corrupted by measurement errors, those errors will propagate into the state estimate and contribute to the state estimation error. Therefore, to

rigorously describe the propagation of errors into the state estimate from the measurement error itself, a description for the transformation of these measurement errors through the coning, sculling, and sculling corrections must be determined. The state uncertainty contributed by the coning, sculling, and scrolling corrections can be determined given the error propagation for each of the algorithms.

Throughout Section 5, an accounting of the errors in strapdown sensor measurements and their propagation through the coning, sculling, and scrolling algorithms are derived in detail. In Section 5.1, the general methodology for the development of the algorithms is expanded upon. A model used for IMU gyros and accelerometers is presented in Section 5.2, while Sections 5.3 – 5.5 derive and present the mappings of errors through the coning, sculling, and scrolling algorithms presented in Section 4.4. Section 5.6 develops the error dynamics for position, velocity, and attitude when applying coning, sculling, and scrolling algorithms, while Section 5.7 expresses these errors in terms of typically estimated strapdown sensor error sources. Finally, Section 5.8 explains the propagation of covariance in terms of the derived error dynamics.

5.1. METHODOLOGY FOR ERROR PROPAGATION DEVELOPMENT

To determine how the error propagates through the coning, sculling, and scrolling algorithms contained within Section 4.4, the propagation of measurement errors through each correction term is examined. To determine this propagation, consider the error definition as in Equation (3.12); therefore the error in each term is expressed as the difference between the true and estimated quantities. Additionally, as seen in Equation (4.18), Equation (4.20), and Equation (4.24), the output of each algorithm can be expressed as a function of the measurement accumulation and the correction terms, while the error dynamics for covariance propagation must be expressed as a function of the estimate and the error in each quantity. To aid in this development, the result of each algorithm is broken into smaller components and recombined to develop the full error dynamics for a given correction.

For example, to determine the error in the coned measurement, it can simply be recast as functions of the accumulated incremental angle and coning correction errors such that

$$e_{\Delta\phi,k} = e_{\theta,k} + e_{\beta,k}. \tag{5.1}$$

Noting that the coning correction is a function of the measurements, it is then easy to notice that $e_{\theta,k}$ and $e_{\beta,k}$ can be independently expressed as a function of the measurement errors $e_{\Delta\theta,i}$ $\forall i = 1, 2, \ldots \ell$ as

$$e_{\theta,k} = f(e_{\Delta\theta,i}) \qquad \text{and} \qquad e_{\beta,k} = g(e_{\Delta\theta,i}), \tag{5.2}$$

where f and g are taken to be independent functions that describe the propagation of measurement errors into the accumulated incremental angle and coning correction vectors, respectively. Therefore, after developing these expressions, the error in the coned measurement can be written as a function of the measurement errors.

However, given that inertial sensor errors are often estimated, the measurements are generally corrected for these errors prior to the measurements' use in coning correction. Therefore, the measurement errors can be expressed as a function of the estimation error in each of these error sources for an inertial sensor. An error mapping can then be developed through recursive application of these techniques, generating the mapping for each error term through the corrections. After developing a mapping of the estimation errors through the algorithms, a slight simplification can be made to each by assuming that some of the error sources are approximately constant over a single major interval. The error dynamics for the state estimate can then be written as a function of the error in each measurement, as generated by the coning, sculling, and scrolling algorithms.

Finally, it is worth noting that some assumptions are made that simplify the development of the error propagation throughout the development of the error propagation. First and foremost, it is assumed that many of the errors are constant over a major interval; while this may not be true, it allows for the simplification of the methods examined. Usually the major interval is small with respect to the rate at which the error grows, allowing the assumption of negligible variability over the major time interval. The second assumption states that the time between measurements is fixed; this assumption can be difficult to achieve in system implementation, especially when considering low-cost hardware with less reliable measurement capabilities. Each of these assumptions can be relaxed, though this relaxation is not explored within the following sections and may be a topic of investigation for future work.

5.2. STRAPDOWN MEASUREMENT ERROR PROPAGATION

Given an estimate $\hat{\boldsymbol{y}}$ of an error source $\boldsymbol{y}$, the expected value of the incremental angle, $\mathrm{E}\{\Delta\boldsymbol{\theta}_k\}$ or $\Delta\hat{\boldsymbol{\theta}}_k$, and the incremental velocity, $\mathrm{E}\{\Delta\boldsymbol{v}_k\}$ or $\Delta\hat{\boldsymbol{v}}_k$, is, assuming Equations (4.10) hold, simply

$$\Delta\hat{\boldsymbol{\theta}}_k = \Delta\boldsymbol{\theta}_{m,k} - [\Delta\boldsymbol{\theta}_{m,k}\diagdown]\hat{\boldsymbol{s}}_{g,k} + [\Delta\boldsymbol{\theta}_{m,k}\times]\hat{\boldsymbol{m}}_{g,k} - [\Delta\boldsymbol{\theta}_{m,k}*]\hat{\boldsymbol{n}}_{g,k} - \hat{\boldsymbol{b}}_{g,k} \tag{5.3a}$$

$$\Delta\hat{\boldsymbol{v}}_k = \Delta\boldsymbol{v}_{m,k} - [\Delta\boldsymbol{v}_{m,k}\diagdown]\hat{\boldsymbol{s}}_{a,k} + [\Delta\boldsymbol{v}_{m,k}\times]\hat{\boldsymbol{m}}_{a,k} - [\Delta\boldsymbol{v}_{m,k}*]\hat{\boldsymbol{n}}_{a,k} - \hat{\boldsymbol{b}}_{a,k}, \tag{5.3b}$$

where $\hat{\boldsymbol{b}}_{g,k}$, $\hat{\boldsymbol{s}}_{g,k}$, $\hat{\boldsymbol{n}}_{g,k}$, and $\hat{\boldsymbol{m}}_{g,k}$ are the estimated bias, scale factor, nonorthogonality, and misalignment in the gyroscope measurements, respectively, and $\hat{\boldsymbol{b}}_{a,k}$, $\hat{\boldsymbol{s}}_{a,k}$, $\hat{\boldsymbol{n}}_{a,k}$, and $\hat{\boldsymbol{m}}_{a,k}$ are the estimated or expected bias, scale factor, nonorthogonality, and misalignment in the accelerometer measurements, respectively. Note that the noise is defined to be zero-mean and the expected value is, therefore, zero. By subtracting Equations (5.3) from

Equations (4.10) and simplifying, the error in the measurements can be expressed as

$$
\begin{aligned}
\boldsymbol{e}_{\Delta\theta,k} &= \Delta\boldsymbol{\theta}_k - \Delta\hat{\boldsymbol{\theta}}_k \\
&= -[\Delta\boldsymbol{\theta}_{m,k}\diagdown]\boldsymbol{e}_{s_g,k} + [\Delta\boldsymbol{\theta}_{m,k}\times]\boldsymbol{e}_{m_g,k} - [\Delta\boldsymbol{\theta}_{m,k}*]\boldsymbol{e}_{n_g,k} - \boldsymbol{e}_{b_g,k} - \boldsymbol{w}_{g,k} \qquad (5.4a)
\end{aligned}
$$

$$
\begin{aligned}
\boldsymbol{e}_{\Delta v,k} &= \Delta\boldsymbol{v}_k - \Delta\hat{\boldsymbol{v}}_k \\
&= -[\Delta\boldsymbol{v}_{m,k}\diagdown]\boldsymbol{e}_{s_a,k} + [\Delta\boldsymbol{v}_{m,k}\times]\boldsymbol{e}_{m_a,k} - [\Delta\boldsymbol{v}_{m,k}*]\boldsymbol{e}_{n_a,k} - \boldsymbol{e}_{b_a,k} - \boldsymbol{w}_{a,k}, \qquad (5.4b)
\end{aligned}
$$

where the errors in the bias, scale-factor, misalignment, and nonorthogonality estimates for the gyroscopes are defined to be

$$
\boldsymbol{e}_{b_g,k} \overset{\Delta}{=} \boldsymbol{b}_{g,k} - \hat{\boldsymbol{b}}_{g,k}, \quad \boldsymbol{e}_{s_g,k} \overset{\Delta}{=} \boldsymbol{s}_{g,k} - \hat{\boldsymbol{s}}_{g,k}, \quad \boldsymbol{e}_{m_g,k} \overset{\Delta}{=} \boldsymbol{m}_{g,k} - \hat{\boldsymbol{m}}_{g,k}, \quad \text{and} \quad \boldsymbol{e}_{n_g,k} \overset{\Delta}{=} \boldsymbol{n}_{g,k} - \hat{\boldsymbol{n}}_{g,k},
$$

respectively, and, similarly, the error in the bias, scale-factor, misalignment, and nonorthogonality estimates for the accelerometers are

$$
\boldsymbol{e}_{b_a,k} \overset{\Delta}{=} \boldsymbol{b}_{a,k} - \hat{\boldsymbol{b}}_{a,k}, \quad \boldsymbol{e}_{s_a,k} \overset{\Delta}{=} \boldsymbol{s}_{a,k} - \hat{\boldsymbol{s}}_{a,k}, \quad \boldsymbol{e}_{m_a,k} \overset{\Delta}{=} \boldsymbol{m}_{a,k} - \hat{\boldsymbol{m}}_{a,k}, \quad \text{and} \quad \boldsymbol{e}_{n_a,k} \overset{\Delta}{=} \boldsymbol{n}_{a,k} - \hat{\boldsymbol{n}}_{a,k},
$$

respectively.

5.3. CONING ALGORITHM ERROR PROPAGATION

By performing the coning correction, the raw measurements are corrected to better represent the true dynamics of the body's rotation. However, when considering the propagation of errors through the coning correction, it is clear that if the manufacturer-provided performance specifications are for the raw measurements, then the statistics will be inconsistent with the output of the coning algorithm since the statistics lack any contributions resulting from the coning correction. To have an accurate uncertainty representation, the navigation filter's covariance prediction requires an accounting of these errors and their

propagation through the coning correction. Some manufacturers of inertial sensors report a measurement that has already been corrected for the effects of coning, prior to communicating the measurement; it is again unclear what performance measures and statistics are truly applicable to the result when this is done. In both cases, by examining the coning correction term and the error mapping through it, the alterations to common navigation architectures are found to be minimal.

To determine how the error propagates through the coning algorithm, the errors in each measurement and the correlations introduced by the coning correction must be examined further. As given in Equation (5.1), the error in the coned measurement, the result of the coning algorithm, is the sum of the error in the accumulated measurement and coning correction terms; the error in each of these terms is considered separately in the following sections. After developing a mapping of the measurement error through the coning algorithm, a slight simplification is made by assuming that several error sources are approximately constant over a single major interval.

5.3.1. Error in the Accumulated Measurements. The first term in Equation (5.1) contains the errors introduced by the accumulation of the measurements. To stay consistent with the error definition in Equation (3.12), define the error in the measurement accumulation and the measurement to be

$$\boldsymbol{e}_{\theta,\ell} \overset{\Delta}{=} \boldsymbol{\theta}_\ell - \hat{\boldsymbol{\theta}}_\ell \quad \text{and} \quad \boldsymbol{e}_{\Delta\theta,i} \overset{\Delta}{=} \Delta\boldsymbol{\theta}_i - \Delta\hat{\boldsymbol{\theta}}_i, \tag{5.5}$$

respectively, where $\boldsymbol{\theta}_\ell$ is the true rotation vector over the major interval, $\hat{\boldsymbol{\theta}}_\ell$ is the estimated rotation vector, $\Delta\hat{\boldsymbol{\theta}}_i$ is the estimated incremental angle vector at t_i over the minor interval, and $\Delta\boldsymbol{\theta}_i$ is the true incremental angle vector. Similar to how the measurement accumulation is expressed as a sum of the measurements in Equation (4.15), the errors can also be expressed as a sum of the errors in each measurement. By deconstructing $\boldsymbol{e}_{\theta,\ell}$ and applying

the definitions in Equations (4.15) and (5.5), the error is given by

$$\boldsymbol{e}_{\theta,\ell} = \boldsymbol{\theta}_\ell - \hat{\boldsymbol{\theta}}_\ell = (\boldsymbol{\theta}_{\ell-1} + \Delta\boldsymbol{\theta}_\ell) - (\hat{\boldsymbol{\theta}}_{\ell-1} + \Delta\hat{\boldsymbol{\theta}}_\ell).$$

Therefore the accumulation is simply a sum of the errors in the last measurement and the previous accumulation, such that

$$\boldsymbol{e}_{\theta,\ell} = (\boldsymbol{\theta}_{\ell-1} - \hat{\boldsymbol{\theta}}_{\ell-1}) + (\Delta\boldsymbol{\theta}_\ell - \Delta\hat{\boldsymbol{\theta}}_\ell) = \boldsymbol{e}_{\theta,\ell-1} + \boldsymbol{e}_{\Delta\theta,\ell},$$

from which it follows that the error in the measurement accumulation is simply the summation of errors in the individual measurements, i.e.

$$\boldsymbol{e}_{\theta,\ell} = \sum_{i=1}^{\ell} \boldsymbol{e}_{\Delta\theta,i}. \tag{5.6}$$

5.3.2. Error in the Accumulated Coning Correction. The development for the second term in Equation (5.1) is more involved, as it accumulates the error generated through the coning correction term. The error in the coning correction term and its accumulation are defined as

$$\boldsymbol{e}_{\Delta\beta,i} \triangleq \Delta\boldsymbol{\beta}_i - \Delta\hat{\boldsymbol{\beta}}_i \quad \text{and} \quad \boldsymbol{e}_{\beta,\ell} \triangleq \boldsymbol{\beta}_\ell - \hat{\boldsymbol{\beta}}_\ell, \tag{5.7}$$

where $\boldsymbol{\beta}_\ell$ is the true coning correction over the major interval, $\hat{\boldsymbol{\beta}}_\ell$ is the estimated coning correction, $\Delta\hat{\boldsymbol{\beta}}_i$ is the estimated coning correction at t_i over the minor interval, and $\Delta\boldsymbol{\beta}_i$ is the true coning correction. The error in the accumulated coning correction terms can then be expressed as a sum of the errors in each coning correction term $\boldsymbol{e}_{\Delta\beta,i}$, i.e.

$$\boldsymbol{e}_{\beta,\ell} = \sum_{i=1}^{\ell} \boldsymbol{e}_{\Delta\beta,i}. \tag{5.8}$$

Examining the coning correction term defined in Equation (4.17), it is clear that the coning correction is dependent upon the measurements. Therefore, the error in the coning correction is dependent upon the measurement errors. Equation (4.17) can be substituted for each term in Equation (5.7) to define the coning correction $e_{\Delta\beta,i}$ in terms of the true and estimated incremental angle, given by

$$e_{\Delta\beta,i} = \left(\frac{1}{2}\left[\boldsymbol{\theta}_{i-1} + \frac{1}{6}\Delta\boldsymbol{\theta}_{i-1}\right] \times \Delta\boldsymbol{\theta}_i\right) - \left(\frac{1}{2}\left[\hat{\boldsymbol{\theta}}_{i-1} + \frac{1}{6}\Delta\hat{\boldsymbol{\theta}}_{i-1}\right] \times \Delta\hat{\boldsymbol{\theta}}_i\right). \tag{5.9}$$

From Equation (5.9), the cross-products can be distributed, providing

$$e_{\Delta\beta,i} = \frac{1}{2}\left[\left(\boldsymbol{\theta}_{i-1} \times \Delta\boldsymbol{\theta}_i + \frac{1}{6}\Delta\boldsymbol{\theta}_{i-1} \times \Delta\boldsymbol{\theta}_i\right) - \left(\hat{\boldsymbol{\theta}}_{i-1} \times \Delta\hat{\boldsymbol{\theta}}_i + \frac{1}{6}\Delta\hat{\boldsymbol{\theta}}_{i-1} \times \Delta\hat{\boldsymbol{\theta}}_i\right)\right].$$

Using the definitions in Equation (5.5), $\boldsymbol{\theta}_i$ and $\Delta\boldsymbol{\theta}_i$ can be rewritten in terms of the estimates and the estimation errors, resulting in

$$e_{\Delta\beta,i} = \frac{1}{2}\left[\left(\hat{\boldsymbol{\theta}}_{i-1} + \boldsymbol{e}_{\theta,i-1}\right) \times \left(\Delta\hat{\boldsymbol{\theta}}_i + \boldsymbol{e}_{\Delta\theta,i}\right) + \frac{1}{6}\left(\Delta\hat{\boldsymbol{\theta}}_{i-1} + \boldsymbol{e}_{\Delta\theta,i-1}\right) \times \left(\Delta\hat{\boldsymbol{\theta}}_i + \boldsymbol{e}_{\Delta\theta,i}\right)\right]$$
$$- \frac{1}{2}\left(\hat{\boldsymbol{\theta}}_{i-1} \times \Delta\hat{\boldsymbol{\theta}}_i + \frac{1}{6}\Delta\hat{\boldsymbol{\theta}}_{i-1} \times \Delta\hat{\boldsymbol{\theta}}_i\right).$$

Distributing the cross-products once again, $e_{\Delta\beta,i}$ can be expressed as

$$e_{\Delta\beta,i} = \frac{1}{2}\left(\hat{\boldsymbol{\theta}}_{i-1} \times \Delta\hat{\boldsymbol{\theta}}_i + \hat{\boldsymbol{\theta}}_{i-1} \times \boldsymbol{e}_{\Delta\theta,i} + \boldsymbol{e}_{\theta,i-1} \times \Delta\hat{\boldsymbol{\theta}}_i\right) - \frac{1}{2}\hat{\boldsymbol{\theta}}_{i-1} \times \Delta\hat{\boldsymbol{\theta}}_i$$
$$+ \frac{1}{12}\left(\Delta\hat{\boldsymbol{\theta}}_{i-1} \times \Delta\hat{\boldsymbol{\theta}}_i + \Delta\hat{\boldsymbol{\theta}}_{i-1} \times \boldsymbol{e}_{\Delta\theta,i} + \boldsymbol{e}_{\Delta\theta,i-1} \times \Delta\hat{\boldsymbol{\theta}}_i\right) - \frac{1}{12}\Delta\hat{\boldsymbol{\theta}}_{i-1} \times \Delta\hat{\boldsymbol{\theta}}_i,$$

and recognizing that several terms cancel, it follows that

$$e_{\Delta\beta,i} = \frac{1}{2}\left(\hat{\boldsymbol{\theta}}_{i-1} \times \boldsymbol{e}_{\Delta\theta,i} + \boldsymbol{e}_{\theta,i-1} \times \Delta\hat{\boldsymbol{\theta}}_i\right) + \frac{1}{12}\left(\Delta\hat{\boldsymbol{\theta}}_{i-1} \times \boldsymbol{e}_{\Delta\theta,i} + \boldsymbol{e}_{\Delta\theta,i-1} \times \Delta\hat{\boldsymbol{\theta}}_i\right). \tag{5.10}$$

Using the cross-product relationship $\boldsymbol{a} \times \boldsymbol{b} = -\boldsymbol{b} \times \boldsymbol{a}$, Equation (5.10) becomes

$$\boldsymbol{e}_{\Delta\beta,i} = \frac{1}{2}\left(\hat{\boldsymbol{\theta}}_{i-1} \times \boldsymbol{e}_{\Delta\theta,i} - \Delta\hat{\boldsymbol{\theta}}_i \times \boldsymbol{e}_{\theta,i-1}\right) + \frac{1}{12}\left(\Delta\hat{\boldsymbol{\theta}}_{i-1} \times \boldsymbol{e}_{\Delta\theta,i} - \Delta\hat{\boldsymbol{\theta}}_i \times \boldsymbol{e}_{\Delta\theta,i-1}\right).$$

Replacing each cross product term with the skew-symmetric cross-product matrix and combining terms, the error in the coning correction as a function of the accumulated and individual measurement errors is determined to be

$$\boldsymbol{e}_{\Delta\beta,i} = \left(\frac{1}{2}[\hat{\boldsymbol{\theta}}_{i-1}\times] + \frac{1}{12}[\Delta\hat{\boldsymbol{\theta}}_{i-1}\times]\right)\boldsymbol{e}_{\Delta\theta,i} - [\Delta\hat{\boldsymbol{\theta}}_i\times]\left(\frac{1}{2}\boldsymbol{e}_{\theta,i-1} + \frac{1}{12}\boldsymbol{e}_{\Delta\theta,i-1}\right). \tag{5.11}$$

By combining Equations (5.8) and (5.11), the accumulated error due to the coning correction term is then expressed as

$$\boldsymbol{e}_{\beta,\ell} = \sum_{i=1}^{\ell}\left[\left(\frac{1}{2}[\hat{\boldsymbol{\theta}}_{i-1}\times] + \frac{1}{12}[\Delta\hat{\boldsymbol{\theta}}_{i-1}\times]\right)\boldsymbol{e}_{\Delta\theta,i} - [\Delta\hat{\boldsymbol{\theta}}_i\times]\left(\frac{1}{2}\boldsymbol{e}_{\theta,i-1} + \frac{1}{12}\boldsymbol{e}_{\Delta\theta,i-1}\right)\right]. \tag{5.12}$$

5.3.3. Combined Propagation of Errors. A representation for the estimation error propagation through the coning algorithm can be developed from the results in Equations (5.6) and (5.12). Initially, consider these errors to be separated into two components: the measurement error accumulation and coning correction error accumulation, where the measurement error accumulation is defined in Equation (5.6). Inspecting the coning correction accumulation error in Equation (5.12) and expanding for a variable number of measurements, the errors can be shown to accumulate such that

$$\boldsymbol{e}_{\beta,\ell} = \sum_{i=1}^{\ell}\boldsymbol{\Xi}_{con,i}\boldsymbol{e}_{\Delta\theta,i}, \tag{5.13}$$

where $\boldsymbol{\Xi}_{con,i} \overset{\Delta}{=} [\boldsymbol{\xi}_{con,i} \times]$ and

$$\boldsymbol{\xi}_{con,i} \overset{\Delta}{=} \frac{1}{2} \left[\sum_{j=1}^{i-1} \Delta\hat{\boldsymbol{\theta}}_j - \sum_{j=i+1}^{\ell} \Delta\hat{\boldsymbol{\theta}}_j \right] - \frac{1}{12} \left(\Delta\hat{\boldsymbol{\theta}}_{i+1} - \Delta\hat{\boldsymbol{\theta}}_{i-1} \right). \qquad (5.14)$$

With Equation (5.14), it can be shown that the error in the ith coning correction term will not be correlated to the errors in the ith measurement, but only to those prior to and following its processing. Additionally, if $i + 1 \geq \ell$ or $i - 1 \leq 0$, then $\Delta\hat{\boldsymbol{\theta}}_{i+1} = \mathbf{0}$ or $\Delta\hat{\boldsymbol{\theta}}_{i-1} = \mathbf{0}$, respectively. To generate $\boldsymbol{\xi}_{con,i}$ as stated in Equation (5.14), the entire array of ℓ measurements must be known; fortunately, this can be restated so that the error terms can be accumulated in a navigation preprocessor algorithm, much like the coning algorithm itself.

By combining the measurement error accumulation in Equation (5.6) and coning correction error accumulation in Equation (5.13), the error in the coned equivalent measurement is given by

$$\boldsymbol{e}_{\Delta\phi} = \sum_{i=1}^{\ell} \left(\boldsymbol{e}_{\Delta\theta,i} + \boldsymbol{\Xi}_{con,i} \boldsymbol{e}_{\Delta\theta,i} \right) = \sum_{i=1}^{\ell} \left(\boldsymbol{I}_{3\times3} + \boldsymbol{\Xi}_{con,i} \right) \boldsymbol{e}_{\Delta\theta,i}. \qquad (5.15)$$

Equation (5.15) describes the propagation of measurement and estimation errors through the coning algorithm into the coned measurement accumulation. Employing a model for IMU measurements, an accounting of the uncertainty in the system due to the estimation and measurement errors can be developed for a particular navigation system that relies upon a coning algorithm.

5.4. SCULLING ALGORITHM ERROR PROPAGATION

Through the application of a sculling algorithm, a correction for the measured non-gravitational motion and its integration into the vehicle's velocity is made using the incremental angle and velocity measurements over the major interval. Whereas the coning correction's application alters the measurement statistics for the incremental angle, the

sculling correction affects the those for the incremental velocity. Noting the equation governing the sculling-corrected non-gravitational term in Equation (4.20), the error can be written as a sum of errors in each of the components, i.e.

$$e_{\Delta v_{ng},\ell} = e_{v,\ell} + e_{\Delta v_{scul},\ell} + e_{\Delta v_{rot},\ell}, \tag{5.16}$$

where $e_{v,\ell}$ is the error in the incremental angle accumulation, $e_{\Delta v_{scul},\ell}$ is the error in the sculling correction, and $e_{\Delta v_{rot},\ell}$ is the error in correction for the vehicle's rotation during the measurement accumulation. Sections 5.4.1 – 5.4.3 derive the mappings of the measurement error through each of these terms, respectively.

5.4.1. Error in the Incremental Velocity Accumulation. The error in the incremental velocity vector and its accumulation can be expressed such that

$$e_{v,\ell} \triangleq v_\ell - \hat{v}_\ell \quad \text{and} \quad e_{\Delta v,i} \triangleq \Delta v_i - \Delta \hat{v}_i, \tag{5.17}$$

where v_ℓ and $\hat{v}_\ell$ are the true and estimated accumulated velocity vector over the major interval, respectively, Δv_i and $\Delta \hat{v}_i$ are the true and estimated incremental velocity vector at t_i, over the minor interval $[t_{i-1}, t_i]$, respectively. By the definition of the velocity accumulation in Equation (4.19) and the definition of the error in Equation (5.17), the error in the accumulation can be expressed as

$$e_{v,\ell} = (v_{\ell-1} + \Delta v_\ell) - (\hat{v}_{\ell-1} + \Delta \hat{v}_\ell)$$

$$= (v_{\ell-1} - \hat{v}_{\ell-1}) + (\Delta v_\ell - \Delta \hat{v}_\ell)$$

$$= e_{v_{\ell-1}} + e_{\Delta v,\ell}.$$

Recursively applying the definitions in Equation (5.17), the error in the accumulation is simply a sum of the measurement errors, or

$$\boldsymbol{e}_{v,\ell} = \sum_{i=1}^{\ell} \boldsymbol{e}_{\Delta v,i}. \tag{5.18}$$

5.4.2. Error in the Sculling Correction. To determine the error in the sculling correction, first recognize that the sculling correction is a sum of the incremental sculling corrections, as shown in Equation (4.21), where the increments are defined by Equation (4.22). Therefore, in order to determine the error in the sculling correction, the error in the increments must first be determined. Define the error in the sculling increment $\boldsymbol{e}_{\delta v_{scul,i}}$ such that

$$\boldsymbol{e}_{\delta v_{scul,i}} = \delta \boldsymbol{v}_{scul,i} - \delta \hat{\boldsymbol{v}}_{scul,i}, \tag{5.19}$$

and substitute for the definition of $\boldsymbol{e}_{\delta v_{scul,i}}$ composed with the true and estimated measurements and their accumulation, yielding

$$\boldsymbol{e}_{\delta v_{scul,i}} = \frac{1}{2}\left[\left(\boldsymbol{\theta}_{i-1} + \frac{1}{6}\Delta\boldsymbol{\theta}_{i-1}\right) \times \Delta\boldsymbol{v}_i + \left(\boldsymbol{v}_{i-1} + \frac{1}{6}\Delta\boldsymbol{v}_{i-1}\right) \times \Delta\boldsymbol{\theta}_i\right]$$
$$- \frac{1}{2}\left[\left(\hat{\boldsymbol{\theta}}_{i-1} + \frac{1}{6}\Delta\hat{\boldsymbol{\theta}}_{i-1}\right) \times \Delta\hat{\boldsymbol{v}}_i + \left(\hat{\boldsymbol{v}}_{i-1} + \frac{1}{6}\Delta\hat{\boldsymbol{v}}_{i-1}\right) \times \Delta\hat{\boldsymbol{\theta}}_i\right]. \tag{5.20}$$

Solving each error definition for the true quantity and substituting, Equation (5.20) becomes

$$\boldsymbol{e}_{\delta v_{scul,i}} = \frac{1}{2}\left(\hat{\boldsymbol{\theta}}_{i-1} + \boldsymbol{e}_{\theta,i-1} + \frac{1}{6}\left(\Delta\hat{\boldsymbol{\theta}}_{i-1} + \boldsymbol{e}_{\Delta\theta,i-1}\right)\right) \times \left(\Delta\hat{\boldsymbol{v}}_i + \boldsymbol{e}_{\Delta v,i}\right)$$
$$+ \frac{1}{2}\left(\hat{\boldsymbol{v}}_{i-1} + \boldsymbol{e}_{v,i-1} + \frac{1}{6}\left(\Delta\hat{\boldsymbol{v}}_{i-1} + \boldsymbol{e}_{\Delta v,i-1}\right)\right) \times \left(\Delta\hat{\boldsymbol{\theta}}_i + \boldsymbol{e}_{\Delta\theta,i}\right)$$
$$- \frac{1}{2}\left(\hat{\boldsymbol{\theta}}_{i-1} + \frac{1}{6}\Delta\hat{\boldsymbol{\theta}}_{i-1}\right) \times \Delta\hat{\boldsymbol{v}}_i - \frac{1}{2}\left(\hat{\boldsymbol{v}}_{i-1} + \frac{1}{6}\Delta\hat{\boldsymbol{v}}_{i-1}\right) \times \Delta\hat{\boldsymbol{\theta}}_i. \tag{5.21}$$

Simplifying and neglecting higher-order terms, the error in the sculling increments can be approximated to first-order as

$$e_{\delta v_{scul},i} \approx \left(\hat{\theta}_{i-1} + \frac{1}{6}\Delta\hat{\theta}_{i-1}\right) \times e_{\Delta v,i} - \Delta\hat{\theta}_i \times \left(e_{v,i-1} + \frac{1}{6}e_{\Delta v,i-1}\right) \quad (5.22)$$
$$+ \left(\hat{v}_{i-1} + \frac{1}{6}\Delta\hat{v}_{i-1}\right) \times e_{\Delta\theta,i} - \Delta\hat{v}_i \times \left(e_{\theta,i-1} + \frac{1}{6}e_{\Delta\theta,i-1}\right)$$

By the definition of the accumulated incremental sculling corrections given in Equation (4.21),

$$e_{\Delta v_{scul},\ell} = (\Delta v_{scul,\ell-1} + \delta v_{scul,i}) - (\Delta\hat{v}_{scul,\ell-1} + \delta\hat{v}_{scul,i})$$
$$= (\Delta v_{scul,\ell-1} - \Delta\hat{v}_{scul,\ell-1}) + (\delta v_{scul,i} - \delta\hat{v}_{scul,i})$$
$$= e_{\Delta v_{scul},\ell-1} + e_{\delta v_{scul},\ell}.$$

This result may be recursively applied, allowing the definition of the error in the accumulation to simply be the sum of the errors in each incremental sculling correction, or

$$e_{\Delta v_{scul},\ell} = \sum_{i=1}^{\ell} e_{\delta v_{scul},i}. \quad (5.23)$$

Now that an expression for the error in the accumulated sculling error is known, the explicit mapping of the error in each measurement into the accumulated error is desired. Examining Equation (5.11), notice that Equation (5.22) has two components that parallel the form of the propagation of the incremental angle measurements through the coning correction. The first is the previously defined $\Xi_{con,i}$ crossed with the incremental velocity errors, while a second term is a parallel mapping that can be defined such that $\Xi_{scul,i} \overset{\Delta}{=} [\xi_{scul,i}\times]$, where

$$\xi_{scul,i} \overset{\Delta}{=} \frac{1}{2}\left[\sum_{j=1}^{i-1}\Delta\hat{v}_j - \sum_{j=i+1}^{\ell}\Delta\hat{v}_j\right] - \frac{1}{12}(\Delta\hat{v}_{i+1} - \Delta\hat{v}_{i-1}) \quad (5.24)$$

and further allows the definition of the mapping of the measurement errors through the incremental sculling correction to be

$$\boldsymbol{e}_{\Delta v_{scul},\ell} = \sum_{i=1}^{\ell} \boldsymbol{\Xi}_{con,i} \boldsymbol{e}_{\Delta v,i} + \boldsymbol{\Xi}_{scul,i} \boldsymbol{e}_{\Delta\theta,i}. \tag{5.25}$$

5.4.3. Error in the Rotational Correction. The direction of the incremented velocity vector must be compensated for the vehicle's rotation during the major interval; this is done via the rotational correction term. To determine the mapping of the measurement errors through the rotational correction term, define the error in the rotational correction as

$$\boldsymbol{e}_{\Delta v_{rot},\ell} = \Delta \boldsymbol{v}_{rot,\ell} - \Delta \hat{\boldsymbol{v}}_{rot,\ell}. \tag{5.26}$$

Expanding Equation (5.26) with the definition of $\Delta \boldsymbol{v}_{rot,\ell}$ in Equation (4.23), and simplifying, the error in the rotational correction is then

$$
\begin{aligned}
\boldsymbol{e}_{\Delta v_{rot},\ell} &= \frac{1}{2} \left(\boldsymbol{\theta}_\ell \times \boldsymbol{v}_\ell \right) - \frac{1}{2} \left(\hat{\boldsymbol{\theta}}_\ell \times \hat{\boldsymbol{v}}_\ell \right) \\
&= \frac{1}{2} \left[\left(\hat{\boldsymbol{\theta}}_\ell + \boldsymbol{e}_{\theta,\ell} \right) \times \left(\hat{\boldsymbol{v}}_\ell + \boldsymbol{e}_{v,\ell} \right) \right] - \frac{1}{2} \left(\hat{\boldsymbol{\theta}}_\ell \times \hat{\boldsymbol{v}}_\ell \right) \\
&= \frac{1}{2} \left[\hat{\boldsymbol{\theta}}_\ell \times \boldsymbol{e}_{v,\ell} - \hat{\boldsymbol{v}}_\ell \times \boldsymbol{e}_{\theta,\ell} \right],
\end{aligned} \tag{5.27}
$$

neglecting higher-order error terms. Given that the error in the accumulations are simply a sum of the errors in each of the measurements, the error propagation for the rotational correction is

$$\boldsymbol{e}_{\Delta v_{rot},\ell} = \frac{1}{2} \left(\sum_{i=1}^{\ell} \left[\hat{\boldsymbol{\theta}}_\ell \times \right] \boldsymbol{e}_{\Delta v,i} - \left[\hat{\boldsymbol{v}}_\ell \times \right] \boldsymbol{e}_{\Delta\theta,i} \right). \tag{5.28}$$

5.4.4. Combined Propagation of Sculling Errors. To produce the error propagation for the sculled, non-gravitational change in velocity, Equation (5.16) can be combined with the definitions for each component defined in Equation (5.18), Equation (5.25), and Equation (5.28). Therefore, the error in the sculling term as a function of the estimated incremental angles and velocities mapped into the errors in each of those terms is

$$\boldsymbol{e}_{\Delta v_{ng},\ell} = \sum_{i=1}^{\ell} \boldsymbol{e}_{\Delta v,i} + \sum_{i=1}^{\ell} \left(\boldsymbol{\Xi}_{con,i} \boldsymbol{e}_{\Delta v,i} + \boldsymbol{\Xi}_{scul,i} \boldsymbol{e}_{\Delta \theta,i} \right) + \frac{1}{2} \sum_{i=1}^{\ell} \left(\left[\hat{\boldsymbol{\theta}}_{\ell} \times \right] \boldsymbol{e}_{\Delta v,i} - [\hat{\boldsymbol{v}}_{\ell} \times] \boldsymbol{e}_{\Delta \theta,i} \right),$$

which simplifies to

$$\boldsymbol{e}_{\Delta v_{ng},\ell} = \sum_{i=1}^{\ell} \left(\boldsymbol{I}_{3\times 3} + \boldsymbol{\Xi}_{con,i} + \frac{1}{2} \left[\hat{\boldsymbol{\theta}}_{\ell} \times \right] \right) \boldsymbol{e}_{\Delta v,i} + \left(\boldsymbol{\Xi}_{scul,i} - \frac{1}{2} [\hat{\boldsymbol{v}}_{\ell} \times] \right) \boldsymbol{e}_{\Delta \theta,i}. \qquad (5.29)$$

The errors in each of these measurement sources, however, is a function of well-known and commonly estimated error sources. In Section 5.6, the error propagation for the sculling correction is integrated into the velocity error dynamics, while Section 5.7 also incorporates the error propagation for a strapdown sensor into the sculling-corrected non-gravitational change in velocity.

5.5. SCROLLING ALGORITHM ERROR PROPAGATION

Through the application of a scrolling algorithm, a correction for the measured non-gravitational motion and its integration into the vehicle's position is made using the incremental angle and velocity measurements over the major interval. Whereas the coning correction's application alters the measurement statistics for incremental angle measurements, the sculling and scrolling corrections effect those for incremental velocity. Noting the equation governing the scrolling-corrected non-gravitational term in Equation (4.24),

the error can be written as a sum of errors in each of the components, i.e.

$$e_{\Delta r_{ng},k} = e_{s_v,\ell} + e_{\Delta r_{rot},\ell} + e_{\Delta r_{scrl},\ell}, \tag{5.30}$$

where $e_{s_v,\ell}$ is the error in the incremental angle accumulation, $e_{\Delta r_{scrl},\ell}$ is the error in the scrolling correction, and $e_{\Delta r_{rot},\ell}$ is the error in correction for the vehicle's rotation during the measurement accumulation. Sections 5.5.1 – 5.5.3 derive the mapping of measurement errors through each term, separately.

5.5.1. Error in the Integrated Incremental Velocity Accumulation. The first term in Equation (5.30) describes the error introduced through the integration of the incremental velocity vectors to determine the change in the vehicle's position, with increment and accumulation defined in Equations (4.26) and (4.25), respectively. The error must then be expressed in terms of the error in the accumulation and increment; the error in the accumulation is simply a sum of the error in each increment, i.e.

$$e_{s_v,\ell} = \sum_{i=1}^{\ell} e_{\Delta s_v,i}. \tag{5.31}$$

The error in the increment is then defined to be the difference between the estimated and true increments, which is given by

$$e_{\Delta s_v,i} = \Delta s_{v,i} - \Delta \hat{s}_{v,i}. \tag{5.32}$$

Substituting for the definition of the increment and truth, the error in the increment can be simplified and expressed as

$$e_{\Delta s_v,i} = e_{v,i-1}\Delta t_\ell + \frac{1}{12}\left(5e_{\Delta v,i} + e_{\Delta v,i-1}\right)\Delta t_\ell, \tag{5.33}$$

allowing Equation (5.31) to be expressed as a sum of the errors in each increment. Note that the $e_{\Delta v, i-1}$ term has been deconstructed and expressed as a sum of the increments by applying Equation (5.18). Expanding for a variable number of steps, the propagation of incremental velocity errors into the accumulated integrated velocity is given by

$$e_{s_v,\ell} = -\frac{\Delta t_\ell}{12} e_{\Delta v,\ell} + \Delta t_\ell \sum_{i=1}^{\ell} \left(\frac{1}{2} + \ell - i \right) e_{\Delta v,i},$$ (5.34)

or

$$e_{s_v,\ell} = \Delta t_\ell \sum_{i=1}^{\ell} c_{i,\ell} e_{\Delta v,i}$$ (5.35)

with the coefficient $c_{i,j}$ defined to be

$$c_{i,j} = \begin{cases} \frac{1}{2} + j - i & i < j \\ \frac{5}{12} & i = j \end{cases},$$ (5.36)

where i is the coefficient associated with the ith measurement error $e_{\Delta\theta,i}$, and j is the number of measurements contained within the $e_{s_v,\ell}$ term. In most cases $j = \ell$, though this is not always true.

5.5.2. Error in the Rotational Correction. To more accurately predict how the non-gravitational incremental velocity and angle cause the state to propagate, the rotation of the vectors during the measurement period is accounted for and defined in Equation (4.27). However, to more accurately predict the uncertainty in the new estimate, the contribution of errors in those measurements to this correction must be determined. Define the error in the rotational component to be

$$e_{\Delta r_{rot},k} = \Delta r_{rot,k} - \Delta\hat{r}_{rot,k}.$$ (5.37)

Substituting for the components from Equation (4.27) the error in the position rotational correction can be expressed as a function of the errors in the incremental angle and velocity measurements to first order as

$$
\begin{aligned}
\boldsymbol{e}_{\Delta r_{rot},k} =& \frac{1}{6} \left(\boldsymbol{s}_{\theta,\ell} \times \boldsymbol{v}_\ell + \boldsymbol{\theta}_\ell \times \boldsymbol{s}_{v,\ell} - \hat{\boldsymbol{s}}_{\theta,\ell} \times \hat{\boldsymbol{v}}_\ell - \hat{\boldsymbol{\theta}}_\ell \times \hat{\boldsymbol{s}}_{v,\ell} \right) \\
=& \frac{1}{6} \Big[\left(\hat{\boldsymbol{s}}_{\theta,\ell} + \boldsymbol{e}_{s_\theta,\ell} \right) \times \left(\hat{\boldsymbol{v}}_\ell + \boldsymbol{e}_{v,\ell} \right) + \left(\hat{\boldsymbol{\theta}}_\ell + \boldsymbol{e}_{\theta,\ell} \right) \times \left(\hat{\boldsymbol{s}}_{v,\ell} + \boldsymbol{e}_{s_v,\ell} \right) \\
& - \hat{\boldsymbol{s}}_{\theta,\ell} \times \hat{\boldsymbol{v}}_\ell - \hat{\boldsymbol{\theta}}_\ell \times \hat{\boldsymbol{s}}_{v,\ell} \Big] \\
=& \frac{1}{6} \left(\hat{\boldsymbol{s}}_{\theta,\ell} \times \boldsymbol{e}_{v,\ell} + \hat{\boldsymbol{\theta}}_\ell \times \boldsymbol{e}_{s_v,\ell} - \hat{\boldsymbol{v}}_\ell \times \boldsymbol{e}_{s_\theta,\ell} - \hat{\boldsymbol{s}}_{v,\ell} \times \boldsymbol{e}_{\theta,\ell} \right) .
\end{aligned}
\tag{5.38}
$$

The error in the integrated incremental angle $\boldsymbol{e}_{s_\theta,\ell}$ can be expressed similarly to how the incremental velocity was defined in Equation (5.35), as

$$
\boldsymbol{e}_{s_\theta,\ell} = \Delta t_\ell \sum_{i=1}^{\ell} c_{i,\ell} \boldsymbol{e}_{\Delta\theta,i},
\tag{5.39}
$$

with $c_{i,\ell}$ defined in Equation (5.36). Finally, the error in the rotational scrolling term can be expressed as a function of the measurement errors by substituting the definitions for the incremental angle and velocity integration in Equations (5.39) and (5.35) and the definitions for the error accumulations in Equations (5.6) and (5.18), which yields

$$
\begin{aligned}
\boldsymbol{e}_{\Delta r_{rot},k} =& \frac{1}{6} \Bigg[\hat{\boldsymbol{s}}_{\theta,k} \times \sum_{i=1}^{\ell} \boldsymbol{e}_{\Delta v,i} + \hat{\boldsymbol{\theta}}_k \times \left(\Delta t_\ell \sum_{i=1}^{\ell} c_{i,\ell} \boldsymbol{e}_{\Delta v,i} \right) \\
& - \hat{\boldsymbol{v}}_k \times \left(\Delta t_\ell \sum_{i=1}^{\ell} c_{i,\ell} \boldsymbol{e}_{\Delta\theta,i} \right) - \hat{\boldsymbol{s}}_{v,k} \times \sum_{i=1}^{\ell} \boldsymbol{e}_{\Delta\theta,i} \Bigg] \\
=& \frac{1}{6} \sum_{i=1}^{\ell} \left(\left[\hat{\boldsymbol{s}}_{\theta,k} + c_{i,\ell} \Delta t_\ell \hat{\boldsymbol{\theta}}_k \right] \times \boldsymbol{e}_{\Delta v,i} - \left[\hat{\boldsymbol{s}}_{v,k} + c_{i,\ell} \Delta t_\ell \hat{\boldsymbol{v}}_k \right] \times \boldsymbol{e}_{\Delta\theta,i} \right)
\end{aligned}
$$

Therefore, the propagation of measurement errors through the rotational term can be expressed as

$$e_{\Delta r_{rot},k} = \frac{1}{6} \sum_{i=1}^{\ell} \Lambda_{\Delta\theta,i} e_{\Delta v,i} - \Lambda_{\Delta v,i} e_{\Delta\theta,i}, \tag{5.40}$$

where $\Lambda_{\Delta\theta,i} = \left[\lambda_{\Delta\theta,i}\times\right]$, $\Lambda_{\Delta v,i} = \left[\lambda_{\Delta v,i}\times\right]$, and

$$\lambda_{\Delta\theta,i} = \hat{s}_{\theta,k} + c_{i,\ell}\Delta t_{\ell}\hat{\theta}_k \tag{5.41a}$$

$$\lambda_{\Delta v,i} = \hat{s}_{v,k} + c_{i,\ell}\Delta t_{\ell}\hat{v}_k. \tag{5.41b}$$

With $\Lambda_{\Delta\theta,i}$ and $\Lambda_{\Delta v,i}$ defined, the propagation of each measurement error into the position rotational correction are known.

5.5.3. Error in the Scrolling Correction. The scrolling correction term, as described by Equation (4.28), is composed of an accumulation of two incremental corrections, a correction for the presence of sculling motion and its integration into the position, and a correction for the presence of other, higher-order effects. The error in the scrolling correction term is defined as

$$e_{\Delta r_{scrl},\ell} = e_{\Delta r_{scrl},\ell-1} + e_{\delta r_{scrl/scul},\ell} + e_{\delta r_{scrl/other},\ell}. \tag{5.42}$$

Recursively applying the definition in Equation (5.42), $e_{\Delta r_{scrl},\ell}$ can be expressed as a sum of errors in the incremental scrolling corrections for sculling and higher-order effects made over the major interval such that

$$e_{\Delta r_{scrl},\ell} = \sum_{i=1}^{\ell} e_{\delta r_{scrl/scul},i} + \sum_{i=1}^{\ell} e_{\delta r_{scrl/other},i}, \tag{5.43}$$

with the error in each term defined to be

$$e_{\delta r_{scrl/scul},i} = \delta \boldsymbol{r}_{scrl/scul,i} - \delta \hat{\boldsymbol{r}}_{scrl/scul,i} \tag{5.44a}$$

$$e_{\delta r_{scrl/other},i} = \delta \boldsymbol{r}_{scrl/other,i} - \delta \hat{\boldsymbol{r}}_{scrl/other,i}. \tag{5.44b}$$

Within the following sections, 5.5.3.1 and 5.5.3.2, the propagation of errors through each of these components and their accumulation are derived.

5.5.3.1. Error in the scrolling correction due to sculling corrections. Applying the definition in Equation (5.44a) to Equation (4.30), the error in the scrolling correction due to the correction for sculling motion is expressed as

$$
\begin{aligned}
e_{\delta r_{scrl/scul},i} = {} & \Delta \boldsymbol{v}_{scul,i-1} \Delta t_\ell - \Delta \hat{\boldsymbol{v}}_{scul,i-1} \Delta t_\ell \\
& + \frac{1}{2} \left[\boldsymbol{\theta}_{i-1} - \frac{1}{12} (\Delta \boldsymbol{\theta}_i - \Delta \boldsymbol{\theta}_{i-1}) \right] \times (\Delta \boldsymbol{s}_{v_i} - \boldsymbol{v}_{i-1} \Delta t_\ell) \\
& - \frac{1}{2} \left[\hat{\boldsymbol{\theta}}_{i-1} - \frac{1}{12} (\Delta \hat{\boldsymbol{\theta}}_i - \Delta \hat{\boldsymbol{\theta}}_{i-1}) \right] \times (\Delta \hat{\boldsymbol{s}}_{v_i} - \hat{\boldsymbol{v}}_{i-1} \Delta t_\ell) \\
& + \frac{1}{2} \left[\boldsymbol{v}_{i-1} - \frac{1}{12} (\Delta \boldsymbol{v}_i - \Delta \boldsymbol{v}_{i-1}) \right] \times (\Delta \boldsymbol{s}_{\theta_i} - \boldsymbol{\theta}_{i-1} \Delta t_\ell) \\
& - \frac{1}{2} \left[\hat{\boldsymbol{v}}_{i-1} - \frac{1}{12} (\Delta \hat{\boldsymbol{v}}_i - \Delta \hat{\boldsymbol{v}}_{i-1}) \right] \times \left(\Delta \hat{\boldsymbol{s}}_{\theta_i} - \hat{\boldsymbol{\theta}}_{i-1} \Delta t_\ell \right),
\end{aligned}
\tag{5.45}
$$

which can be simplified to

$$
\begin{aligned}
e_{\delta r_{scrl/scul},i} = {} & \Delta t_\ell e_{\Delta v_{scul},i-1} + \frac{\Delta t_\ell}{24} \left(\hat{\boldsymbol{\theta}}_{i-1} - \frac{1}{2} \Delta \hat{\boldsymbol{\theta}}_i \right) \times e_{\Delta v,i-1} - \frac{\Delta t_\ell}{24} \left(5\Delta \hat{\boldsymbol{\theta}}_i + \Delta \hat{\boldsymbol{\theta}}_{i-1} \right) \times e_{v,i-1} \\
& + \frac{\Delta t_\ell}{24} \left(5\hat{\boldsymbol{\theta}}_{i-1} + \frac{1}{2} \Delta \hat{\boldsymbol{\theta}}_{i-1} \right) \times e_{\Delta v,i} + \frac{\Delta t_\ell}{24} \left(\hat{\boldsymbol{v}}_{i-1} - \frac{1}{2} \Delta \hat{\boldsymbol{v}}_i \right) \times e_{\Delta \theta,i-1} \\
& - \frac{\Delta t_\ell}{24} (5\Delta \hat{\boldsymbol{v}}_i + \Delta \hat{\boldsymbol{v}}_{i-1}) \times e_{\theta,i-1} + \frac{\Delta t_\ell}{24} \left(5\hat{\boldsymbol{v}}_{i-1} + \frac{1}{2} \Delta \hat{\boldsymbol{v}}_{i-1} \right) \times e_{\Delta \theta,i}
\end{aligned}
\tag{5.46}
$$

by substituting the definition $\delta \boldsymbol{r}_{scrl/scul,i} = \delta \hat{\boldsymbol{r}}_{scrl/scul,i} + \boldsymbol{e}_{\delta r_{scrl/scul},i}$. In Section 5.4.2, the error propagation for the sculling term is defined and can be substituted into Equation (5.46), giving

$$
\begin{aligned}
\boldsymbol{e}_{\delta r_{scrl/scul},i} = \Delta t_\ell &\left(\sum_{j=1}^{i-1} \boldsymbol{\Xi}_{con,j} \boldsymbol{e}_{\Delta v,j} + \boldsymbol{\Xi}_{scul,j} \boldsymbol{e}_{\Delta\theta,j} \right) + \frac{\Delta t_\ell}{24} \left(\hat{\boldsymbol{\theta}}_{i-1} - \frac{1}{2}\Delta\hat{\boldsymbol{\theta}}_i \right) \times \boldsymbol{e}_{\Delta v,i-1} \\
&- \frac{\Delta t_\ell}{24} \left(5\Delta\hat{\boldsymbol{\theta}}_i + \Delta\hat{\boldsymbol{\theta}}_{i-1} \right) \times \boldsymbol{e}_{v,i-1} + \frac{\Delta t_\ell}{24} \left(5\hat{\boldsymbol{\theta}}_{i-1} + \frac{1}{2}\Delta\hat{\boldsymbol{\theta}}_{i-1} \right) \times \boldsymbol{e}_{\Delta v,i} \\
&+ \frac{\Delta t_\ell}{24} \left(\hat{\boldsymbol{v}}_{i-1} - \frac{1}{2}\Delta\hat{\boldsymbol{v}}_i \right) \times \boldsymbol{e}_{\Delta\theta,i-1} - \frac{\Delta t_\ell}{24} \left(5\Delta\hat{\boldsymbol{v}}_i + \Delta\hat{\boldsymbol{v}}_{i-1} \right) \times \boldsymbol{e}_{\theta,i-1} \\
&+ \frac{\Delta t_\ell}{24} \left(5\hat{\boldsymbol{v}}_{i-1} + \frac{1}{2}\Delta\hat{\boldsymbol{v}}_{i-1} \right) \times \boldsymbol{e}_{\Delta\theta,i} \,,
\end{aligned} \tag{5.47}
$$

which is reorganized to

$$
\begin{aligned}
\boldsymbol{e}_{\delta r_{scrl/scul},i} = \Delta t_\ell \sum_{j=1}^{i-1} &\left(\boldsymbol{\Xi}_{con,j} - \frac{1}{24} \left[\left(5\Delta\hat{\boldsymbol{\theta}}_i + \Delta\hat{\boldsymbol{\theta}}_{i-1} \right) \times \right] \right) \boldsymbol{e}_{\Delta v,j} \\
&+ \frac{\Delta t_\ell}{24} \left(\hat{\boldsymbol{\theta}}_{i-1} - \frac{1}{2}\Delta\hat{\boldsymbol{\theta}}_i \right) \times \boldsymbol{e}_{\Delta v,i-1} + \frac{\Delta t_\ell}{24} \left(5\hat{\boldsymbol{\theta}}_{i-1} + \frac{1}{2}\Delta\hat{\boldsymbol{\theta}}_{i-1} \right) \times \boldsymbol{e}_{\Delta v,i} \\
&+ \Delta t_\ell \sum_{j=1}^{i-1} \left(\boldsymbol{\Xi}_{scul,j} - \frac{1}{24} \left[(5\Delta\hat{\boldsymbol{v}}_i + \Delta\hat{\boldsymbol{v}}_{i-1}) \times \right] \right) \boldsymbol{e}_{\Delta\theta,j} \\
&+ \frac{\Delta t_\ell}{24} \left(\hat{\boldsymbol{v}}_{i-1} - \frac{1}{2}\Delta\hat{\boldsymbol{v}}_i \right) \times \boldsymbol{e}_{\Delta\theta,i-1} + \frac{\Delta t_\ell}{24} \left(5\hat{\boldsymbol{v}}_{i-1} + \frac{1}{2}\Delta\hat{\boldsymbol{v}}_{i-1} \right) \times \boldsymbol{e}_{\Delta\theta,i}
\end{aligned} \tag{5.48}
$$

by expanding the definition of $\boldsymbol{e}_{\theta,i-1}$.

The propagation of the measurement errors through the scrolling algorithm's correction for sculling motion is a sum of errors in each increment generated across the major interval. Expanding manually, it can be shown that the error in the scrolling correction for the sculling motion is then expressed as

$$e_{\Delta r_{scrl/scul},\ell} = \Delta t_\ell \left(\sum_{i=1}^{\ell} \left[(\ell - i) \, \Xi_{con,i} + \frac{1}{24} \Gamma_{\Delta\theta,i} \right] e_{\Delta v,i} \right.$$

$$\left. + \sum_{i=1}^{\ell} \left[(\ell - i) \, \Xi_{scul,i} + \frac{1}{24} \Gamma_{\Delta v,i} \right] e_{\Delta\theta,i} \right) \qquad (5.49)$$

with the mappings defined such that $\Gamma_{\Delta\theta,i} = \left[\boldsymbol{\gamma}_{\Delta\theta,i} \times \right]$ and $\Gamma_{\Delta v,i} = \left[\boldsymbol{\gamma}_{\Delta v,i} \times \right]$, where

$$\boldsymbol{\gamma}_{\Delta\theta,i} = \begin{cases} 6 \left(\sum_{j=1}^{i-1} \Delta\hat{\boldsymbol{\theta}}_j - \sum_{j=i+1}^{\ell} \Delta\hat{\boldsymbol{\theta}}_j \right) + \frac{1}{2} \left(\Delta\hat{\boldsymbol{\theta}}_{i-1} - \Delta\hat{\boldsymbol{\theta}}_{i+1} \right) + \Delta\hat{\boldsymbol{\theta}}_\ell & i < \ell \\ 5 \sum_{j=1}^{i-1} \Delta\hat{\boldsymbol{\theta}}_j + \frac{1}{2} \Delta\hat{\boldsymbol{\theta}}_{i-1} & i = \ell \end{cases}$$

and

$$\boldsymbol{\gamma}_{\Delta v,i} = \begin{cases} 6 \left(\sum_{j=1}^{i-1} \Delta\hat{\boldsymbol{v}}_j - \sum_{j=i+1}^{\ell} \Delta\hat{\boldsymbol{v}}_j \right) + \frac{1}{2} \left(\Delta\hat{\boldsymbol{v}}_{i-1} - \Delta\hat{\boldsymbol{v}}_{i+1} \right) + \Delta\hat{\boldsymbol{v}}_\ell & i < \ell \\ 5 \sum_{j=1}^{i-1} \Delta\hat{\boldsymbol{v}}_j + \frac{1}{2} \Delta\hat{\boldsymbol{v}}_{i-1} & i = \ell. \end{cases}$$

The definitions for $\boldsymbol{\gamma}_{\Delta\theta,i}$ and $\boldsymbol{\gamma}_{\Delta v,i}$ can be further expressed as

$$\boldsymbol{\gamma}_{\Delta\theta,i} = \begin{cases} 12\hat{\boldsymbol{\theta}}_i - 6\Delta\hat{\boldsymbol{\theta}}_i - 6\hat{\boldsymbol{\theta}}_\ell + \frac{1}{2} \left(\Delta\hat{\boldsymbol{\theta}}_{i-1} - \Delta\hat{\boldsymbol{\theta}}_{i+1} \right) + \Delta\hat{\boldsymbol{\theta}}_\ell & i < \ell \\ 5\hat{\boldsymbol{\theta}}_{i-1} + \frac{1}{2}\Delta\hat{\boldsymbol{\theta}}_{i-1} & i = \ell \end{cases} \qquad (5.50)$$

and

$$\boldsymbol{\gamma}_{\Delta v,i} = \begin{cases} 12\hat{\boldsymbol{v}}_i - 6\Delta\hat{\boldsymbol{v}}_i - 6\hat{\boldsymbol{v}}_\ell + \frac{1}{2} \left(\Delta\hat{\boldsymbol{v}}_{i-1} - \Delta\hat{\boldsymbol{v}}_{i+1} \right) + \Delta\hat{\boldsymbol{v}}_\ell & i < \ell \\ 5\hat{\boldsymbol{v}}_{i-1} + \frac{1}{2}\Delta\hat{\boldsymbol{v}}_{i-1} & i = \ell, \end{cases} \qquad (5.51)$$

by substituting the accumulated variables for the summations.

5.5.3.2. Error in the scrolling correction due to higher-order effect corrections.

As previously shown in Equation (5.44b), the error introduced in the scrolling correction, due to the correction for higher-order effects, is a sum of the error in each increment over the major interval. Therefore, in any given increment, the error can be expressed as a function

of the measurements and their errors throughout the current major interval. Substituting for the definition of the scrolling correction made for higher-order effects provided in Equation (4.31), and simplifying, the error in an individual increment can be expressed as

$$
\begin{aligned}
\boldsymbol{e}_{\delta r_{scrl/other},i} =& \frac{\Delta t_\ell}{6} \sum_{j=1}^{i-1} \left(\left[\hat{\boldsymbol{\theta}}_{i-1} - \frac{1}{6} \left(\Delta\hat{\boldsymbol{\theta}}_i - \Delta\hat{\boldsymbol{\theta}}_{i-1} \right) - c_{j,\,i-1}\Delta\hat{\boldsymbol{\theta}}_i \right] \times \boldsymbol{e}_{\Delta v,j} \right) \\
& - \frac{\Delta t_\ell}{6} \sum_{j=1}^{i-1} \left(\left[\hat{\boldsymbol{v}}_{i-1} - \frac{1}{6} (\Delta\hat{\boldsymbol{v}}_i - \Delta\hat{\boldsymbol{v}}_{i-1}) - c_{j,\,i-1}\Delta\hat{\boldsymbol{v}}_i \right] \times \boldsymbol{e}_{\Delta\theta,j} \right) \\
& + \frac{\Delta t_\ell}{6} \left[\frac{1}{6}\hat{\boldsymbol{\theta}}_{i-1} - \frac{1}{40} \left(\Delta\hat{\boldsymbol{\theta}}_i - \Delta\hat{\boldsymbol{\theta}}_{i-1} \right) + \Delta\hat{\boldsymbol{\theta}}_i \right] \times \boldsymbol{e}_{\Delta v,i-1} \\
& - \frac{\Delta t_\ell}{6} \left[\frac{1}{6}\hat{\boldsymbol{v}}_{i-1} - \frac{1}{40} (\Delta\hat{\boldsymbol{v}}_i - \Delta\hat{\boldsymbol{v}}_{i-1}) + \Delta\hat{\boldsymbol{v}}_i \right] \times \boldsymbol{e}_{\Delta\theta,i-1} \\
& + \frac{\Delta t_\ell}{6} \left[\frac{7}{120} \left(\Delta\hat{\boldsymbol{\theta}}_i - \Delta\hat{\boldsymbol{\theta}}_{i-1} \right) - \frac{1}{24}\Delta\hat{\boldsymbol{\theta}}_{i-1} + \sum_{j=1}^{i-1} \left(i - j - \frac{1}{3} \right) \Delta\hat{\boldsymbol{\theta}}_j \right] \times \boldsymbol{e}_{\Delta v,i} \\
& - \frac{\Delta t_\ell}{6} \left[\frac{7}{120} (\Delta\hat{\boldsymbol{v}}_i - \Delta\hat{\boldsymbol{v}}_{i-1}) - \frac{1}{24}\Delta\hat{\boldsymbol{v}}_{i-1} + \sum_{j=1}^{i-1} \left(i - j - \frac{1}{3} \right) \Delta\hat{\boldsymbol{v}}_j \right] \times \boldsymbol{e}_{\Delta\theta,i}, \quad (5.52)
\end{aligned}
$$

where $c_{j,i-1}$ is defined in Equation (5.36).

Manually expanding each term, the measurement accumulation that generates the mapping of the measurement errors into the scrolling correction term that accounts for higher-order effects is then expressed as

$$
\begin{aligned}
\boldsymbol{e}_{\Delta r_{scrl/other},\ell} &= \sum_{i=1}^{\ell} \boldsymbol{e}_{\delta r_{scrl/other},i} \\
&= \frac{\Delta t_\ell}{6} \left(\sum_{i=1}^{\ell} \boldsymbol{M}_{\Delta v,i}\boldsymbol{e}_{\Delta\theta,i} - \boldsymbol{M}_{\Delta\theta,i}\boldsymbol{e}_{\Delta v,i} \right), \quad (5.53)
\end{aligned}
$$

with $M_{\Delta\theta,i} = \left[\mu_{\Delta\theta,i}\times\right]$ and $M_{\Delta v,i} = \left[\mu_{\Delta v,i}\times\right]$ where $\mu_{\Delta\theta,i}$ and $\mu_{\Delta v,i}$ are

$$
\mu_{\Delta\theta,i} = \begin{cases} \frac{7}{120}\left(\Delta\hat{\theta}_i - \Delta\hat{\theta}_{i-1}\right) + \frac{1}{40}\left(\Delta\hat{\theta}_i + \Delta\hat{\theta}_{i+1}\right) + \frac{1}{6}\left(\hat{\theta}_i + \Delta\hat{\theta}_i - \Delta\hat{\theta}_\ell\right) & i < \ell \\[2mm] \qquad + \frac{1}{12}\Delta\hat{\theta}_{i+1} - \frac{1}{24}\Delta\hat{\theta}_{i-1} + (\ell - i)\,\hat{\theta}_i + \Delta\hat{\theta}_i + \sum_{j=1}^{i-1}\left(i - j - \frac{1}{3}\right)\Delta\hat{\theta}_j \\[2mm] \qquad + \sum_{j=i+1}^{\ell}(\ell - j)\,\Delta\hat{\theta}_j + \left(i - j + \frac{1}{2}\right)\Delta\hat{\theta}_j \\[8mm] \frac{7}{120}\left(\Delta\hat{\theta}_i - \Delta\hat{\theta}_{i-1}\right) - \frac{1}{24}\Delta\hat{\theta}_{i-1} + \sum_{j=1}^{i-1}\left(i - j - \frac{1}{3}\right)\Delta\hat{\theta}_j & i = \ell \end{cases}
$$

and

$$
\mu_{\Delta v,i} = \begin{cases} \frac{7}{120}\left(\Delta\hat{v}_i - \Delta\hat{v}_{i-1}\right) + \frac{1}{40}\left(\Delta\hat{v}_i + \Delta\hat{v}_{i+1}\right) + \frac{1}{6}\left(\hat{v}_i + \Delta\hat{v}_i - \Delta\hat{v}_\ell\right) & i < \ell \\[2mm] \qquad + \frac{1}{12}\Delta\hat{v}_{i+1} - \frac{1}{24}\Delta\hat{v}_{i-1} + (\ell - i)\,\hat{v}_i + \Delta\hat{v}_i + \sum_{j=1}^{i-1}\left(i - j - \frac{1}{3}\right)\Delta\hat{v}_j \\[2mm] \qquad + \sum_{j=i+1}^{\ell}(\ell - j)\,\Delta\hat{v}_j + \left(i - j + \frac{1}{2}\right)\Delta\hat{v}_j \\[8mm] \frac{7}{120}\left(\Delta\hat{v}_i - \Delta\hat{v}_{i-1}\right) - \frac{1}{24}\Delta\hat{v}_{i-1} + \sum_{j=1}^{i-1}\left(i - j - \frac{1}{3}\right)\Delta\hat{v}_j & i = \ell \end{cases} \quad ,
$$

which can be further simplified to

$$
\mu_{\Delta\theta,i} = \begin{cases} \left(\ell - i + \frac{1}{6}\right)\hat{\theta}_i - \frac{1}{10}\Delta\hat{\theta}_{i-1} + \frac{5}{4}\Delta\hat{\theta}_i + \frac{13}{120}\Delta\hat{\theta}_{i+1} - \frac{1}{6}\Delta\hat{\theta}_\ell & i < \ell \\[2mm] \qquad + \sum_{j=1}^{i-1}\left(i - j - \frac{1}{3}\right)\Delta\hat{\theta}_j + \sum_{j=i+1}^{\ell}\left(\ell + i - 2j + \frac{1}{2}\right)\Delta\hat{\theta}_j \\[8mm] \frac{7}{120}\Delta\hat{\theta}_i - \frac{1}{10}\Delta\hat{\theta}_{i-1} + \sum_{j=1}^{i-1}\left(i - j - \frac{1}{3}\right)\Delta\hat{\theta}_j & i = \ell \end{cases} . \quad (5.54)
$$

and

$$
\mu_{\Delta v,i} = \begin{cases} \left(\ell - i + \frac{1}{6}\right) \hat{\boldsymbol{v}}_i - \frac{1}{10}\Delta\hat{\boldsymbol{v}}_{i-1} + \frac{5}{4}\Delta\hat{\boldsymbol{v}}_i + \frac{13}{120}\Delta\hat{\boldsymbol{v}}_{i+1} - \frac{1}{6}\Delta\hat{\boldsymbol{v}}_\ell & i < \ell \\ \qquad + \sum_{j=1}^{i-1} \left(i - j - \frac{1}{3}\right) \Delta\hat{\boldsymbol{v}}_j + \sum_{j=i+1}^{\ell} \left(\ell + i - 2j + \frac{1}{2}\right) \Delta\hat{\boldsymbol{v}}_j & \\ & \\ \frac{7}{120}\Delta\hat{\boldsymbol{v}}_i - \frac{1}{10}\Delta\hat{\boldsymbol{v}}_{i-1} + \sum_{j=1}^{i-1} \left(i - j - \frac{1}{3}\right) \Delta\hat{\boldsymbol{v}}_j & i = \ell \end{cases}
\tag{5.55}
$$

5.5.4. Combined Propagation of Scrolling Errors. From the definitions and derivations for the propagation of measurement errors through the corrections for the incremental velocity integration, presented in Section 5.5.1, the correction for frame rotation, as seen in Section 5.5.2, and the correction for the scrolling errors, developed throughout 5.5.3, the error in the scrolling-corrected non-gravitational change in position can be constructed. Substituting the components from Equation (5.35), Equation (5.40), Equation (5.49), and Equation (5.53), the propagation of errors is expressed as

$$
\begin{aligned}
\boldsymbol{e}_{\Delta r_{ng},k} = {} & \sum_{i=1}^{\ell} \left[\Delta t_\ell \left((\ell - i)\boldsymbol{\Xi}_{scul,i} + \frac{1}{24}\boldsymbol{\Gamma}_{\Delta v,i} + \frac{1}{6}\boldsymbol{M}_{\Delta v,i} \right) - \frac{1}{6}\boldsymbol{\Lambda}_{\Delta v,i} \right] \boldsymbol{e}_{\Delta\theta,i} \\
& + \sum_{i=1}^{\ell} \left[\Delta t_\ell \left(c_{i,\ell}\boldsymbol{I}_{3\times 3} + (\ell - i)\boldsymbol{\Xi}_{con,i} + \frac{1}{24}\boldsymbol{\Gamma}_{\Delta\theta,i} - \frac{1}{6}\boldsymbol{M}_{\Delta\theta,i} \right) + \frac{1}{6}\boldsymbol{\Lambda}_{\Delta\theta,i} \right] \boldsymbol{e}_{\Delta v,i}.
\end{aligned}
\tag{5.56}
$$

To simplify the notation, define

$$
\boldsymbol{X}_{\Delta v,i} = \Delta t_\ell \left((\ell - i)\boldsymbol{\Xi}_{scul,i} + \frac{1}{24}\boldsymbol{\Gamma}_{\Delta v,i} + \frac{1}{6}\boldsymbol{M}_{\Delta v,i} \right) - \frac{1}{6}\boldsymbol{\Lambda}_{\Delta v,i}
$$

$$
\boldsymbol{X}_{\Delta\theta,i} = \Delta t_\ell \left(c_{i,\ell}\boldsymbol{I}_{3\times 3} + (\ell - i)\boldsymbol{\Xi}_{con,i} + \frac{1}{24}\boldsymbol{\Gamma}_{\Delta\theta,i} - \frac{1}{6}\boldsymbol{M}_{\Delta\theta,i} \right) + \frac{1}{6}\boldsymbol{\Lambda}_{\Delta\theta,i}
$$

allowing Equation (5.56) to be expressed as

$$
\boldsymbol{e}_{\Delta r_{ng},k} = \sum_{i=1}^{\ell} \left(\boldsymbol{X}_{\Delta v,i}\boldsymbol{e}_{\Delta\theta,i} + \boldsymbol{X}_{\Delta\theta,i}\boldsymbol{e}_{\Delta v,i} \right).
\tag{5.57}
$$

5.6. VEHICLE STATE ERROR DYNAMICS

For inertial navigation system implementation within an MEKF, the error dynamics for each of the states must be determined as a function of the estimation errors in order to propagate the uncertainty. Within this section, the error dynamics for Equation (4.33) are derived in terms of the corrections made for coning, sculling, and scrolling considerations. Section 5.6.1 details the propagation of the errors in the coned incremental angle vector into the attitude states, while Section 5.6.2 performs a derivation of the error dynamics for the velocity uncertainty as affected by the coning and sculling results. Finally, Section 5.6.3 builds upon Section 5.6.2 to derive the error dynamics for the position in terms of the coning and scrolling results.

5.6.1. Attitude Error Dynamics. Through the definition of the attitude estimation error shown in Equation (3.27) and allowing the rotation vector to be the result of the coning algorithm, i.e. letting $\Delta\hat{\boldsymbol{\theta}}_k \to \Delta\hat{\boldsymbol{\phi}}_k$, the attitude error propagation can be expressed in terms of the error in the previous attitude error and the error in the coned rotation as

$$\boldsymbol{e}_{A,k} = \boldsymbol{T}(\Delta\hat{\boldsymbol{\phi}}_k)\boldsymbol{e}_{A,k-1} + \boldsymbol{e}_{\Delta\phi,k}. \tag{5.58}$$

Substituting the error dynamics for the coned rotation vector, shown in Equation (5.15), the error dynamics in the attitude estimate are expressed as a function of the measurement errors from the ℓ measurements sampled over the $[t_{k-1}, t_k]$ interval as

$$\boldsymbol{e}_{A,k} = \boldsymbol{T}(\Delta\hat{\boldsymbol{\phi}}_k)\boldsymbol{e}_{A,k-1} + \sum_{i=1}^{\ell} \left(\boldsymbol{I}_{3\times3} + \boldsymbol{\Xi}_{con,i}\right) \boldsymbol{e}_{\Delta\theta,i}. \tag{5.59}$$

It is noted that should the error propagation be considered simply a sum of the measurement errors that the contribution due to the coning correction will be neglected. By mapping the uncertainty through the coning algorithm, the additional mapping for each error term into the uncertainty of the attitude estimate has been shown in Equation (5.59).

5.6.2. Velocity Error Dynamics. To determine the propagation of the measurement errors through the velocity states, the error in the velocity is simply defined as

$$e_{v,k} = v_k - \hat{v}_k. \tag{5.60}$$

With the velocity propagation for a vehicle aided by strapdown inertial sensors shown in Equation (4.33b), assuming that $\Delta t_k = \Delta \hat{t}_k$, the error in the velocity propagation is

$$
\begin{aligned}
e_{v,k} =& v_{k-1} + T_{k-1}^T \Delta v_{ng,k} + \left(g_{k-1} - \frac{1}{2} G_{k-1} T_{k-1}^T \left[r_{cg/c,k-1} \times \right] \Delta \phi_k \right) \Delta t_k \\
& - \hat{v}_{k-1} - \hat{T}_{k-1}^T \Delta \hat{v}_{ng,k} - \left(\hat{g}_{k-1} - \frac{1}{2} \hat{G}_{k-1} \hat{T}_{k-1}^T \left[\hat{r}_{cg/c,k-1} \times \right] \Delta \hat{\phi}_k \right) \Delta t_k,
\end{aligned}
$$

which can be rearranged to

$$
\begin{aligned}
e_{v,k} =& v_{k-1} - \hat{v}_{k-1} + T_{k-1}^T \Delta v_{ng,k} - \hat{T}_{k-1}^T \Delta \hat{v}_{ng,k} + (g_{k-1} - \hat{g}_{k-1}) \Delta t_k \\
& - \frac{1}{2} \left(G_{k-1} T_{k-1}^T \left[r_{cg/c,k-1} \times \right] \Delta \phi_k - \frac{1}{2} \hat{G}_{k-1} \hat{T}_{k-1}^T \left[\hat{r}_{cg/c,k-1} \times \right] \Delta \hat{\phi}_k \right) \Delta t_k. \tag{5.61}
\end{aligned}
$$

To further simplify, the terms within Equation (5.61) are considered separately. By the definition of the quaternion error in Equation (3.20), it follows that

$$\delta T_{k-1} = T_{k-1} \hat{T}_{k-1}^T.$$

To first order, the error in the rotation can be expressed as [5]

$$\delta T_{k-1} = I_{3\times3} - \left[e_{A,k-1} \times \right],$$

such that the true transformation matrix has the first-order expansion

$$T_{k-1} = \hat{T}_{k-1} - \left[e_{A,k-1} \times \right] \hat{T}_{k-1},$$

which is found through the right-side multiplication by $\hat{T}_{k-1}$. Transposing, and noting that $\left[e_{A,k-1} \times \right]$ is skew-symmetric provides

$$T_{k-1}^T = \hat{T}_{k-1}^T + \hat{T}_{k-1}^T \left[e_{A,k-1} \times \right] . \tag{5.62}$$

Incorporating the result from Equation (5.62), then

$$
\begin{aligned}
T_{k-1}^T \Delta v_{ng,k} &= \left(\hat{T}_{k-1}^T + \hat{T}_{k-1}^T \left[e_{A,k-1} \times \right] \right) \left(\Delta \hat{v}_{ng,k} + e_{\Delta v_{ng},k} \right) \\
&= \hat{T}_{k-1}^T \Delta \hat{v}_{ng,k} + \hat{T}_{k-1}^T e_{\Delta v_{ng},k} + \hat{T}_{k-1}^T \left[e_{A,k-1} \times \right] \Delta \hat{v}_{ng,k} \\
&= \hat{T}_{k-1}^T \Delta \hat{v}_{ng,k} + \hat{T}_{k-1}^T e_{\Delta v_{ng},k} - \hat{T}_{k-1}^T \left[\Delta \hat{v}_{ng,k} \times \right] e_{A,k-1}
\end{aligned} \tag{5.63}
$$

to first-order in the error terms. Next, noting that g_{k-1} is evaluated at the vehicle center of gravity, it can be expressed as

$$g_{k-1} = \hat{g}_{k-1} + \hat{G}_{k-1} e_{r_{cg},k-1} \tag{5.64}$$

where $e_{r_{cg},k-1} = r_{cg,k-1} - \hat{r}_{cg,k-1}$. Given Equation (5.62), it then follows that

$$
\begin{aligned}
e_{r_{cg},k-1} &= r_{k-1} + T_{k-1}^T r_{cg/c,k-1} - \hat{r}_{k-1} - \hat{T}_{k-1}^T \hat{r}_{cg/c,k-1} \\
&= e_{r,k-1} + \hat{T}_{k-1}^T e_{r_{cg/c},k} + \hat{T}_{k-1}^T \left[e_{A,k-1} \times \right] \hat{r}_{cg/c,k-1} \\
&= e_{r,k-1} + \hat{T}_{k-1}^T e_{r_{cg/c},k} - \hat{T}_{k-1}^T \left[\hat{r}_{cg/c,k-1} \times \right] e_{A,k-1}
\end{aligned} \tag{5.65}
$$

to first-order, showing that Equation (5.64) can be expanded to first order as

$$g_{k-1} = \hat{g}_{k-1} + \hat{G}_{k-1} e_{r,k-1} + \hat{G}_{k-1} \hat{T}_{k-1}^T e_{r_{cg/c},k-1} - \hat{G}_{k-1} \hat{T}_{k-1}^T \left[\hat{r}_{cg/c,k-1} \times \right] e_{A,k-1} . \tag{5.66}$$

By substituting the definition from Equation (5.62), $\hat{r}_{cg/c,k-1} = \hat{r}_{cg/c,k-1} + e_{r_{cg/c},k-1}$ and $\Delta\phi_k = \Delta\hat{\phi}_k + e_{\Delta\phi,k}$ into $T_{k-1}^T \left[r_{cg/c,k-1} \times \right] \Delta\phi_k$, the first-order expansion of the term becomes

$$
\begin{aligned}
T_{k-1}^T \left[r_{cg/c,k-1} \times \right] \Delta\phi_k &= \left(\hat{T}_{k-1}^T + \hat{T}_{k-1}^T \left[e_{A,k-1} \times \right] \right) \left[\left(\hat{r}_{cg/c,k-1} + e_{r_{cg/c},k-1} \right) \times \right] \left(\Delta\hat{\phi}_k + e_{\Delta\phi,k} \right) \\
&= \hat{T}_{k-1}^T \left[\hat{r}_{cg/c,k-1} \times \right] \Delta\hat{\phi}_k + \hat{T}_{k-1}^T \left[\hat{r}_{cg/c,k-1} \times \right] e_{\Delta\phi,k} \\
&\quad + \hat{T}_{k-1}^T \left[e_{r_{cg/c},k-1} \times \right] \Delta\hat{\phi}_k + \hat{T}_{k-1}^T \left[e_{A,k-1} \times \right] \left[\hat{r}_{cg/c,k-1} \times \right] \Delta\hat{\phi}_k \\
&= \hat{T}_{k-1}^T \left[\hat{r}_{cg/c,k-1} \times \right] \Delta\hat{\phi}_k + \hat{T}_{k-1}^T \left[\hat{r}_{cg/c,k-1} \times \right] e_{\Delta\phi,k} \\
&\quad - \hat{T}_{k-1}^T \left[\Delta\hat{\phi}_k \times \right] e_{r_{cg/c},k-1} - \hat{T}_{k-1}^T \left[\hat{r}_{cg/c,k-1} \times \right] \left[\Delta\hat{\phi}_k \times \right] e_{A,k-1}.
\end{aligned}
$$

$$(5.67)$$

It can then be shown that

$$
G_{k-1} \hat{T}_{k-1}^T \left[\hat{r}_{cg/c,k-1} \times \right] \Delta\hat{\phi}_k = \hat{G}_{k-1} \hat{T}_{k-1}^T \left[\hat{r}_{cg/c,k-1} \times \right] \Delta\hat{\phi}_k + \hat{U}_{k-1} e_{r_{cg},k-1}
$$

where $\hat{U}_{k-1} \in \mathbb{R}^{3\times3}$, with an element in the ith row and j^{th} column given by [32]

$$
\hat{U}_{k-1}(i,j) = \left[\sum_{m=1}^{3} \frac{\partial^2 g(i)}{\partial r(j) \partial r(m)} u(m) \Bigg|_{r=\hat{r}_{cg,k-1}} \right]. \tag{5.68}
$$

It should be noted that $r(j)$ and $r(i)$ denote the ith and j^{th} elements of the $r_{cg,k-1}$ vector, while $g(i)$ similarly denotes the ith component of g_{k-1}. Therefore, $G_{k-1} T_{k-1}^T \left[r_{cg/c,k-1} \times \right] \Delta\phi_k$ can be expressed to first-order as

$$
\begin{aligned}
G_{k-1} T_{k-1}^T \left[r_{cg/c,k-1} \times \right] \Delta\phi_k &= \hat{G}_{k-1} \hat{T}_{k-1}^T \left[\hat{r}_{cg/c,k-1} \times \right] \Delta\hat{\phi}_k + \hat{U}_{k-1} e_{r_{cg},k-1} \\
&\quad + \hat{G}_{k-1} \hat{T}_{k-1}^T \left[\hat{r}_{cg/c,k-1} \times \right] e_{\Delta\phi,k} - \hat{G}_{k-1} \hat{T}_{k-1}^T \left[\Delta\hat{\phi}_k \times \right] e_{r_{cg/c},k-1} \\
&\quad - \hat{G}_{k-1} \hat{T}_{k-1}^T \left[\hat{r}_{cg/c,k-1} \times \right] \left[\Delta\hat{\phi}_k \times \right] e_{A,k-1}.
\end{aligned}
$$

$$(5.69)$$

Additionally, substituting the definition of $e_{r_{cg},k-1}$ from Equation (5.65),

$$\hat{U}_{k-1}e_{r_{cg},k-1} = \hat{U}_{k-1}e_{r,k-1} - \hat{U}_{k-1}\hat{T}_{k-1}^T \left[\hat{r}_{cg/c,k-1}\times\right] e_{A,k-1} + \hat{U}_{k-1}\hat{T}_{k-1}^T e_{r_{cg/c},k-1}. \quad (5.70)$$

The error propagation for the velocity states can then be expressed as

$$\begin{aligned}
e_{v,k} =& e_{v,k-1} - \hat{T}_{k-1}^T \left[\Delta\hat{v}_{ng,k}\times\right] e_{A,k-1} + \hat{T}_{k-1}^T e_{\Delta v_{ng},k} \\
&+ \hat{G}_{k-1}\left(e_{r,k-1} + \hat{T}_{k-1}^T e_{r_{cg/c},k-1} - \hat{T}_{k-1}^T \left[\hat{r}_{cg/c,k-1}\times\right] e_{A,k-1}\right)\Delta t_k - \frac{\Delta t_k}{2}\left(\hat{U}_{k-1}e_{r,k-1}\right. \\
&- \hat{U}_{k-1}\hat{T}_{k-1}^T \left[\hat{r}_{cg/c,k-1}\times\right] e_{A,k-1} + \hat{U}_{k-1}\hat{T}_{k-1}^T e_{r_{cg/c},k-1} + \hat{G}_{k-1}\hat{T}_{k-1}^T \left[\hat{r}_{cg/c,k-1}\times\right] e_{\Delta\phi,k} \\
&\left.- \hat{G}_{k-1}\hat{T}_{k-1}^T \left[\Delta\hat{\phi}_k\times\right] e_{r_{cg/c},k-1} - \hat{G}_{k-1}\hat{T}_{k-1}^T \left[\hat{r}_{cg/c,k-1}\times\right]\left[\Delta\hat{\phi}_k\times\right] e_{A,k-1}\right). \quad (5.71)
\end{aligned}$$

Finally, given the error dynamics for the coned rotation and sculled velocity vectors, the results in Equations (5.15) and (5.29) can be substituting, giving the error propagation in terms of the measurement errors as

$$\begin{aligned}
e_{v,k} =& \Delta t_k\left(\hat{G}_{k-1} - \frac{1}{2}\hat{U}_{k-1}\right)e_{r,k-1} + e_{v,k-1} \\
&+ \left\{\frac{\Delta t_k}{2}\hat{G}_{k-1}\hat{T}_{k-1}^T \left[\hat{r}_{cg/c,k-1}\times\right]\left[\Delta\hat{\phi}_k\times\right] - \hat{T}_{k-1}^T \left[\Delta\hat{v}_{ng,k}\times\right]\right. \\
&\left.\qquad - \Delta t_k\left(\hat{G}_{k-1} - \frac{1}{2}\hat{U}_{k-1}\right)\hat{T}_{k-1}^T \left[\hat{r}_{cg/c,k-1}\times\right]\right\}e_{A,k-1} \\
&+ \Delta t_k\left\{\left(\hat{G}_{k-1} - \frac{1}{2}\hat{U}_{k-1}\right)\hat{T}_{k-1}^T + \frac{1}{2}\hat{G}_{k-1}\hat{T}_{k-1}^T \left[\Delta\hat{\phi}_k\times\right]\right\}e_{r_{cg/c},k-1} \\
&+ \sum_{i=1}^{\ell}\left(\hat{T}_{k-1}^T + \hat{T}_{k-1}^T\Xi_{con,i} + \frac{1}{2}\hat{T}_{k-1}^T \left[\hat{\theta}_\ell\times\right]\right)e_{\Delta v,i} \\
&+ \sum_{i=1}^{\ell}\left\{\hat{T}_{k-1}^T\Xi_{scul,i} - \frac{1}{2}\hat{T}_{k-1}^T \left[\hat{v}_\ell\times\right] - \frac{\Delta t_k}{2}\hat{G}_{k-1}\hat{T}_{k-1}^T \left[\hat{r}_{cg/c,k-1}\times\right]\left(I_{3\times3} + \Xi_{con,i}\right)\right\}e_{\Delta\theta,i}.
\end{aligned}$$

$$(5.72)$$

Therefore, Equation (5.72) expresses the propagation of estimation errors in the vehicle's center of gravity location and its position, attitude, and the individual incremental angle and velocity measurements into the estimation error for velocity. It should be noted that measurements $\Delta\boldsymbol{\theta}_i$, $\Delta\boldsymbol{v}_i$ $\forall i \in \{1, 2, \ldots, \ell\}$ are obtained and processed during the interval $[t_{k-1}, t_k]$.

5.6.3. Position Error Dynamics. Similar to the expression of velocity error, the position error is simply defined as

$$\boldsymbol{e}_{r,k} = \boldsymbol{r}_k - \hat{\boldsymbol{r}}_k. \tag{5.73}$$

Combining the propagation of the position estimate for a vehicle aided by strapdown inertial sensors is shown in Equation (4.33a), and noting that Δt_k is taken to be deterministic, the error dynamics for the position estimate can be stated as

$$
\begin{aligned}
\boldsymbol{e}_{r,k} =& \boldsymbol{r}_{k-1} - \hat{\boldsymbol{r}}_{k-1} + \Delta t_k \left(\boldsymbol{v}_{k-1} - \hat{\boldsymbol{v}}_{k-1} \right) + \boldsymbol{T}_{k-1}^T \Delta \boldsymbol{r}_{ng,k} - \hat{\boldsymbol{T}}_{k-1}^T \Delta \hat{\boldsymbol{r}}_{ng,k} + \frac{\Delta t_k^2}{2} \left(\boldsymbol{g}_{k-1} - \hat{\boldsymbol{g}}_{k-1} \right) \\
& - \frac{1}{6} \left(\boldsymbol{G}_{k-1} \boldsymbol{T}_{k-1}^T \left[\boldsymbol{r}_{cg/c,k-1} \times \right] \Delta \boldsymbol{\phi}_k - \hat{\boldsymbol{G}}_{k-1} \hat{\boldsymbol{T}}_{k-1}^T \left[\hat{\boldsymbol{r}}_{cg/c,k-1} \times \right] \Delta \hat{\boldsymbol{\phi}}_k \right) \Delta t_k^2.
\end{aligned}
\tag{5.74}
$$

Using the results of Section 5.6.2, many terms within Equation (5.74) can be simplified. Given the results in Equation (5.62), and the definition that $\Delta \boldsymbol{r}_{ng,k} = \Delta \hat{\boldsymbol{r}}_{ng,k} + \boldsymbol{e}_{\Delta r_{ng},k}$, it can be shown that

$$\boldsymbol{T}_{k-1}^T \Delta \boldsymbol{r}_{ng,k} - \hat{\boldsymbol{T}}_{k-1}^T \Delta \hat{\boldsymbol{r}}_{ng,k} = \hat{\boldsymbol{T}}_{k-1}^T \boldsymbol{e}_{\Delta r_{ng},k} - \hat{\boldsymbol{T}}_{k-1}^T \left[\Delta \hat{\boldsymbol{r}}_{ng,k} \times \right] \boldsymbol{e}_{A,k-1}. \tag{5.75}$$

Additionally, from Equation (5.66),

$$\boldsymbol{g}_{k-1} - \hat{\boldsymbol{g}}_{k-1} = \hat{\boldsymbol{G}}_{k-1} \boldsymbol{e}_{r,k-1} + \hat{\boldsymbol{G}}_{k-1} \hat{\boldsymbol{T}}_{k-1}^T \boldsymbol{e}_{r_{cg/c},k-1} - \hat{\boldsymbol{G}}_{k-1} \hat{\boldsymbol{T}}_{k-1}^T \left[\hat{\boldsymbol{r}}_{cg/c,k-1} \times \right] \boldsymbol{e}_{A,k-1}.$$

The error dynamics, dictating the propagation of the error in the position estimate are then stated as

$$
\begin{aligned}
\boldsymbol{e}_{r,k} =& \boldsymbol{e}_{r,k-1} + \Delta t_k \boldsymbol{e}_{v,k-1} + \hat{\boldsymbol{T}}_{k-1}^T \boldsymbol{e}_{\Delta r_{ng},k} - \hat{\boldsymbol{T}}_{k-1}^T \left[\Delta \hat{\boldsymbol{r}}_{ng,k} \times \right] \boldsymbol{e}_{A,k-1} \\
&+ \frac{\Delta t_k^2}{2} \left(\hat{\boldsymbol{G}}_{k-1} \boldsymbol{e}_{r,k-1} + \hat{\boldsymbol{G}}_{k-1} \hat{\boldsymbol{T}}_{k-1}^T \boldsymbol{e}_{r_{cg/c},k-1} - \hat{\boldsymbol{G}}_{k-1} \hat{\boldsymbol{T}}_{k-1}^T \left[\hat{\boldsymbol{r}}_{cg/c,k-1} \times \right] \boldsymbol{e}_{A,k-1} \right) \\
&- \frac{\Delta t_k^2}{6} \Bigg\{ \hat{\boldsymbol{U}}_{k-1} \boldsymbol{e}_{r,k-1} - \hat{\boldsymbol{U}}_{k-1} \hat{\boldsymbol{T}}_{k-1}^T \left[\hat{\boldsymbol{r}}_{cg/c,k-1} \times \right] \boldsymbol{e}_{A,k-1} + \hat{\boldsymbol{U}}_{k-1} \hat{\boldsymbol{T}}_{k-1}^T \boldsymbol{e}_{r_{cg/c},k-1} \\
&\qquad\qquad + \hat{\boldsymbol{G}}_{k-1} \hat{\boldsymbol{T}}_{k-1}^T \left[\hat{\boldsymbol{r}}_{cg/c,k-1} \times \right] \boldsymbol{e}_{\Delta \phi,k} - \hat{\boldsymbol{G}}_{k-1} \hat{\boldsymbol{T}}_{k-1}^T \left[\Delta \hat{\boldsymbol{\phi}}_k \times \right] \boldsymbol{e}_{r_{cg/c},k-1} \\
&\qquad\qquad - \hat{\boldsymbol{G}}_{k-1} \hat{\boldsymbol{T}}_{k-1}^T \left[\hat{\boldsymbol{r}}_{cg/c,k-1} \times \right] \left[\Delta \hat{\boldsymbol{\phi}}_k \times \right] \boldsymbol{e}_{A,k-1} \Bigg\}.
\end{aligned}
\tag{5.76}
$$

and can be reorganized to

$$
\begin{aligned}
\boldsymbol{e}_{r,k} =& \left\{ \boldsymbol{I}_{3 \times 3} + \frac{\Delta t_k^2}{2} \left(\hat{\boldsymbol{G}}_{k-1} - \frac{1}{3} \hat{\boldsymbol{U}}_{k-1} \right) \right\} \boldsymbol{e}_{r,k-1} + \Delta t_k \boldsymbol{e}_{v,k-1} \\
&+ \Bigg\{ \frac{\Delta t_k^2}{6} \hat{\boldsymbol{G}}_{k-1} \hat{\boldsymbol{T}}_{k-1}^T \left[\hat{\boldsymbol{r}}_{cg/c,k-1} \times \right] \left[\Delta \hat{\boldsymbol{\phi}}_k \times \right] - \hat{\boldsymbol{T}}_{k-1}^T \left[\Delta \hat{\boldsymbol{r}}_{ng,k} \times \right] \\
&\qquad - \frac{\Delta t_k^2}{2} \left(\hat{\boldsymbol{G}}_{k-1} - \frac{1}{3} \hat{\boldsymbol{U}}_{k-1} \right) \hat{\boldsymbol{T}}_{k-1}^T \left[\hat{\boldsymbol{r}}_{cg/c,k-1} \times \right] \Bigg\} \boldsymbol{e}_{A,k-1} \\
&+ \frac{\Delta t_k^2}{2} \left\{ \left(\hat{\boldsymbol{G}}_{k-1} - \frac{1}{3} \hat{\boldsymbol{U}}_{k-1} \right) \hat{\boldsymbol{T}}_{k-1}^T + \frac{1}{3} \hat{\boldsymbol{G}}_{k-1} \hat{\boldsymbol{T}}_{k-1}^T \left[\Delta \hat{\boldsymbol{\phi}}_k \times \right] \right\} \boldsymbol{e}_{r_{cg/c},k-1} \\
&+ \hat{\boldsymbol{T}}_{k-1}^T \boldsymbol{e}_{\Delta r_{ng},k} - \frac{\Delta t_k^2}{6} \hat{\boldsymbol{G}}_{k-1} \hat{\boldsymbol{T}}_{k-1}^T \left[\hat{\boldsymbol{r}}_{cg/c,k-1} \times \right] \boldsymbol{e}_{\Delta \phi,k}.
\end{aligned}
\tag{5.77}
$$

The previously determined propagation of errors through the coning algorithm in Equation (5.15) allows the expression

$$
\hat{\boldsymbol{G}}_{k-1} \hat{\boldsymbol{T}}_{k-1}^T \left[\hat{\boldsymbol{r}}_{cg/c,k-1} \times \right] \boldsymbol{e}_{\Delta \phi,k} = \sum_{i=1}^{\ell} \hat{\boldsymbol{G}}_{k-1} \hat{\boldsymbol{T}}_{k-1}^T \left[\hat{\boldsymbol{r}}_{cg/c,k-1} \times \right] \left(\boldsymbol{I}_{3 \times 3} + \boldsymbol{\Xi}_{con,i} \right) \boldsymbol{e}_{\Delta \theta,i}, \tag{5.78}
$$

which describes the propagation of errors in the incremental angle measurements through the coning-compensated rotation. Similarly, substituting Equation (5.56), the term containing the error in the scrolling-corrected change in position can be expressed as

$$\hat{T}_{k-1}^T e_{\Delta r_{ng},k} = \sum_{i=1}^{\ell} \hat{T}_{k-1}^T X_{\Delta v,i} e_{\Delta\theta,i} + \sum_{i=1}^{\ell} \hat{T}_{k-1}^T X_{\Delta\theta,i} e_{\Delta v,i}. \tag{5.79}$$

Therefore, Equation (5.77) can be restated by substituting Equations (5.78) and (5.79), including the contribution of errors from the measurements and performed coning and scrolling corrections, as

$$\begin{aligned}
e_{r,k} =& \left\{ I_{3\times3} + \frac{\Delta t_k^2}{2} \left(\hat{G}_{k-1} - \frac{1}{3}\hat{U}_{k-1} \right) \right\} e_{r,k-1} + \Delta t_k e_{v,k-1} \\
&+ \left\{ \frac{\Delta t_k^2}{6} \hat{T}_{k-1}^T \left[\hat{r}_{cg/c,k-1}\times \right] \left[\Delta\hat{\phi}_k\times \right] - \hat{T}_{k-1}^T \left[\Delta\hat{r}_{ng,k}\times \right] \right. \\
&\qquad \left. - \frac{\Delta t_k^2}{2} \left(\hat{G}_{k-1} - \frac{1}{3}\hat{U}_{k-1} \right) \hat{T}_{k-1}^T \left[\hat{r}_{cg/c,k-1}\times \right] \right\} e_{A,k-1} \\
&+ \frac{\Delta t_k^2}{2} \left\{ \left(\hat{G}_{k-1} - \frac{1}{3}\hat{U}_{k-1} \right) \hat{T}_{k-1}^T + \frac{1}{3}\hat{G}_{k-1}\hat{T}_{k-1}^T \left[\Delta\hat{\phi}_k\times \right] \right\} e_{r_{cg/c},k-1} \\
&+ \sum_{i=1}^{\ell} \left\{ \hat{T}_{k-1}^T X_{\Delta v,i} - \frac{\Delta t_k^2}{6}\hat{G}_{k-1}\hat{T}_{k-1}^T \left[\hat{r}_{cg/c,k-1}\times \right] (I_{3\times3} + \Xi_{con,i}) \right\} e_{\Delta\theta,i} \\
&+ \sum_{i=1}^{\ell} \hat{T}_{k-1}^T X_{\Delta\theta,i} e_{\Delta v,i} \tag{5.80}
\end{aligned}$$

5.7. INCORPORATING THE STRAPDOWN SENSOR MODEL

As shown in Section 4.3, a number of parameters corrupt the strapdown inertial sensor measurements including bias, scale-factor, axes nonorthogonality, frame misalignment, and white noise. In Section 5.2 the contribution of common strapdown sensor error sources to the error in each individual measurement error was shown. Often, information about these errors is available, either provided by the manufacturer or determined experimentally

by the user. Given an initial distribution of each error source and a description for the temporal evolution of those error sources, the dynamics and contribution of each error source into the state estimation error can be determined. As such, these sources of corruption are often estimated directly through the augmentation of the vehicle's state vector with the estimated parameters, or, alternatively, their effects on the state uncertainty can be directly acknowledged through consider filtering [33].

To determine the contribution to the state estimation error by the error in the estimated strapdown sensor corruption sources, the position, velocity, and attitude errors must be expressed as functions of the estimation error for each of these parameters. Section 5.7.1 derives the propagation of gyro measurement errors into the attitude estimate, while Sections 5.7.2 and 5.7.3 derive the propagation of gyro and accelerometer errors into the velocity and position estimates, respectively.

5.7.1. Attitude. Considering the gyro measurements to be corrupted by bias, scale factor, misalignment, nonorthogonality, and noise error sources, the propagation of these errors into the attitude estimate is given by the combination of Equations (5.4a) and (5.59), giving the component containing the measurement errors as

$$
\begin{aligned}
\sum_{i=1}^{\ell} \left(I_{3\times3} + \Xi_{con,i} \right) e_{\Delta\theta,i} = &- \sum_{i=1}^{\ell} \left(I_{3\times3} + \Xi_{con,i} \right) [\Delta\theta_{m,i} \diagdown] e_{s_g,i} \\
&+ \sum_{i=1}^{\ell} \left(I_{3\times3} + \Xi_{con,i} \right) [\Delta\theta_{m,i} \times] e_{m_g,i} \\
&- \sum_{i=1}^{\ell} \left(I_{3\times3} + \Xi_{con,i} \right) [\Delta\theta_{m,i} *] e_{n_g,i} \\
&- \sum_{i=1}^{\ell} \left(I_{3\times3} + \Xi_{con,i} \right) e_{b_g,i} - \sum_{i=1}^{\ell} \left(I_{3\times3} + \Xi_{con,i} \right) w_{g,i}. \quad (5.81)
\end{aligned}
$$

Using the model in Equation (5.81), there are no assumptions about the error sources themselves that are not implicit to the IMU model itself. To simplify for algorithmic implementation, recognize that the change in the error sources over any given interval is

expected to be small, such that $\boldsymbol{b}_{g,i}$, $\boldsymbol{s}_{g,i}$, $\boldsymbol{n}_{g,i}$, and $\boldsymbol{m}_{g,i}$ can be approximated as constant over the coning interval, or

$$\dot{\boldsymbol{b}}_{g,i} \approx \boldsymbol{0}, \qquad \dot{\boldsymbol{s}}_{g,i} \approx \boldsymbol{0}, \qquad \dot{\boldsymbol{n}}_{g,i} \approx \boldsymbol{0}, \qquad \text{and} \qquad \dot{\boldsymbol{m}}_{g,i} \approx \boldsymbol{0},$$

Equation (5.81) can be expressed as

$$\sum_{i=1}^{\ell} \left(\boldsymbol{I}_{3\times3} + \boldsymbol{\Xi}_{con,i} \right) \boldsymbol{e}_{\Delta\theta,i} = -\boldsymbol{L}_{s_g} \boldsymbol{e}_{s_g,k} + \boldsymbol{L}_{m_g} \boldsymbol{e}_{m_g,k} - \boldsymbol{L}_{n_g} \boldsymbol{e}_{n_g,k} - \boldsymbol{L}_{b_g} \boldsymbol{e}_{b_g,k} - \boldsymbol{w}_{A,g} \qquad (5.82)$$

where

$$\boldsymbol{L}_{s_g} \overset{\Delta}{=} [\boldsymbol{\theta}_{m,\ell}\diagdown] + \sum_{i=1}^{\ell} \boldsymbol{\Xi}_{con,i}[\Delta\boldsymbol{\theta}_{m,i}\diagdown] \qquad (5.83a)$$

$$\boldsymbol{L}_{m_g} \overset{\Delta}{=} [\boldsymbol{\theta}_{m,\ell}\times] + \sum_{i=1}^{\ell} \boldsymbol{\Xi}_{con,i}[\Delta\boldsymbol{\theta}_{m,i}\times] \qquad (5.83b)$$

$$\boldsymbol{L}_{n_g} \overset{\Delta}{=} [\boldsymbol{\theta}_{m,\ell}*] + \sum_{i=1}^{\ell} \boldsymbol{\Xi}_{con,i}[\Delta\boldsymbol{\theta}_{m,i}*] \qquad (5.83c)$$

$$\boldsymbol{L}_{b_g} \overset{\Delta}{=} \ell\boldsymbol{I}_{3\times3} + \sum_{i=1}^{\ell} \boldsymbol{\Xi}_{con,i} \qquad (5.83d)$$

$$\boldsymbol{w}_{A,g} \overset{\Delta}{=} \sum_{i=1}^{\ell} \left(\boldsymbol{I}_{3\times3} + \boldsymbol{\Xi}_{con,i} \right) \boldsymbol{w}_{g,i}. \qquad (5.83e)$$

are defined to simplify the notation and isolate the propagation of the gyro bias, scale factor, misalignment, nonorthogonality, and noise into the attitude estimate. Additionally, note that $\boldsymbol{\theta}_{m,\ell}$ is simply the sum of the measurements, i.e. $\boldsymbol{\theta}_{m,\ell} = \sum_{i=1}^{\ell} \Delta\boldsymbol{\theta}_{m,i}$. Therefore, the attitude error, including the contribution from each of the gyro error sources, is

$$\boldsymbol{e}_{A,k} = \boldsymbol{T}(\Delta\hat{\boldsymbol{\phi}}_k)\boldsymbol{e}_{A,k-1} - \boldsymbol{L}_{s_g} \boldsymbol{e}_{s_g,k} + \boldsymbol{L}_{m_g} \boldsymbol{e}_{m_g,k} - \boldsymbol{L}_{n_g} \boldsymbol{e}_{n_g,k} - \boldsymbol{L}_{b_g} \boldsymbol{e}_{b_g,k} - \boldsymbol{w}_{A,g}. \qquad (5.84)$$

It is important to note that the noise is not assumed to be constant over the coning interval and requires special attention for implementation.

5.7.2. Velocity. Given that both the gyros and accelerometers can be corrupted by bias, scale factor, misalignment, nonorthogonality, and noise error sources, the error in the velocity estimate will be dependent upon the error in these parameters. Therefore, combining Equation (5.4a) with Equation (5.72), the component mapping errors in the accelerometer measurements to the velocity becomes

$$
\begin{aligned}
\sum_{i=1}^{\ell} \hat{\boldsymbol{T}}_{k-1}^T \left(\boldsymbol{N}_\theta + \boldsymbol{\Xi}_{con,i} \right) \boldsymbol{e}_{\Delta v,i} = & -\sum_{i=1}^{\ell} \hat{\boldsymbol{T}}_{k-1}^T \left(\boldsymbol{N}_\theta + \boldsymbol{\Xi}_{con,i} \right) [\Delta \boldsymbol{v}_{m,i} \diagdown] \boldsymbol{e}_{s_a,i} \\
& + \sum_{i=1}^{\ell} \hat{\boldsymbol{T}}_{k-1}^T \left(\boldsymbol{N}_\theta + \boldsymbol{\Xi}_{con,i} \right) [\Delta \boldsymbol{v}_{m,i} \times] \boldsymbol{e}_{m_a,i} \\
& - \sum_{i=1}^{\ell} \hat{\boldsymbol{T}}_{k-1}^T \left(\boldsymbol{N}_\theta + \boldsymbol{\Xi}_{con,i} \right) [\Delta \boldsymbol{v}_{m,i} *] \boldsymbol{e}_{n_a,i} \\
& - \sum_{i=1}^{\ell} \hat{\boldsymbol{T}}_{k-1}^T \left(\boldsymbol{N}_\theta + \boldsymbol{\Xi}_{con,i} \right) \boldsymbol{e}_{b_a,i} \\
& - \sum_{i=1}^{\ell} \hat{\boldsymbol{T}}_{k-1}^T \left(\boldsymbol{N}_\theta + \boldsymbol{\Xi}_{con,i} \right) \boldsymbol{w}_{a,i}, \qquad (5.85)
\end{aligned}
$$

where

$$
\boldsymbol{N}_\theta = \boldsymbol{I}_{3\times 3} + \frac{1}{2} \left[\hat{\boldsymbol{\theta}}_\ell \times \right] \qquad (5.86)
$$

is defined to simplify notation. Again applying the assumption that the bias, scale factor, misalignment, and nonorthogonality errors are constant over the major interval, and defining

$$
\boldsymbol{V}_{s_a} \overset{\Delta}{=} \hat{\boldsymbol{T}}_{k-1}^T \left\{ \boldsymbol{N}_\theta [\boldsymbol{v}_{m,\ell} \diagdown] + \sum_{i=1}^{\ell} \boldsymbol{\Xi}_{con,i} [\Delta \boldsymbol{v}_{m,i} \diagdown] \right\} \qquad (5.87a)
$$

$$
\boldsymbol{V}_{m_a} \overset{\Delta}{=} \hat{\boldsymbol{T}}_{k-1}^T \left\{ \boldsymbol{N}_\theta [\boldsymbol{v}_{m,\ell} \times] + \sum_{i=1}^{\ell} \boldsymbol{\Xi}_{con,i} [\Delta \boldsymbol{v}_{m,i} \times] \right\} \qquad (5.87b)
$$

$$V_{n_a} \triangleq \hat{T}_{k-1}^T \left\{ N_\theta [\boldsymbol{v}_{m,\ell}*] + \sum_{i=1}^{\ell} \boldsymbol{\Xi}_{con,i} [\Delta \boldsymbol{v}_{m,i}*] \right\} \qquad (5.87c)$$

$$V_{b_a} \triangleq \hat{T}_{k-1}^T \left(\ell N_\theta + \sum_{i=1}^{\ell} \boldsymbol{\Xi}_{con,i} \right) \qquad (5.87d)$$

$$\boldsymbol{w}_{V,a} \triangleq \sum_{i=1}^{\ell} \hat{T}_{k-1}^T \left(N_\theta + \boldsymbol{\Xi}_{con,i} \right) \boldsymbol{w}_{a,i}, \qquad (5.87e)$$

the term describing the propagation of errors from the accelerometer measurements into the velocity estimate is then given by

$$\sum_{i=1}^{\ell} \hat{T}_{k-1}^T \left(N_\theta + \boldsymbol{\Xi}_{con,i} \right) \boldsymbol{e}_{\Delta v,i} = - V_{s_a} \boldsymbol{e}_{s_a,k} + V_{m_a} \boldsymbol{e}_{m_a,k} - V_{n_a} \boldsymbol{e}_{n_a,k} - V_{b_a} \boldsymbol{e}_{b_a,k} - \boldsymbol{w}_{V,a}. \quad (5.88)$$

Similarly, by combining Equation (5.4a) with Equation (5.72), defining the mapping of each error in the gyro measurement into the velocity error as

$$V_{s_g} \triangleq \sum_{i=1}^{\ell} \hat{T}_{k-1}^T \boldsymbol{\Xi}_{scul,i} [\Delta \boldsymbol{\theta}_{m,i} \diagdown]$$
$$- \frac{1}{2} \left(\hat{T}_{k-1}^T [\hat{\boldsymbol{v}}_\ell \times] [\boldsymbol{\theta}_{m,\ell} \diagdown] + \Delta t_k \hat{G}_{k-1} \hat{T}_{k-1}^T \left[\hat{\boldsymbol{r}}_{cg/c,k-1} \times \right] L_{s_g} \right) \qquad (5.89a)$$

$$V_{m_g} \triangleq \sum_{i=1}^{\ell} \hat{T}_{k-1}^T \boldsymbol{\Xi}_{scul,i} [\Delta \boldsymbol{\theta}_{m,i} \times]$$
$$- \frac{1}{2} \left(\hat{T}_{k-1}^T [\hat{\boldsymbol{v}}_\ell \times] [\boldsymbol{\theta}_{m,\ell} \times] + \Delta t_k \hat{G}_{k-1} \hat{T}_{k-1}^T \left[\hat{\boldsymbol{r}}_{cg/c,k-1} \times \right] L_{m_g} \right) \qquad (5.89b)$$

$$V_{n_g} \triangleq \sum_{i=1}^{\ell} \hat{T}_{k-1}^T \boldsymbol{\Xi}_{scul,i} [\Delta \boldsymbol{\theta}_{m,i}*]$$
$$- \frac{1}{2} \left(\hat{T}_{k-1}^T [\hat{\boldsymbol{v}}_\ell \times] [\boldsymbol{\theta}_{m,\ell}*] + \Delta t_k \hat{G}_{k-1} \hat{T}_{k-1}^T \left[\hat{\boldsymbol{r}}_{cg/c,k-1} \times \right] L_{n_g} \right) \qquad (5.89c)$$

$$V_{b_g} \triangleq \sum_{i=1}^{\ell} \hat{T}_{k-1}^T \boldsymbol{\Xi}_{scul,i} - \frac{1}{2} \left(\hat{T}_{k-1}^T [\hat{\boldsymbol{v}}_\ell \times] + \Delta t_k \hat{G}_{k-1} \hat{T}_{k-1}^T \left[\hat{\boldsymbol{r}}_{cg/c,k-1} \times \right] L_{s_b} \right) \qquad (5.89d)$$

$$\boldsymbol{w}_{V,g} \triangleq \sum_{i=1}^{\ell} \hat{T}_{k-1}^T \left(\boldsymbol{\Xi}_{scul,i} - \frac{1}{2} [\hat{\boldsymbol{v}}_\ell \times] \right) \boldsymbol{w}_{g,i} - \frac{\Delta t_k}{2} \hat{G}_{k-1} \hat{T}_{k-1}^T \left[\hat{\boldsymbol{r}}_{cg/c,k-1} \times \right] \boldsymbol{w}_{A,g}, \qquad (5.89e)$$

and incorporating the definitions from Equation (5.87), it can be shown that the velocity error propagation is

$$
\begin{aligned}
\boldsymbol{e}_{v,k} = {} & \Delta t_k \left(\hat{\boldsymbol{G}}_{k-1} - \frac{1}{2} \hat{\boldsymbol{U}}_{k-1} \right) \boldsymbol{e}_{r,k-1} + \boldsymbol{e}_{v,k-1} \\
& + \left\{ \frac{\Delta t_k}{2} \hat{\boldsymbol{G}}_{k-1} \hat{\boldsymbol{T}}_{k-1}^T \left[\hat{\boldsymbol{r}}_{cg/c,k-1} \times \right] \left[\Delta \hat{\boldsymbol{\phi}}_k \times \right] - \hat{\boldsymbol{T}}_{k-1}^T \left[\Delta \hat{\boldsymbol{v}}_{ng,k} \times \right] \right. \\
& \qquad \left. - \Delta t_k \left(\hat{\boldsymbol{G}}_{k-1} - \frac{1}{2} \hat{\boldsymbol{U}}_{k-1} \right) \hat{\boldsymbol{T}}_{k-1}^T \left[\hat{\boldsymbol{r}}_{cg/c,k-1} \times \right] \right\} \boldsymbol{e}_{A,k-1} \\
& + \Delta t_k \left\{ \left(\hat{\boldsymbol{G}}_{k-1} - \frac{1}{2} \hat{\boldsymbol{U}}_{k-1} \right) \hat{\boldsymbol{T}}_{k-1}^T + \frac{1}{2} \hat{\boldsymbol{G}}_{k-1} \hat{\boldsymbol{T}}_{k-1}^T \left[\Delta \hat{\boldsymbol{\phi}}_k \times \right] \right\} \boldsymbol{e}_{r_{cg/c},k-1} \\
& - \boldsymbol{V}_{s_a} \boldsymbol{e}_{s_a,k} + \boldsymbol{V}_{m_a} \boldsymbol{e}_{m_a,k} - \boldsymbol{V}_{n_a} \boldsymbol{e}_{n_a,k} - \boldsymbol{V}_{b_a} \boldsymbol{e}_{b_a,k} - \boldsymbol{w}_{V,a} \\
& - \boldsymbol{V}_{s_g} \boldsymbol{e}_{s_g,k} + \boldsymbol{V}_{m_g} \boldsymbol{e}_{m_g,k} - \boldsymbol{V}_{n_g} \boldsymbol{e}_{n_g,k} - \boldsymbol{V}_{b_g} \boldsymbol{e}_{b_g,k} - \boldsymbol{w}_{V,g}.
\end{aligned}
\tag{5.90}
$$

The error propagation in Equation (5.90) describes the dynamics for the error in the velocity estimate given that the navigation system is dependent upon strapdown inertial sensors and uses a coning and sculling algorithm. To simplify the error propagation, it has been assumed in the derivation of Equation (5.90) that the bias, scale factor, misalignment and nonorthogonality errors in both the accelerometers and gyroscopes are constant over the major time step.

5.7.3. Position. With the definition of the velocity error dynamics written in terms of the strapdown sensor errors in Equation (5.90), their propagation into the position error follows similarly. The mappings defining the propagation of gyro measurement errors into the position estimate, through the application of coning and scrolling algorithms, can then be defined as

$$
\boldsymbol{R}_{s_g} \triangleq \sum_{i=1}^{\ell} \hat{\boldsymbol{T}}_{k-1}^T \boldsymbol{X}_{\Delta\theta,i} \left[\Delta \boldsymbol{v}_{m,i} \searrow \right] - \frac{\Delta t_k^2}{6} \hat{\boldsymbol{G}}_{k-1} \hat{\boldsymbol{T}}_{k-1}^T \left[\hat{\boldsymbol{r}}_{cg/c,k-1} \times \right] \boldsymbol{L}_{s_g}
\tag{5.91a}
$$

$$
\boldsymbol{R}_{m_g} \triangleq \sum_{i=1}^{\ell} \hat{\boldsymbol{T}}_{k-1}^T \boldsymbol{X}_{\Delta\theta,i} \left[\Delta \boldsymbol{v}_{m,i} \times \right] - \frac{\Delta t_k^2}{6} \hat{\boldsymbol{G}}_{k-1} \hat{\boldsymbol{T}}_{k-1}^T \left[\hat{\boldsymbol{r}}_{cg/c,k-1} \times \right] \boldsymbol{L}_{m_g}
\tag{5.91b}
$$

$$R_{n_g} \triangleq \sum_{i=1}^{\ell} \hat{T}_{k-1}^T X_{\Delta\theta,i}[\Delta v_{m,i}*] - \frac{\Delta t_k^2}{6} \hat{G}_{k-1}\hat{T}_{k-1}^T \left[\hat{r}_{cg/c,k-1}\times\right] L_{n_g} \tag{5.91c}$$

$$R_{b_g} \triangleq \sum_{i=1}^{\ell} \hat{T}_{k-1}^T X_{\Delta\theta,i} - \frac{\Delta t_k^2}{6} \hat{G}_{k-1}\hat{T}_{k-1}^T \left[\hat{r}_{cg/c,k-1}\times\right] L_{b_g} \tag{5.91d}$$

$$w_{R,g} \triangleq \sum_{i=1}^{\ell} \hat{T}_{k-1}^T X_{\Delta\theta,i} w_{a,i} - \frac{\Delta t_k^2}{6} \hat{G}_{k-1}\hat{T}_{k-1}^T \left[\hat{r}_{cg/c,k-1}\times\right] w_{A,g}. \tag{5.91e}$$

Additionally, the mapping for the errors in the accelerometer measurements can be defined as

$$R_{s_a} \triangleq \sum_{i=1}^{\ell} \hat{T}_{k-1}^T X_{\Delta v,i} \left[\Delta\theta_{m,i}\diagdown\right] \tag{5.92a}$$

$$R_{m_a} \triangleq \sum_{i=1}^{\ell} \hat{T}_{k-1}^T X_{\Delta v,i} \left[\Delta\theta_{m,i}\times\right] \tag{5.92b}$$

$$R_{n_a} \triangleq \sum_{i=1}^{\ell} \hat{T}_{k-1}^T X_{\Delta v,i}[\Delta\theta_{m,i}*] \tag{5.92c}$$

$$R_{b_a} \triangleq \sum_{i=1}^{\ell} \hat{T}_{k-1}^T X_{\Delta v,i} \tag{5.92d}$$

$$w_{R,a} \triangleq \sum_{i=1}^{\ell} \hat{T}_{k-1}^T X_{\Delta v,i} w_{a,i}. \tag{5.92e}$$

Finally, with the mappings defined in Equations (5.91) and Equations (5.92), the error dynamics for the position become

$$
\begin{aligned}
e_{r,k} =& \left\{I_{3\times3} + \frac{\Delta t_k^2}{2}\left(\hat{G}_{k-1} - \frac{1}{3}\hat{U}_{k-1}\right)\right\} e_{r,k-1} + \Delta t_k e_{v,k-1} \\
&+ \left\{\frac{\Delta t_k^2}{6}\hat{T}_{k-1}^T \left[\hat{r}_{cg/c,k-1}\times\right] \left[\Delta\hat{\phi}_k\times\right] - \hat{T}_{k-1}^T \left[\Delta\hat{r}_{ng,k}\times\right]\right. \\
&\qquad\left. - \frac{\Delta t_k^2}{2}\left(\hat{G}_{k-1} - \frac{1}{3}\hat{U}_{k-1}\right)\hat{T}_{k-1}^T \left[\hat{r}_{cg/c,k-1}\times\right]\right\} e_{A,k-1} \\
&+ \frac{\Delta t_k^2}{2}\left\{\left(\hat{G}_{k-1} - \frac{1}{3}\hat{U}_{k-1}\right)\hat{T}_{k-1}^T + \frac{1}{3}\hat{G}_{k-1}\hat{T}_{k-1}^T \left[\Delta\hat{\phi}_k\times\right]\right\} e_{r_{cg/c},k-1}
\end{aligned}
$$

$$- R_{s_a} e_{s_a,k} + R_{m_a} e_{m_a,k} - R_{n_a} e_{n_a,k} - R_{b_a} e_{b_a,k} - w_{R,a}$$

$$- R_{s_g} e_{s_g,k} + R_{m_g} e_{m_g,k} - R_{n_g} e_{n_g,k} - R_{b_g} e_{b_g,k} - w_{R,g} \tag{5.93}$$

Equation (5.93) describes the error dynamics for the position estimate, influenced by accelerometer and gyro bias, scale factor, misalignment, and nonorthogonality which are assumed to be constant from t_{k-1} to t_k. The noise, however, is not assumed constant over the interval and thus provides a separate contribution from each measurement, requiring the definition of $w_{R,g}$ and $w_{R,a}$. Additionally, the propagation of errors through coning and scrolling corrections are accounted for in the development of the mapping terms for each error source.

5.8. COVARIANCE PROPAGATION

Let the state vector be given by the concatenated position, velocity, and attitude vectors, augmented by the estimated inertial sensor parameters, or

$$\hat{x}_k = \begin{bmatrix} \hat{r}_k^T & \hat{v}_k^T & \hat{\bar{q}}_k^T & \hat{\omega}_{\text{aug},k}^T & \hat{a}_{\text{aug},k}^T \end{bmatrix}^T ,$$

where the estimated error parameters for the gyro and accelerometer are then defined to be

$$\hat{\omega}_{\text{aug},k} = \begin{bmatrix} \hat{b}_{g,k}^T & \hat{s}_{g,k}^T & \hat{m}_{g,k}^T & \hat{n}_{g,k}^T \end{bmatrix}^T \quad \text{and} \quad \hat{a}_{\text{aug},k} = \begin{bmatrix} \hat{b}_{a,k}^T & \hat{s}_{a,k}^T & \hat{m}_{a,k}^T & \hat{n}_{a,k}^T \end{bmatrix}^T ,$$

respectively. A concatenation of the noise vectors can also be expressed as

$$w_k = \begin{bmatrix} w_{a,k}^T & w_{g,k}^T \end{bmatrix}^T . \tag{5.94}$$

As discussed in Section 3, the state uncertainty can be propagated by the navigation system within the EKF architecture via Equation (3.18). Additionally, as mentionend within the EKF development, the linearization of the dynamics about the mean of the distribution is necessary in order to propagate the covariance. Elements of the dynamics Jacobian, required for the covariance propagation, follow directly from the system error dynamics developed in Equation (5.93), Equation (5.90), and Equation (5.84), which are collected here as

$$
\begin{aligned}
\boldsymbol{e}_{r,k} =& \left\{ \boldsymbol{I}_{3\times 3} + \frac{\Delta t_k^2}{2}\left(\hat{\boldsymbol{G}}_{k-1} - \frac{1}{3}\hat{\boldsymbol{U}}_{k-1}\right) \right\} \boldsymbol{e}_{r,k-1} + \Delta t_k \boldsymbol{e}_{v,k-1} \\
&+ \left\{ \frac{\Delta t_k^2}{6}\hat{\boldsymbol{T}}_{k-1}^T \left[\hat{\boldsymbol{r}}_{cg/c,k-1}\times\right]\left[\Delta\hat{\boldsymbol{\phi}}_k\times\right] - \hat{\boldsymbol{T}}_{k-1}^T \left[\Delta\hat{\boldsymbol{r}}_{ng,k}\times\right] \right.\\
&\qquad\qquad \left. - \frac{\Delta t_k^2}{2}\left(\hat{\boldsymbol{G}}_{k-1} - \frac{1}{3}\hat{\boldsymbol{U}}_{k-1}\right) \hat{\boldsymbol{T}}_{k-1}^T \left[\hat{\boldsymbol{r}}_{cg/c,k-1}\times\right] \right\} \boldsymbol{e}_{A,k-1} \\
&+ \frac{\Delta t_k^2}{2}\left\{ \left(\hat{\boldsymbol{G}}_{k-1} - \frac{1}{3}\hat{\boldsymbol{U}}_{k-1}\right) \hat{\boldsymbol{T}}_{k-1}^T + \frac{1}{3}\hat{\boldsymbol{G}}_{k-1}\hat{\boldsymbol{T}}_{k-1}^T \left[\Delta\hat{\boldsymbol{\phi}}_k\times\right] \right\} \boldsymbol{e}_{r_{cg/c},k-1} \\
&- \boldsymbol{R}_{s_a}\boldsymbol{e}_{s_a,k} + \boldsymbol{R}_{m_a}\boldsymbol{e}_{m_a,k} - \boldsymbol{R}_{n_a}\boldsymbol{e}_{n_a,k} - \boldsymbol{R}_{b_a}\boldsymbol{e}_{b_a,k} - \boldsymbol{w}_{R,a} \\
&- \boldsymbol{R}_{s_g}\boldsymbol{e}_{s_g,k} + \boldsymbol{R}_{m_g}\boldsymbol{e}_{m_g,k} - \boldsymbol{R}_{n_g}\boldsymbol{e}_{n_g,k} - \boldsymbol{R}_{b_g}\boldsymbol{e}_{b_g,k} - \boldsymbol{w}_{R,g}
\end{aligned}
\tag{5.95a}
$$

$$
\begin{aligned}
\boldsymbol{e}_{v,k} =& \Delta t_k \left(\hat{\boldsymbol{G}}_{k-1} - \frac{1}{2}\hat{\boldsymbol{U}}_{k-1}\right) \boldsymbol{e}_{r,k-1} + \boldsymbol{e}_{v,k-1} \\
&+ \left\{ \frac{\Delta t_k}{2}\hat{\boldsymbol{G}}_{k-1}\hat{\boldsymbol{T}}_{k-1}^T \left[\hat{\boldsymbol{r}}_{cg/c,k-1}\times\right]\left[\Delta\hat{\boldsymbol{\phi}}_k\times\right] - \hat{\boldsymbol{T}}_{k-1}^T \left[\Delta\hat{\boldsymbol{v}}_{ng,k}\times\right] \right.\\
&\qquad\qquad \left. - \Delta t_k \left(\hat{\boldsymbol{G}}_{k-1} - \frac{1}{2}\hat{\boldsymbol{U}}_{k-1}\right) \hat{\boldsymbol{T}}_{k-1}^T \left[\hat{\boldsymbol{r}}_{cg/c,k-1}\times\right] \right\} \boldsymbol{e}_{A,k-1} \\
&+ \Delta t_k \left\{ \left(\hat{\boldsymbol{G}}_{k-1} - \frac{1}{2}\hat{\boldsymbol{U}}_{k-1}\right) \hat{\boldsymbol{T}}_{k-1}^T + \frac{1}{2}\hat{\boldsymbol{G}}_{k-1}\hat{\boldsymbol{T}}_{k-1}^T \left[\Delta\hat{\boldsymbol{\phi}}_k\times\right] \right\} \boldsymbol{e}_{r_{cg/c},k-1} \\
&- \boldsymbol{V}_{s_a}\boldsymbol{e}_{s_a,k} + \boldsymbol{V}_{m_a}\boldsymbol{e}_{m_a,k} - \boldsymbol{V}_{n_a}\boldsymbol{e}_{n_a,k} - \boldsymbol{V}_{b_a}\boldsymbol{e}_{b_a,k} - \boldsymbol{w}_{V,a} \\
&- \boldsymbol{V}_{s_g}\boldsymbol{e}_{s_g,k} + \boldsymbol{V}_{m_g}\boldsymbol{e}_{m_g,k} - \boldsymbol{V}_{n_g}\boldsymbol{e}_{n_g,k} - \boldsymbol{V}_{b_g}\boldsymbol{e}_{b_g,k} - \boldsymbol{w}_{V,g}
\end{aligned}
\tag{5.95b}
$$

$$
\boldsymbol{e}_{A,k} = \boldsymbol{T}(\Delta\hat{\boldsymbol{\phi}}_k)\boldsymbol{e}_{A,k-1} - \boldsymbol{L}_{s_g}\boldsymbol{e}_{s_g,k} + \boldsymbol{L}_{m_g}\boldsymbol{e}_{m_g,k} - \boldsymbol{L}_{n_g}\boldsymbol{e}_{n_g,k} - \boldsymbol{L}_{b_g}\boldsymbol{e}_{b_g,k} - \boldsymbol{w}_{A,g}.
\tag{5.95c}
$$

Additionally, the strapdown IMU error parameters augmenting the state vector are here taken to be constant through time, giving

$$s_{a,k} = s_{a,k-1} \qquad m_{a,k} = m_{a,k-1} \qquad n_{a,k} = n_{a,k-1} \qquad b_{a,k} = b_{a,k-1}$$

$$s_{g,k} = s_{g,k-1} \qquad m_{g,k} = m_{g,k-1} \qquad n_{g,k} = n_{g,k-1} \qquad b_{g,k} = b_{g,k-1},$$

with initial values $s_{a,0}$, $s_{g,0}$, $m_{a,0}$, $m_{g,0}$, $n_{a,0}$, $n_{g,0}$, $b_{a,0}$, and $b_{g,0}$. Additionally, the estimate is often initialized to the mean for each parameter and is here stated to be zero. With the dynamics described, and without processing external measurements, the estimation error of the IMU error parameters is expected to be constant through time. Therefore, the error dynamics for each of the strapdown IMU error parameters are expressed as

$$e_{s_a,k} = e_{s_a,k-1} \qquad e_{n_a,k} = e_{n_a,k-1} \qquad e_{m_a,k} = e_{m_a,k-1} \qquad e_{b_a,k} = e_{b_a,k-1} \qquad (5.96a)$$

$$e_{s_g,k} = e_{s_g,k-1} \qquad e_{n_g,k} = e_{n_g,k-1} \qquad e_{m_g,k} = e_{m_g,k-1} \qquad e_{b_g,k} = e_{b_g,k-1}. \qquad (5.96b)$$

Given the error dynamics in Equations (5.95) and Equations (5.96), the state estimation error dynamics can then defined by

$$e_k = F_{k-1} e_{k-1} + M_{k-1} w_{k-1}, \qquad (5.97)$$

where F_{k-1} describes the propagation of uncertainty from the previous time step through the dynamics and M_{k-1} maps the process noise, here represented by the strapdown sensor noise, into the state estimation error. The elements of F_{k-1} and M_{k-1} are given by inspection of Equations (5.95) and Equations (5.96).

6. RESULTS AND DISCUSSION

To assess the performance benefits of including the error propagation developed within this thesis, two separate simulations are considered. The first simulation, discussed in Section 6.1, examines a scenario in which attitude is being estimated through discrete attitude dead-reckoning, both with and without application of the coning algorithm. Primarily, the first simulation seeks to analyze the effect of coning motion on attitude estimation and the propagation of uncertainty, comparing the newly developed methods to several alternatives.

The second simulation inspects a lunar descent-to-landing scenario in which position, velocity, and attitude of a spacecraft are estimated through inertial navigation. Two separate navigation system configurations are compared: one employs the coning, sculling, and scrolling algorithms developed in Section 4, and the second applies using traditional dead-reckoning methods at the frequency of the inertial measurements. The trajectory examined for this scenario is limited to 40 Hz data and thus analysis with a large discrepency between the data and navigation frequency cannot be examined. The results within Section 6.2 give a baseline for comparison of the methods used for inertial navigation system employing both the traditional methods and those using coning, sculling, and scrolling corrections.

6.1. CONING SIMULATION OVERVIEW

Methods for both traditional dead-reckoning (TDR) and coned dead-reckoning (CDR) operating at a variety of frequencies are compared for the estimation of attitude within an EKF architecture. For the low-frequency cases, the attitude estimates are provided at 10 Hz, while high-frequency cases operate at 400 Hz, the same rate at which measurements are simulated. Each algorithm is then applied within several 1000 trial Monte Carlo simulations, with varying configurations, that are used to determine the con-

Table 6.1. LN-200S IMU specifications (1σ)

	Gyroscope	Accelerometer
Noise	0.07 °/√hr	35μg/√hr
Bias	1 °/hr	300 μg
Scale factor	300 ppm	100 ppm
Misalignment	0.1 mrad	0.1 mrad
Nonorthogonality	0.1 mrad	0.1 mrad

sistency of the filter's covariance propagation through an examination and comparison of the resulting error statistics. Each trial has an initial error in the attitude estimate that is sampled from a Gaussian distribution of 25 arcseconds, 1σ. For each trial, IMU measurements emulate a Northrop Grumman LN-200S[1] IMU's fiber-optic gyroscopes.

Each measurement contains corruption from scale factor, misalignment, nonorthogonality, bias, and noise error sources. Each source of error is taken to be distributed according to the LN-200S specifications seen in Table 6.1; each specification is assumed to describe the standard deviation of a zero-mean Gaussian distribution from which each error is sampled. Additionally, the measurement noise is sampled for each measurement, while each other source of corruption is taken to be constant through time. Note that the noise and bias error sources are not given in angular units, but instead describe the angle random-walk and bias repeatability as a function of measurement time or sampling frequency; by fixing the sampling frequency to 400 Hz, the distribution is defined for each measurement.

To compare the performance of CDR and TDR algorithms for state and covariance propagation, cases consisting of constant angular velocity and underlying coning motion are examined. The coning motion source is an angular velocity that generates pure coning motion, which is given by

$$\omega_c(t) = \begin{bmatrix} f\sin a\cos(ft) \\ -f\sin a\sin(ft) \\ f(1-\cos a) \end{bmatrix},\tag{6.1}$$

[1]http://www.northropgrumman.com/Capabilities/LN200FOG/Documents/ln200s.pdf

where f is the frequency of the coning motion and a is the amplitude of the coning motion. For the simulated measurements, the primary motion is generated given by an arbitrary constant angular velocity vector, here taken to be $\omega_0 = [1, 2, -3]^T \frac{\deg}{s}$. For cases including underlying coning motion, a rotating component is simply added to the motion such that $\omega(t) = \omega_0 + \omega_c(t)$. Equation (6.1) is used to generate the vector used to simulate coning motion with 50 arcseconds amplitude at coning frequencies of 40 Hz and 200 Hz.

6.1.1. Traditional Dead-Reckoning. The method here considered to be traditional dead-reckoning processes gyro measurements at the IMU sampling frequency and propagates the attitude estimate with Equation (4.3c). To compare TDR to the error propagation of the generalized coning algorithm, an examination of traditional attitude dead-reckoning and a variation thereof, is considered at both high and low-frequencies.

6.1.1.1. High-frequency propagation. Most modern IMUs are capable of providing high-frequency data, typically much more quickly than is feasible or necessary for on-board vehicle navigation systems. With this consideration, 400 Hz data being processed at the same rate is taken to be an infeasible and impractical frequency, as the computational load generated by the propagation of covariance within a navigation filter operating at this frequency would be significant for a space-qualified on-board system. In addition to the processing limitation, having a state estimate available at 400 Hz is often unnecessary. That said, it is desirable to process high-frequency data, which can help to identify underlying vibrational motion. The state estimate for high-frequency TDR is obtained using Equation (4.3c), while the covariance is propagated by Equation (3.18).

6.1.1.2. Low-frequency propagation. Several alternatives to propagating the state and covariance at the gyro measurement frequency exist. One such method assumes that the angular velocity is constant over the major interval and the high-frequency measurements are down-sampled by summing those sampled during the major interval and propagating the state and covariance with the down-sampled data. Therefore, having obtained gyro measurements generated at a high-frequency, i.e. 400 Hz, low-frequency TDR will simul-

taneously process all measurements at the navigation frequency, here chosen to be 10 Hz. Therefore, the state propagation is simply given by

$$\hat{\bar{q}}_k = \bar{q}(\hat{\boldsymbol{\theta}}_k) \otimes \hat{\bar{q}}_{k-1} = \bar{q}(\textstyle\sum_{i=1}^{\ell} \Delta\hat{\boldsymbol{\theta}}_i) \otimes \hat{\bar{q}}_{k-1},$$

which is simply Equation (4.3c) for processing a sum of the gyro measurements. Additionally, assuming that the bias, scale factor, misalignment, and nonorthogonality are constant over the time interval $(t_{k-1}, t_k]$, the error in this summed measurement is given by

$$\boldsymbol{e}_{\Delta\phi,k} = -[\boldsymbol{\theta}_{m,k} \diagdown]\boldsymbol{e}_{s,k} + [\boldsymbol{\theta}_{m,k}\times]\boldsymbol{e}_{m,k} - [\boldsymbol{\theta}_{m,k}*]\boldsymbol{e}_{n,k} - \ell\boldsymbol{e}_{b,k} - \sum_{i=1}^{\ell} \boldsymbol{w}_i, \qquad (6.2)$$

where $\boldsymbol{\theta}_{m,k} = \sum_{i=1}^{\ell} \Delta\boldsymbol{\theta}_{m,i}$ and ℓ is the number of measurements summed. The form of the Jacobian can be inferred from the substitution of Equation (6.2) and $\hat{\boldsymbol{\theta}}_k$ into Equation (3.27) for $\boldsymbol{e}_{\Delta\theta,k}$ and $\Delta\boldsymbol{\theta}_k$, respectively. It is worth noting that in this case, the process noise covariance obtained from the IMU specifications is multiplied by a factor of ℓ to account for the ℓ noise terms in Equation (6.2).

6.1.1.3. Mixed-frequency propagation. As previously mentioned, the covariance propagation is the most computationally taxing component of the inertial navigation system, while the state propagation is not typically an exceedingly complex or taxing undertaking. This is especially true within a system only estimating attitude. Thus, an additional formulation is considered to deal with the inaccuracies in assumptions made for the low-frequency propagation, which assumes that the angular velocity across the major interval is constant. Here, benefits of propagating the state at the measurement frequency are maintained by performing the state propagation as described by Equation (4.3c), while the computational load of covariance propagation is reduced by propagating with the sum of gyro measurements, as described within Section 6.1.1.2.

6.1.2. Coned Dead-Reckoning. The method of dead-reckoning using a coning algorithm, or coned dead-reckoning, is here defined to be inertial navigation with the coned rotation vector. Through the use of the coning algorithm, measurements are processed sequentially until a state estimate is desired; the propagated attitude and covariance are often provided at a lower frequency than that at which the measurements are obtained. To compare the error propagation of the coning algorithm to TDR, high- and low-frequency implementations of the CDR algorithm are considered.

6.1.2.1. High-frequency propagation. Processing gyro measurements at 400 Hz through the use of the coning algorithm leads to a single measurement being processed, simplifying the state propagation to the considered high frequency TDR case. This can be seen by examining the effect of processing a single measurement with Equation (4.17), i.e., the coning correction when a single measurement is processed will be zero. By investigating this case, the expected equivalence between the high-rate TDR and CDR can be explicitly shown. Again, the attitude estimate is propagated via Equation (4.3c), while the covariance propagation is given by Equation (3.31), when only processing a single gyro measurement.

6.1.2.2. Low-frequency propagation. The intended application of the coning algorithm is observed in the case of low-frequency coned dead-reckoning, where the high-frequency data simulated at 400 Hz is used to generate an attitude estimate at a lower frequency, 10 Hz, preserving the information gained from the high-rate data. The extra computational burden of performing the attitude and covariance propagation is removed, while the error in the estimate produced by accumulating the measurements for propagation, as is done for the low-frequency TDR approach, is decreased. The attitude is propagated via Equation (4.33) and covariance via Equation (3.18), where the dynamics Jacobian construction is implied by Equation (5.59).

6.1.3. Simulation Results. To compare the performance of each method examined, several measures of comparison are used. First, to determine whether or not each estimator is consistent, an examination of the results from Monte Carlo simulation are examined

– a comparison between the mean filter standard deviation and the Monte Carlo sample standard deviation are compared graphically for each method. A ratio of uncertainties for each method are then examined for comparison, where the averaged filter and sample standard deviations for each method are normalized by that of the high-frequency traditional dead-reckoning results. It must also be noted that each method examined processes the exact same measurements – i.e. the differences are purely due to the assumptions made in the estimator's development and cannot be attributed to discrepancies in the measurements or trajectory.

The level of credibility and consistency for the filter propagation stage is examined through the averaged normalized estimation error squared (ANEES)[2, 17]. The ANEES, $\bar{\epsilon}$, is calculated by

$$\bar{\epsilon} = \frac{1}{nM} \sum_{i=1}^{M} \epsilon_i,$$

where $\epsilon_i = (\boldsymbol{x}_i - \hat{\boldsymbol{x}}_i)^T \boldsymbol{P}_i^{-1} (\boldsymbol{x}_i - \hat{\boldsymbol{x}}_i) = \boldsymbol{e}_i^T \boldsymbol{P}_i^{-1} \boldsymbol{e}_i$ is the better-known squared Mahalanobis distance for trial i, n is the number of states, and M is the number of trials. The ANEES measure is χ^2-distributed if the estimation errors are Gaussian distributed and allows the rejection of the filter as credible at a particular level, α, given that $Pr\left(\bar{\epsilon} \in [a,b] | nM\bar{\epsilon} \sim \chi^2_{nM}\right) = 1 - \alpha$ for $a < 1 < b$ and $0 < \alpha \ll 1$, where χ^2_{nM} is a χ^2-distribution of nM degrees of freedom [17]. The interval $[a, b]$ contains 95% of the probability mass for the χ^2 distribution having a mean of one and nM degrees of freedom when $\alpha = 0.05$. The lower bound a separates the lower $\alpha/2$ of the probability mass, while the upper bound eliminates the upper $\alpha/2$. If $\bar{\epsilon} = 1$, the ANEES is perfectly consistent with the error distribution. It is necessary to note that ANEES is *not* a credibility measurement but is useful in recognizing if the filter's approximation of the uncertainty is representative of the errors, or that the filter is consistent [16]. Finally, this measure allows the recognition of estimation performance; the estimator overestimates the estimation error when the ANEES is less than one, and underestimates the

error when the ANEES is greater than one. While examining the consistency of the diagonal elements of the filter and Monte Carlo sample covariance matrices is useful, ANEES allows the direct comparison of the entire covariance structure with the estimation errors.

To simplify the presentation, the root of sums squared (RSS) of the mean estimation error, sample covariance, and average filter covariance are examined instead of the three-axis representation; these may be calculated as

$$e_{RSS,k} = \|\bar{e}_{A,k}\| \qquad \text{and} \qquad \sigma_{RSS,k} = \sqrt{\text{trace}\,(P_k)},$$

where $\bar{e}_{A,k}$ is the mean estimation error and P_k is noted to be either the sample covariance or the averaged filter covariance at time t_k. Finally, the uncertainty predicted for the different estimator configurations are directly compared by considering a normalized error between the RSS standard deviations, i.e.

$$e_{\sigma,i} = \frac{\sigma_{RSS,i} - \sigma_{RSS,ref}}{\sigma_{RSS,ref}}, \tag{6.3}$$

where $\sigma_{RSS,i}$ is the σ_{RSS} of a particular configuration and $\sigma_{RSS,ref}$ is the σ_{RSS} of a reference configuration. For all cases shown, the high-frequency traditional dead-reckoning method is taken to be the reference. The measure in Equation (6.3) is examined for both the Monte Carlo sample covariance and average filter covariance of each configuration. It should be noted that this ratio applied to the Monte Carlo sample covariances describes the error in the observed error distribution, while it describes the error in the predicted estimation error distribution by the average filter. Finally, it is useful to note that if $e_{\sigma,i} > 0$, the standard deviation of the uncertainty in the examined configuration is larger than the reference case, and if $e_{\sigma,i} < 0$ it is smaller.

6.1.3.1. No coning motion. In Figures 6.1–6.5, results from 1000 trial Monte Carlo simulations of each method are presented. Notice that when no coning motion is present, the mean estimation error is approximately zero-mean for each method, and the averaged

filter and sample covariance also describe the same uncertainty, as shown by the overlapping $1\sigma_{RSS}$ intervals. Note that only the positive $1\sigma_{RSS}$ interval are shown for each configuration to allow a greater examination of the mean estimation error. In this case, each method appears to be consistent with the Monte Carlo statistics.

Comparisons of each method, made by directly examining the uncertainty intervals, are provided in Figures 6.6–6.8. In Figures 6.6 and 6.7, the error between each configuration's covariance and the covariance for the high-frequency traditional dead-reckoning configuration are shown, where each error is also normalized by the RSS standard deviation for high-frequency traditional dead-reckoning. When examining Figure 6.6, it's clear that all methods perform similarly without coning motion, though some non-zero behavior is observed for summed dead-reckoning. While it can be stated that the state prediction from summed dead-reckoning is no longer exactly consistent with the predictions made by high-frequency traditional dead-reckoning, it should be noted that the error is very small and likely insignificant. From Figure 6.7, it becomes clear that coned dead-reckoning predicts a larger uncertainty than the other approaches, while the mixed-frequency and high-frequency traditional dead-reckoning approaches are consistent with one another and still predict a larger uncertainty than that predicted by traditional dead-reckoning. Examining the ANEES for each method in Figure 6.8 shows that each estimator's predicted uncertainty is consistent with its associated estimation errors and shows no significant deviation between the estimators applied in an environment lacking coning motion. It should again be noted that the scale on the errors is extremely small.

6.1.3.2. 40 Hz coning motion. Figures 6.9–6.13 illustrate the effects that moderate coning motion has on the attitude estimation systems under consideration. Note that, for most configurations considered here, the results are not significantly affected by the presence of coning motion; Figure 6.10 shows a significant growth in the mean error for the summed dead-reckoning method, while the $1\sigma_{RSS}$ for both the averaged filter and Monte Carlo samples are not visibly perturbed.
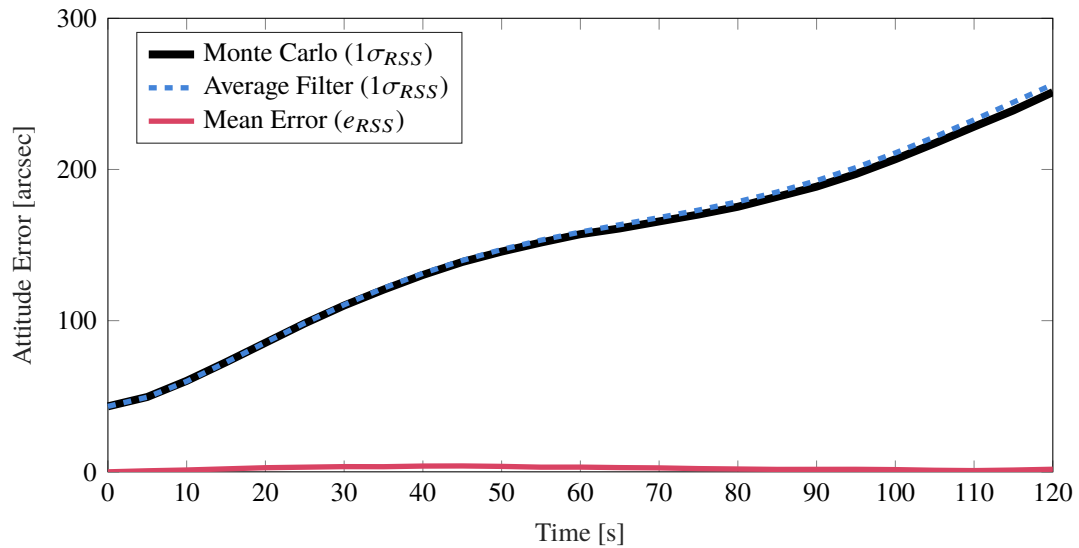
Figure 6.1. Monte Carlo simulation results for high-frequency traditional dead-reckoning; mean attitude error (RSS), averaged filter covariance ($1\sigma_{RSS}$), Monte Carlo sample covariance ($1\sigma_{RSS}$) from 1000 trials with no coning motion
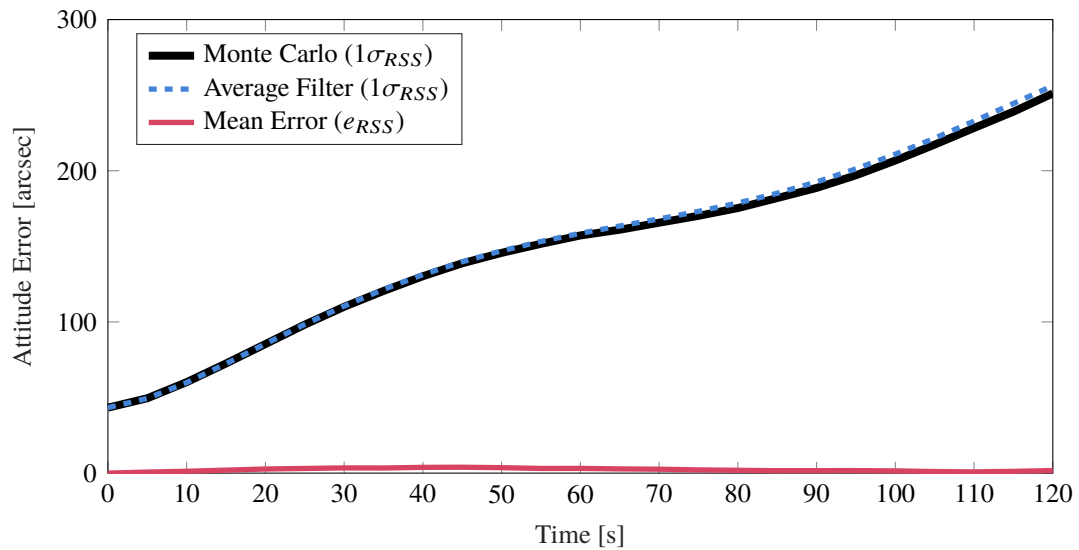

Figure 6.2. Monte Carlo simulation results for low-frequency traditional dead-reckoning; mean attitude error (RSS), averaged filter covariance ($1\sigma_{RSS}$), Monte Carlo sample covariance ($1\sigma_{RSS}$) from 1000 trials with no coning motion
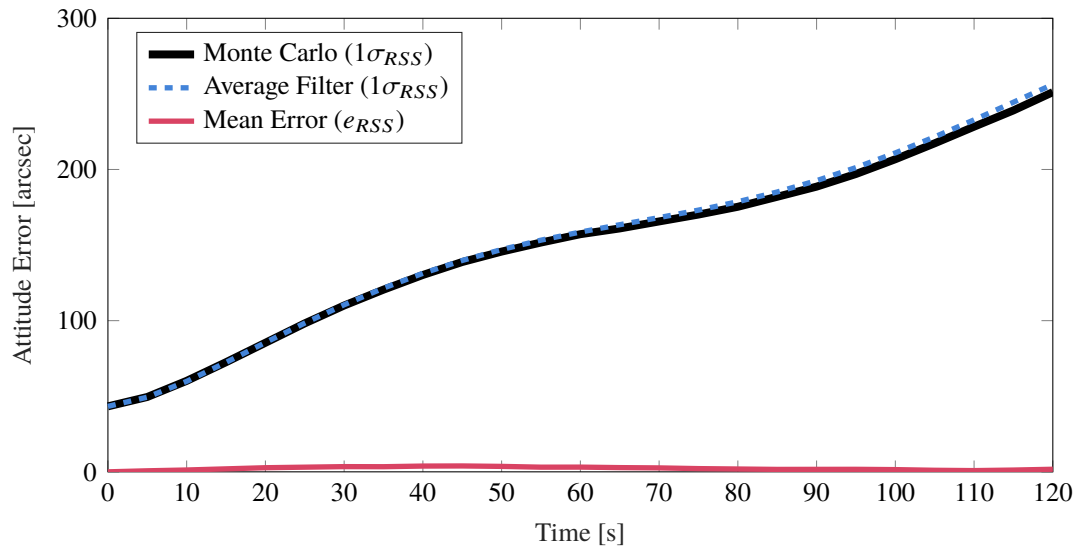
Figure 6.3. Monte Carlo simulation results for mixed-frequency traditional dead-reckoning; mean attitude error (RSS), averaged filter covariance ($1\sigma_{RSS}$), Monte Carlo sample covariance ($1\sigma_{RSS}$) from 1000 trials with no coning motion
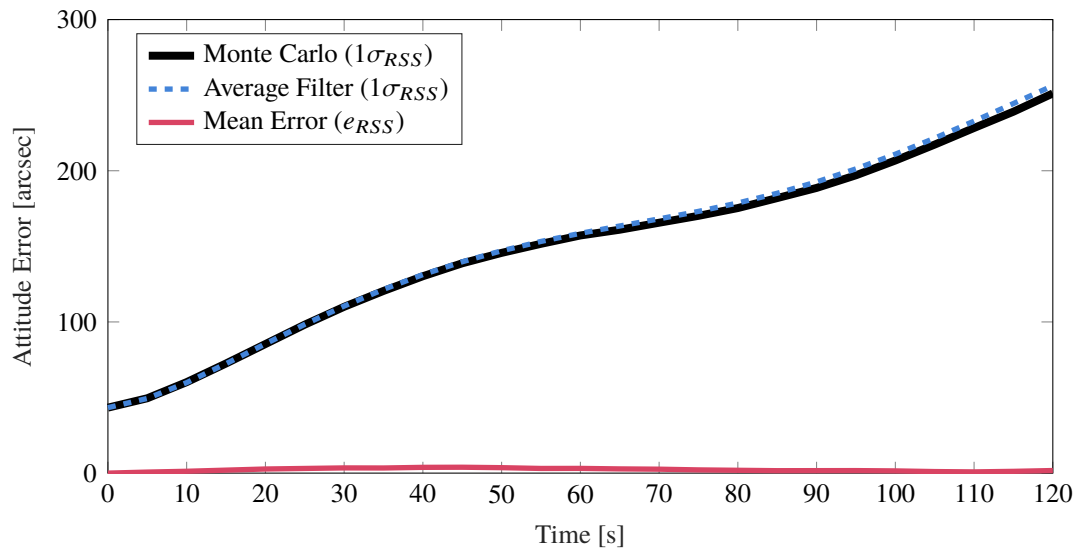
Figure 6.4. Monte Carlo simulation results for low-frequency coned dead-reckoning; mean attitude error (RSS), averaged filter covariance ($1\sigma_{RSS}$), Monte Carlo sample covariance ($1\sigma_{RSS}$) from 1000 trials with no coning motion
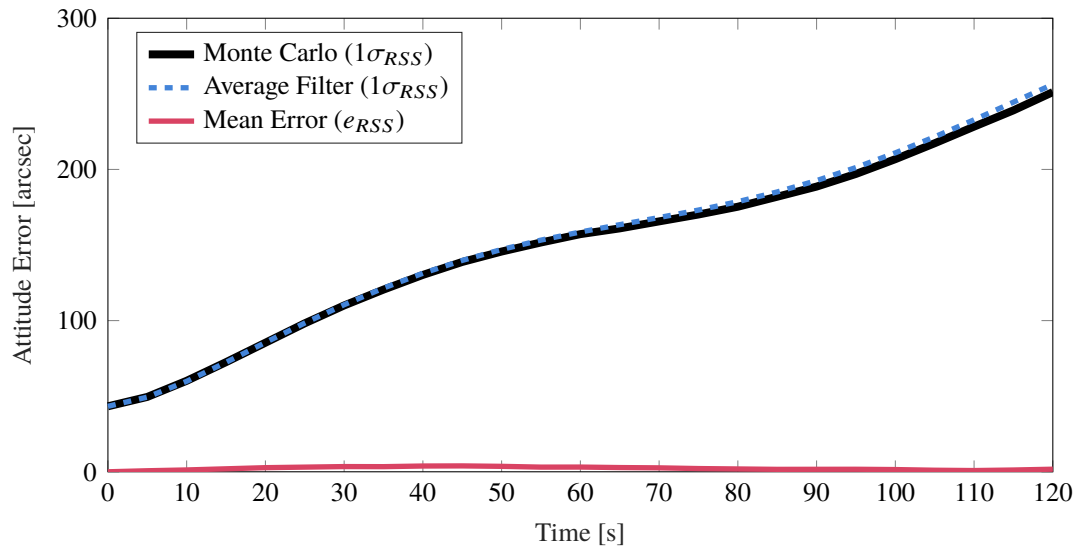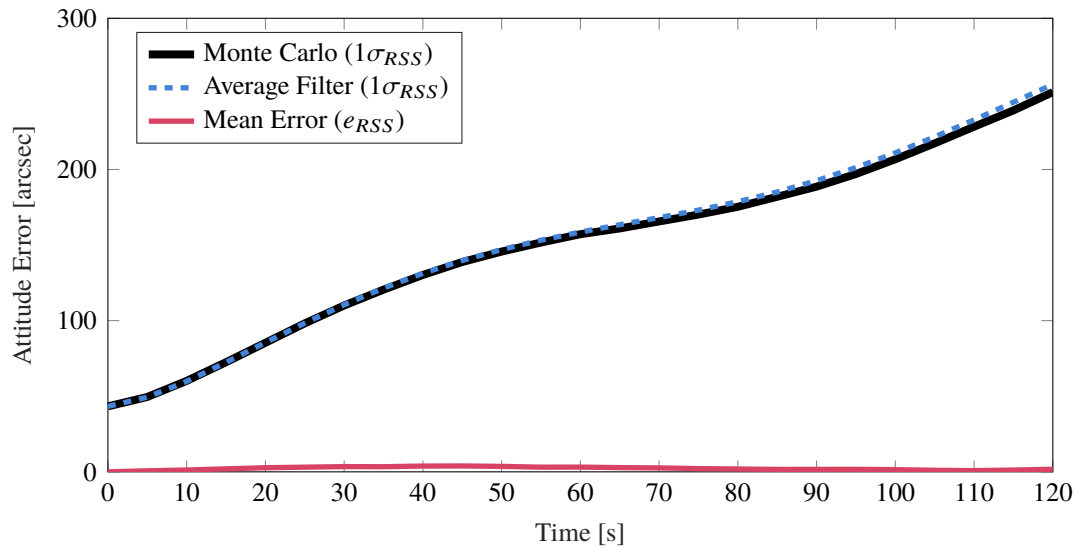
Figure 6.5. Monte Carlo simulation results for high-frequency, coned dead-reckoning; mean attitude error (RSS), averaged filter covariance ($1\sigma_{RSS}$), Monte Carlo sample covariance ($1\sigma_{RSS}$) from 1000 trials with no coning motion
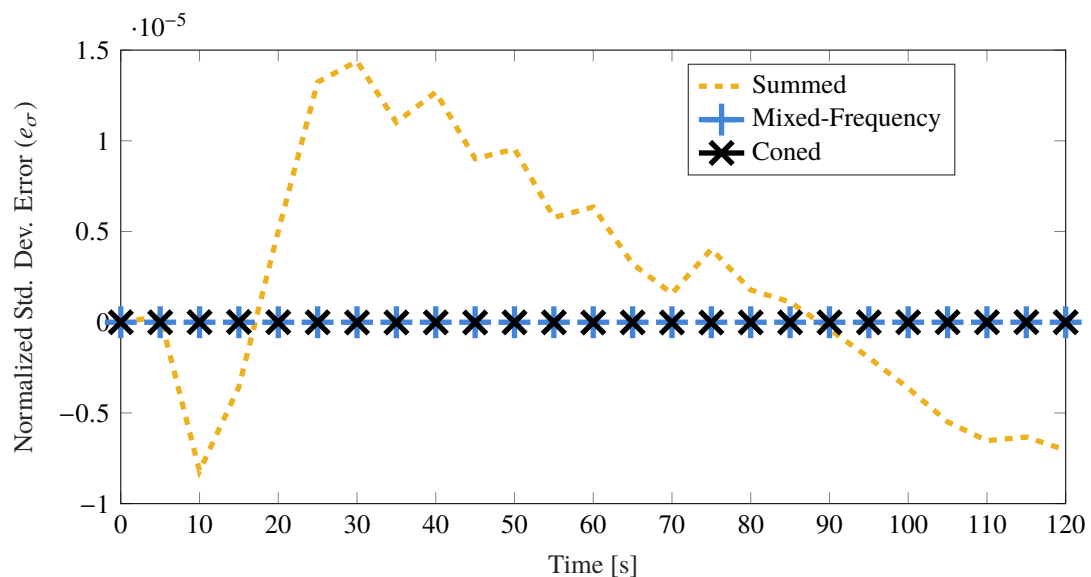

Figure 6.6. Normalized standard deviation error between Monte Carlo sample standard deviation (RSS) for summed TDR, CDR, and mixed-frequency dead-reckoning compared to the high-frequency traditional dead-reckoning Monte Carlo sample standard deviation (RSS) from 1000 trials with no coning motion
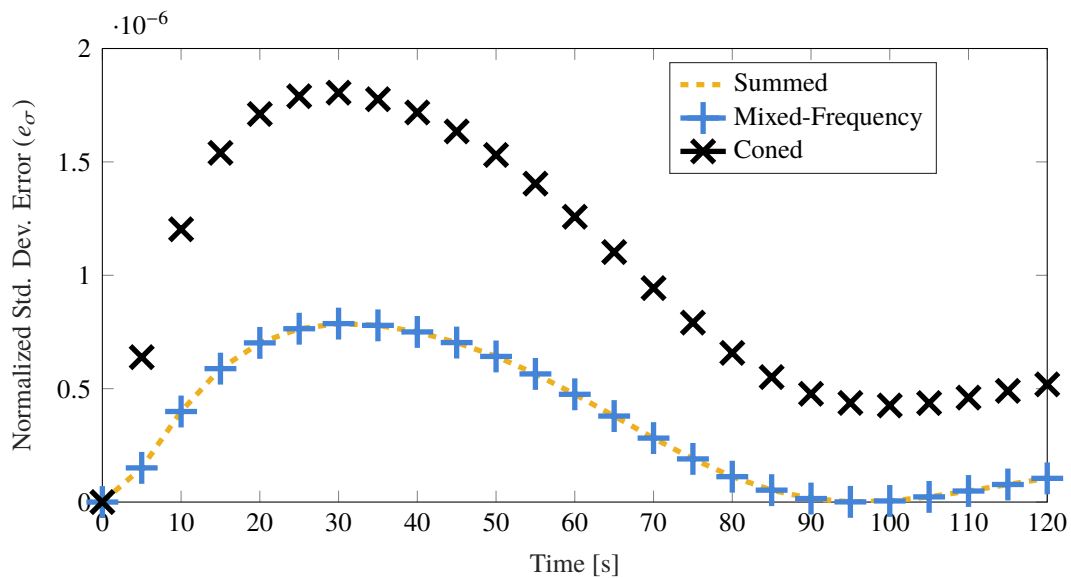
Figure 6.7. Normalized standard deviation error between average filter standard deviation (RSS) for summed TDR, CDR, and mixed-frequency dead-reckoning compared to the high-frequency traditional dead-reckoning average filter standard deviation (RSS) from 1000 trials with no coning motion
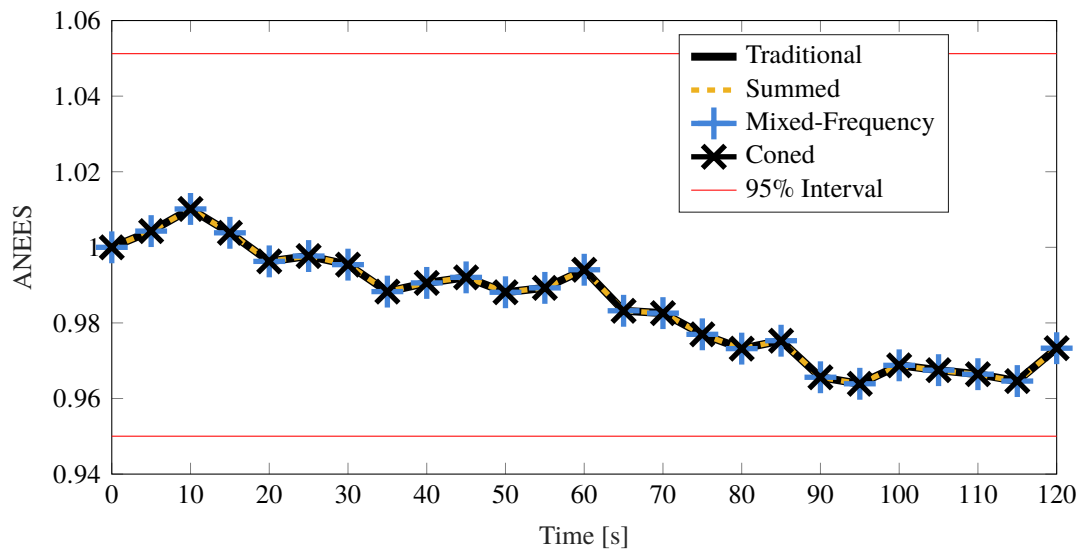
Figure 6.8. ANEES comparison for summed, mixed-frequency, coned, and traditional methods for attitude dead-reckoning from 1000 Monte Carlo trials with no coning motion

Examining Figures 6.14–6.15, it is clear that the spread of the errors about the mean estimation error is similar to those seen in the case of no coning motion for each method implemented. Additionally, it is clear that the uncertainties predicted by the summed and mixed-frequency dead-reckoning approaches are again consistent with one another, while the coned dead-reckoning remains near zero, i.e. comparable to the traditional method of dead-reckoning. When inspecting Figure 6.16, a deviation between summed dead-reckoning and the other approaches is observed. Though no configuration can be deemed inconsistent, the non-zero mean estimation errors present in the summed dead-reckoning configuration make it a poor choice for attitude estimation in a coning environment.

6.1.3.3. 200 Hz coning motion. Results for 1000 trial Monte Carlo simulations of each configuration, estimating the vehicle's attitude in an environment containing significant coning motion, are provided in Figures 6.17–6.21. Continuing the trend observed by the previous cases, summed dead-reckoning sees significant growth in the mean estimation error, while much smaller growth is noticeable in the high- and mixed-frequency methods of traditional dead-reckoning. Coned dead-reckoning sees little error growth that can be directly attributed to the presence of coning motion. Additionally, the averaged filter and Monte Carlo sample covariances appear to be consistent.

Examining Figures 6.22 and 6.23, it is noted that the summed dead-reckoning error distribution continues to grow larger than that of TDR, while CDR sees some error reduction in this environment. Additionally, from Figure 6.23, the filter-predicted uncertainty is larger again for the mixed-frequency TDR and summed TDR, while it is reduced (in general) when compared to TDR. Finally, Figure 6.24 illustrates that each method is consistent with its predictions, aside from the summed dead-reckoning case. It is observed that the summed dead-reckoning method quickly penetrates the 95% consistency interval defined by the ANEES, showing that the assumption of constant angular velocity between attitude estimates has been violated in this case.

Figure 6.9. Monte Carlo simulation results for high-frequency traditional dead-reckoning; mean attitude error (RSS), averaged filter covariance ($1\sigma_{RSS}$), Monte Carlo sample covariance ($1\sigma_{RSS}$) from 1000 trials with 40 Hz coning motion
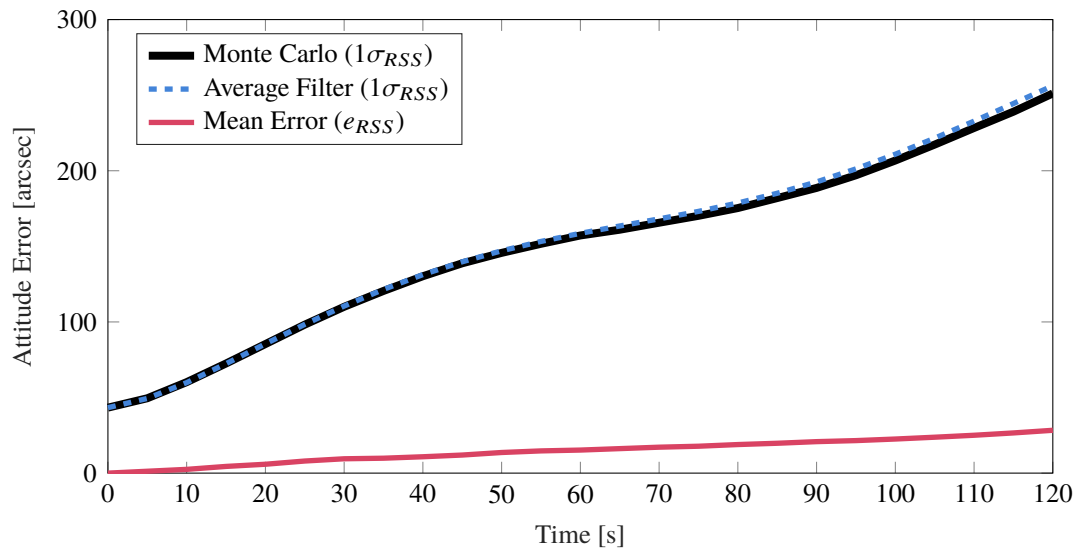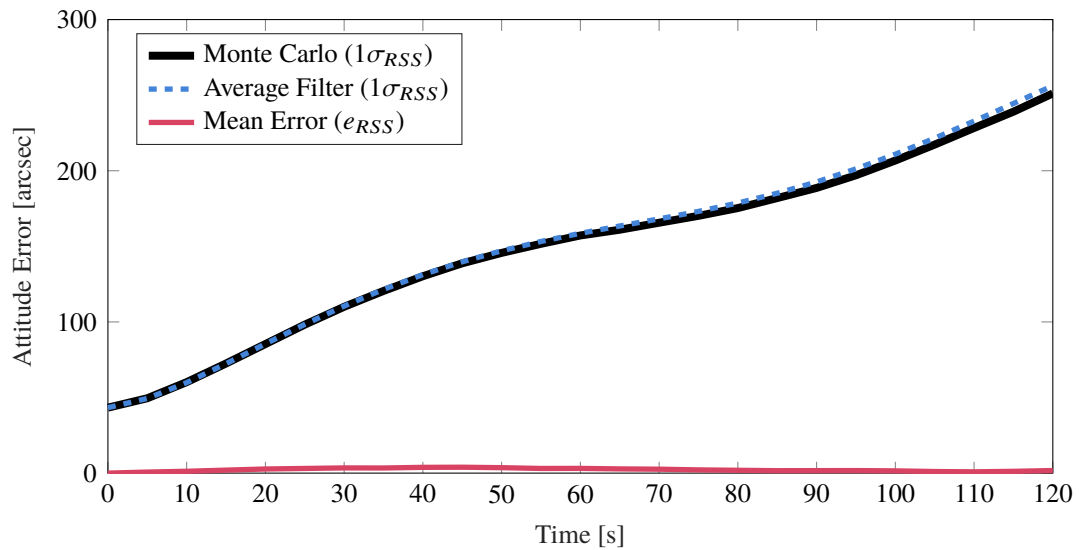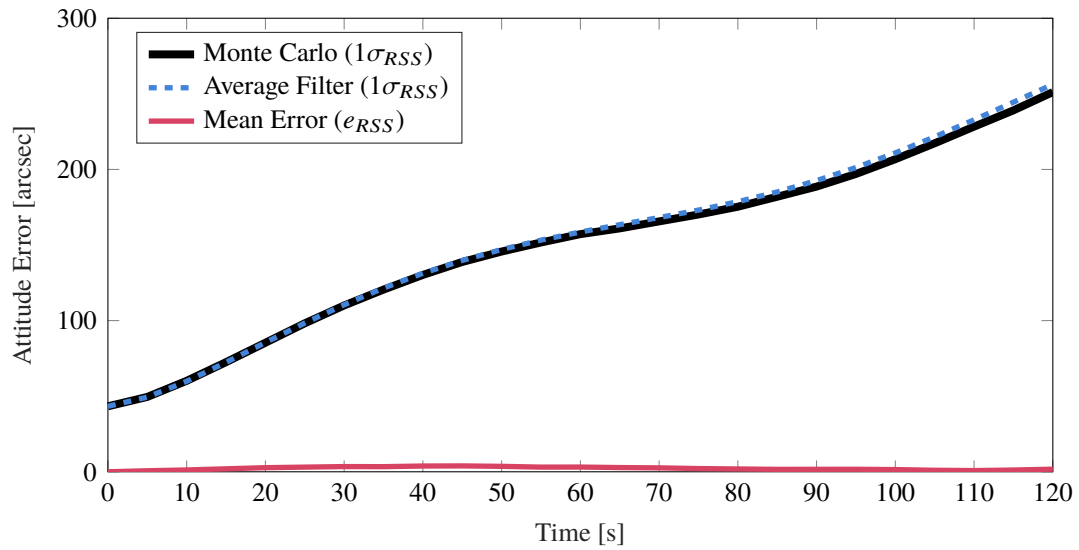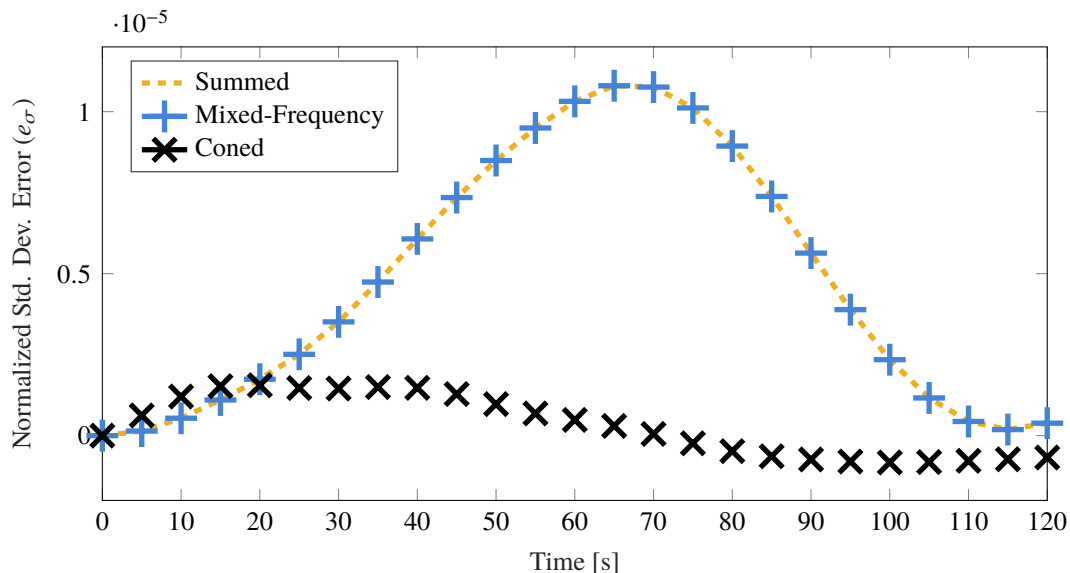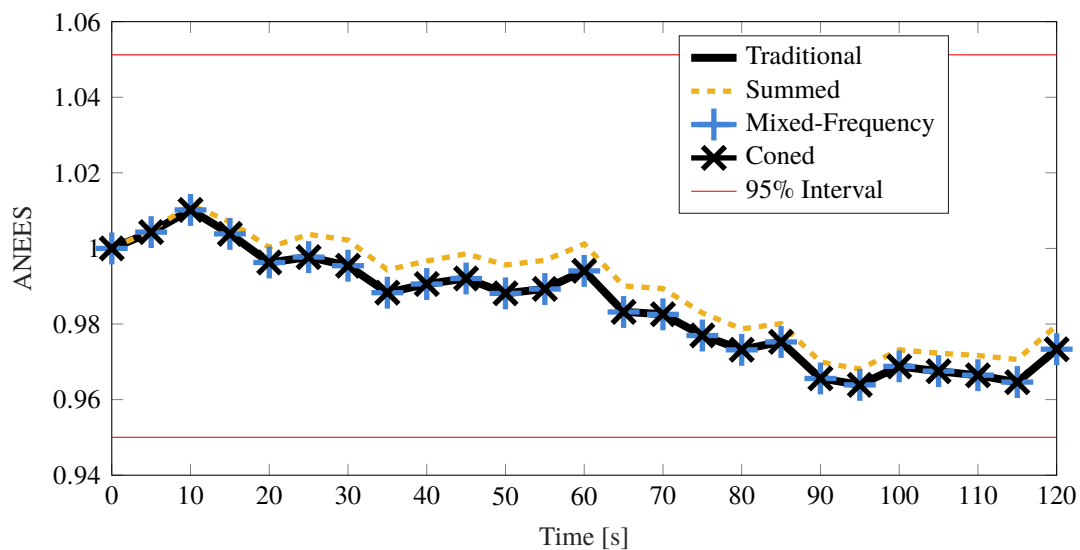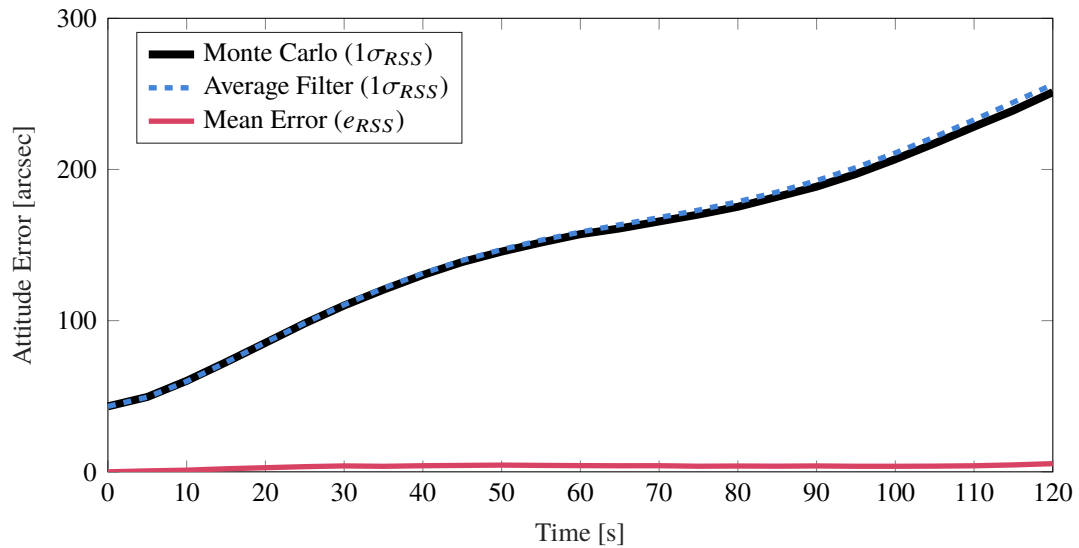

Figure 6.10. Monte Carlo simulation results for low-frequency traditional dead-reckoning; mean attitude error (RSS), averaged filter covariance ($1\sigma_{RSS}$), Monte Carlo sample covariance ($1\sigma_{RSS}$) from 1000 trials with 40 Hz coning motion
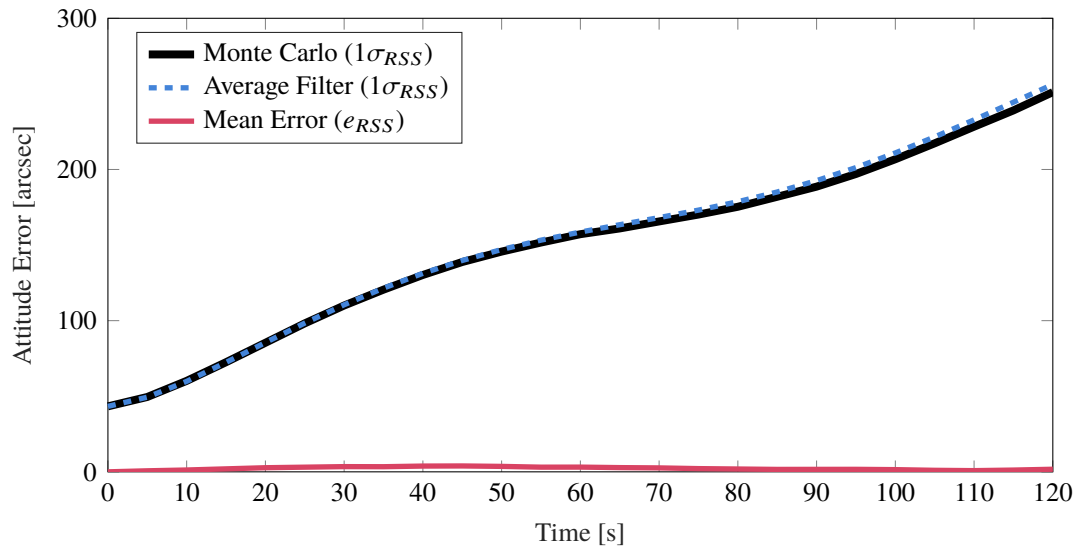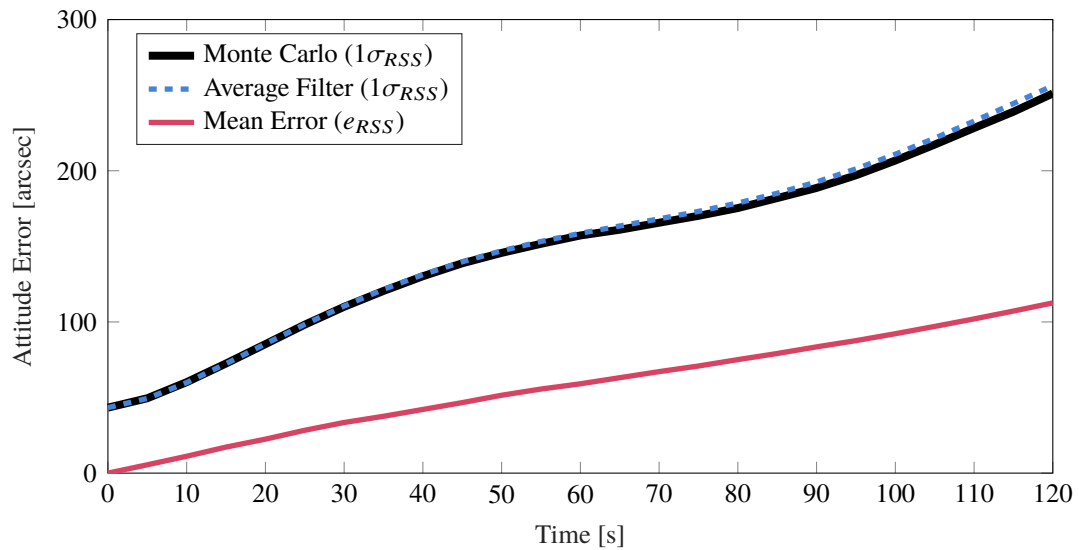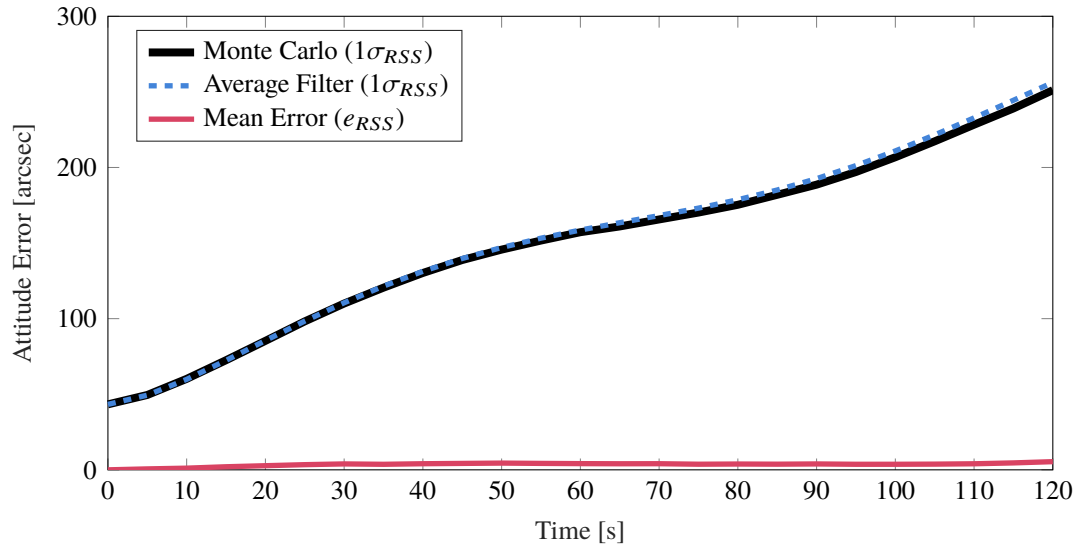
Figure 6.11.   Monte Carlo simulation results for mixed-frequency traditional dead-reckoning; mean attitude error (RSS), averaged filter covariance ($1\sigma_{RSS}$), Monte Carlo sample covariance ($1\sigma_{RSS}$) from 1000 trials with 40 Hz coning motion

Figure 6.12. Monte Carlo simulation results for low-frequency coned dead-reckoning; mean attitude error (RSS), averaged filter covariance ($1\sigma_{RSS}$), Monte Carlo sample covariance ($1\sigma_{RSS}$) from 1000 trials with 40 Hz coning motion

Figure 6.13. Monte Carlo simulation results for high-frequency, coned dead-reckoning; mean attitude error (RSS), averaged filter covariance ($1\sigma_{RSS}$), Monte Carlo sample covariance ($1\sigma_{RSS}$) from 1000 trials with 40 Hz coning motion
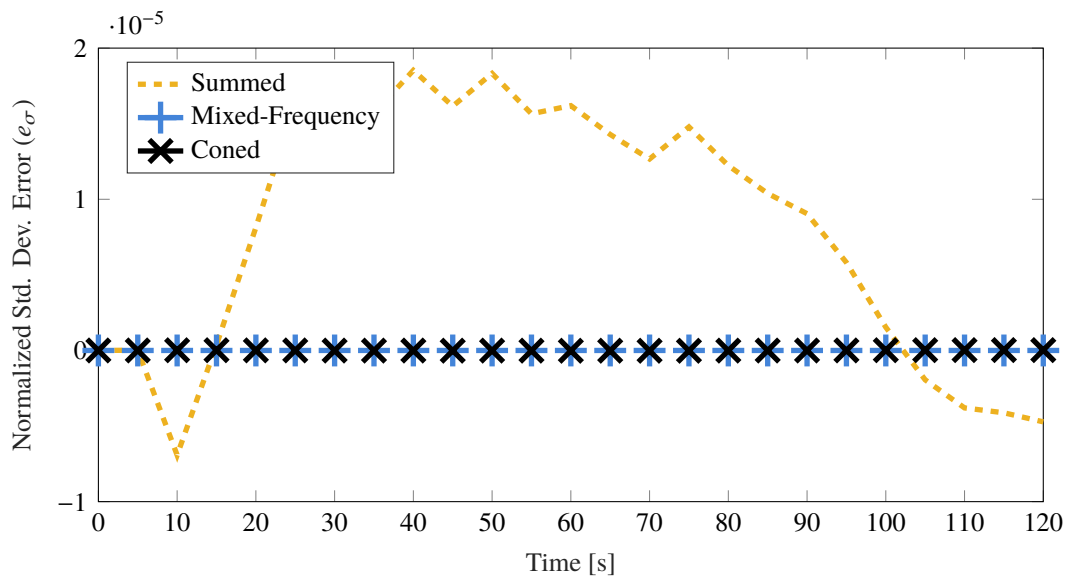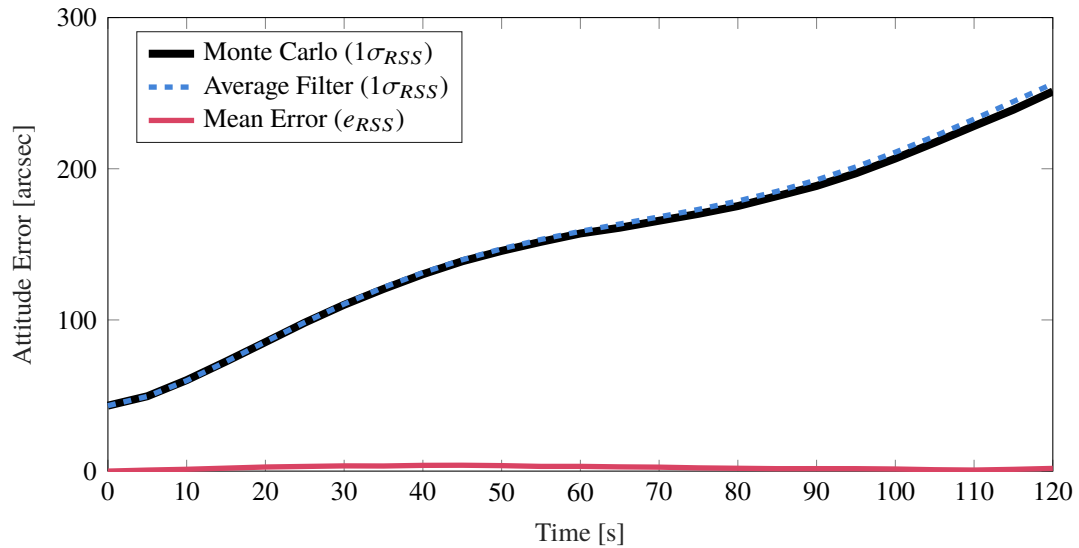

Figure 6.14. Normalized standard deviation error between Monte Carlo sample standard deviation (RSS) for summed TDR, CDR, and mixed-frequency dead-reckoning compared to the high-frequency traditional dead-reckoning Monte Carlo sample standard deviation (RSS) from 1000 trials with 40 Hz coning motion

Figure 6.15. Normalized standard deviation error between average filter standard deviations (RSS) for summed TDR, CDR, and mixed-frequency dead-reckoning compared to the high-frequency traditional dead-reckoning average filter standard deviation (RSS) from 1000 trials with 40 Hz coning motion

Figure 6.16. ANEES comparison for summed, mixed-frequency, coned, and traditional methods for attitude dead-reckoning from 1000 Monte Carlo trials with 40 Hz coning motion

Figure 6.17. Monte Carlo simulation results for high-frequency traditional dead-reckoning; mean attitude error (RSS), averaged filter covariance ($1\sigma_{RSS}$), Monte Carlo sample covariance ($1\sigma_{RSS}$) from 1000 trials with 200 Hz coning motion
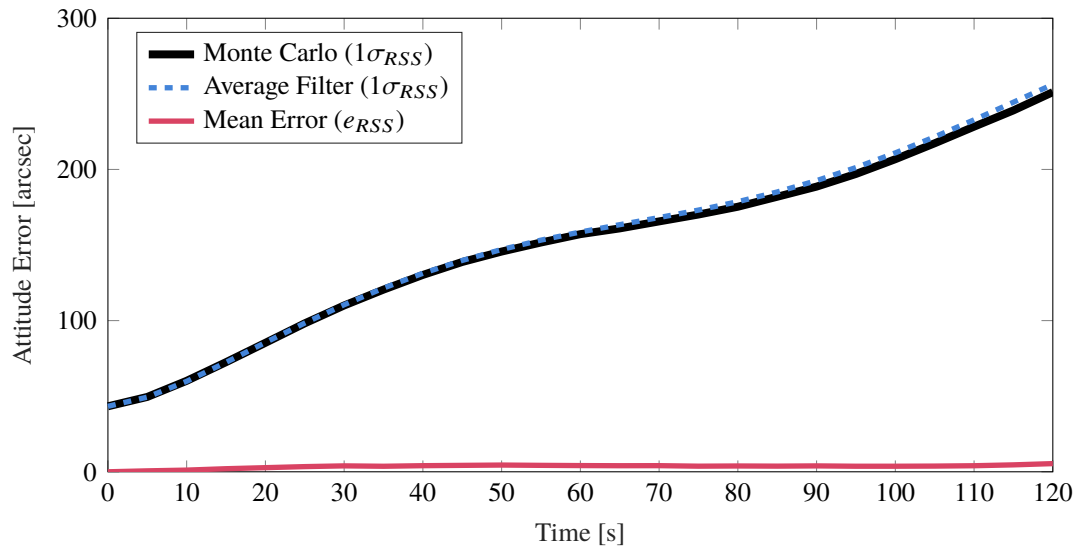

Figure 6.18. Monte Carlo simulation results for low-frequency traditional dead-reckoning; mean attitude error (RSS), averaged filter covariance ($1\sigma_{RSS}$), Monte Carlo sample covariance ($1\sigma_{RSS}$) from 1000 trials with 200 Hz coning motion

Figure 6.19. Monte Carlo simulation results for mixed-frequency traditional dead-reckoning; mean attitude error (RSS), averaged filter covariance ($1\sigma_{RSS}$), Monte Carlo sample covariance ($1\sigma_{RSS}$) from 1000 trials with 200 Hz coning motion

Figure 6.20. Monte Carlo simulation results for low-frequency coned dead-reckoning; mean attitude error (RSS), averaged filter covariance ($1\sigma_{RSS}$), Monte Carlo sample covariance ($1\sigma_{RSS}$) from 1000 trials with 200 Hz coning motion

Figure 6.21. Monte Carlo simulation results for high-frequency, coned dead-reckoning; mean attitude error (RSS), averaged filter covariance ($1\sigma_{RSS}$), Monte Carlo sample covariance ($1\sigma_{RSS}$) from 1000 trials with 200 Hz coning motion
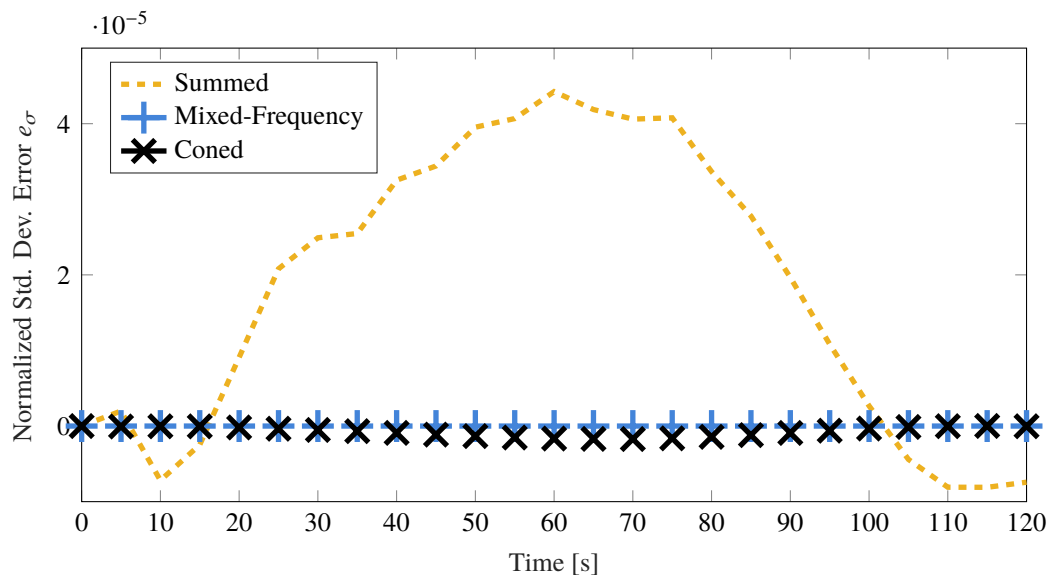
Figure 6.22. Normalized standard deviation error between Monte Carlo sample standard deviation (RSS) for summed TDR, CDR, and mixed-frequency dead-reckoning compared to the high-frequency traditional dead-reckoning Monte Carlo sample standard deviation (RSS) from 1000 trials with 200 Hz coning motion
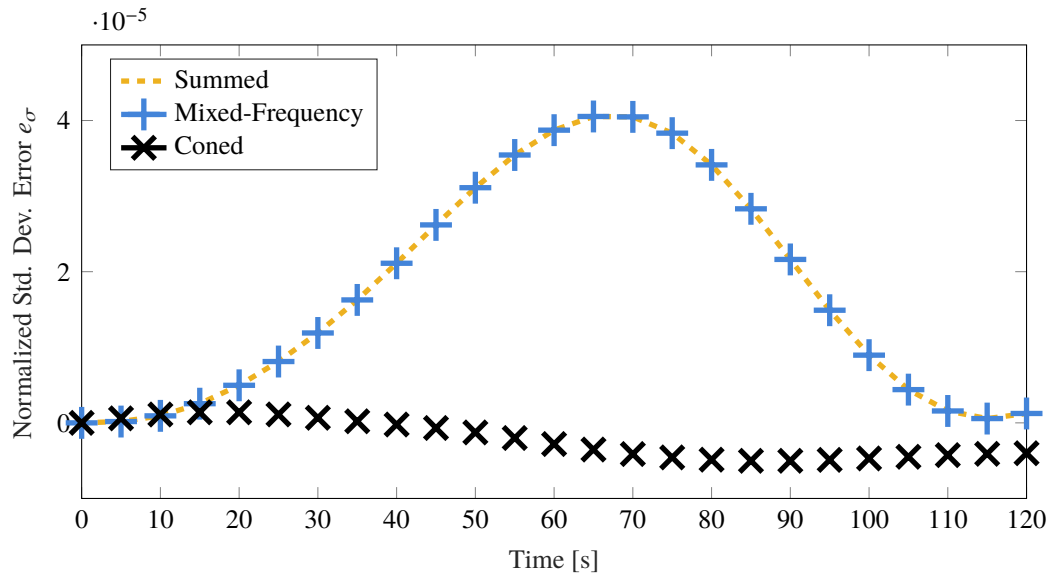
Figure 6.23. Normalized standard deviation error between average filter standard deviations (RSS) for summed TDR, CDR, and mixed-frequency dead-reckoning compared to the high-frequency traditional dead-reckoning average standard deviation (RSS) from 1000 trials with 200 Hz coning motion
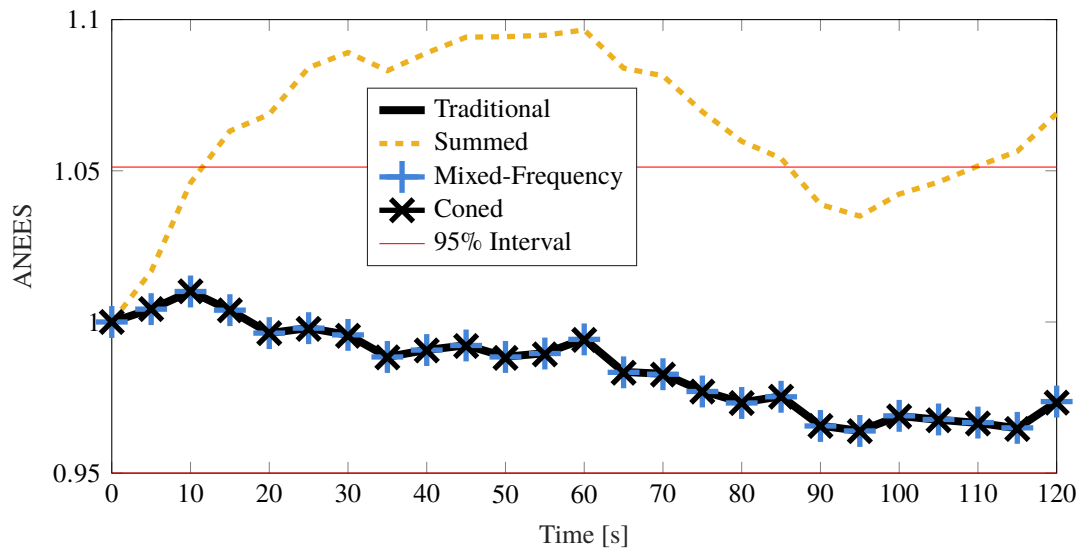
Figure 6.24. ANEES comparison for summed, mixed-frequency, coned, and traditional methods for attitude dead-reckoning from 1000 Monte Carlo trials with 200 Hz coning motion

6.1.4. Summary of Results. In most cases, the simulation results show that each configuration is statistically consistent with small influence due to the presence of coning motion. However, a non-zero bias is realized in the mean estimation error for low-frequency TDR when coning motion is present and begins to manifest in the other methods when not applying the coning correction. This result is to be expected, as the constant angular velocity assumption is violated in the accumulation and processing of the measurements for each, though this assumption is doubly violated by the summed TDR case.

By examining the ratio of the sample and averaged filter covariances, and the ANEES for each case, it is clear that each estimator exhibits roughly the same performance and can be considered consistent with the estimation error when no coning motion is included. However, when coning motion is introduced, the summed TDR configuration is no longer consistent with the other cases. As the coning frequency is further increased, it is clear that each other algorithm manages to maintain the same consistency experienced before, while the summed TDR case quickly penetrates the 95% confidence interval. Therefore, the filter operating upon summed gyroscope measurements can be considered inconsistent and deemed non-credible at a level of 95% when 200 Hz coning motion is present. Finally, CDR manages to maintain a level of consistency for each environment and exhibits improvements in performance as the underlying coning motion increases.

Table 6.2 provides a comparison of mean trial run-time for each configuration, obtained from the 1000 trial set. It is obvious that CDR is more computationally burdensome in general, as is apparent by it requiring approximately 25% more time than TDR when providing estimates at the same frequency. This is not a surprising result as the mechanization of the CDR is more complex. However, when producing estimates at a lower frequency, the mixed-frequency configuration requires less computational resources than CDR, though it fails to reduce the error growth caused by the presence of coning motion. By applying CDR to propagate the state and covariance, the significant computational time is cut, while

Table 6.2. Mean run-time for 1000 Monte Carlo trials

Configuration	Run-Time (s)
Traditional (400 Hz)	7.58
Summed (40 Hz)	0.19
Mixed-Frequency (40 Hz)	2.03
Coned (40 Hz)	2.87
Coned (400 Hz)	9.57

reducing the mean attitude error. Propagating the mean and covariance with a summed batch of measurements significantly reduces the computational load, though the underlying assumptions quickly become unrealistic.

6.2. DESCENT-TO-LANDING SIMULATION OVERVIEW

A series of Monte Carlo simulations are examined to compare traditional dead-reckoning techniques to one employing coning, sculling, and scrolling (CSS) algorithms using the error propagation techniques developed within Section 5. The selected trajectory is chosen not to maximize the effects or usefulness of coning, sculling, and scrolling algorithms, but to represent a scenario in which precision is of the utmost importance. The same trajectory has been examined in References [30] and [31], where the effects of external measurements on the navigation performance are considered. In contrast, the analysis here focuses on the situation where the vehicle is only navigating via a variety of inertial navigation techniques. Understanding how the estimation error propagates through the navigation system in a high-stakes scenario, such as a lunar landing, can be crucial to improving systems currently under development. Comparing a variety of different propagation techniques with this scenario provides a quantifiable differentiation between navigation systems equipped with the coning, sculling, and scrolling algorithms' error

Table 6.3. Initial uncertainty for each state (per component basis, 1σ)

	Uncertainty (1σ)
Position	1000 m
Velocity	0.1 m/s
Attitude	100 arcseconds

propagation and those without. This comparison highlights the improvements expected in a navigation system's performance when employing the error propagation alongside the often implemented coning, sculling, and scrolling algorithms.

To assess performance and compare configurations, Monte Carlo analysis is used. However, this method of analysis typically samples the true state from some distribution about the mean. Breaking convention, the true position, velocity, acceleration, and angular velocity are fixed for this trajectory, as is the case in Reference [31], requiring that the initial estimates be sampled from a distribution about the true states. The initial states are assumed to be initially uncorrelated and sampled from Gaussian distributions, with 1σ uncertainties shown in Table 6.3.

The true vehicle trajectory is illustrated in Figures 6.25–6.28. The altitude profile of the vehicle across the mission is shown in Figure 6.25, where the trajectory is initialized 50 km above the lunar surface. The vehicle slowly descends over the first 24 minutes to an altitude of 16.5 km and enters a powered descent phase after 25.5 minutes mission elapsed time (MET). During powered descent, the vehicle rapidly descends to the surface in just under 7 minutes. Figure 6.26 shows the vehicle attitude, expressed as Euler angles; the attitude profile is only provided for a portion of the mission to show the changes experienced throughout the powered descent phase of the simulation. It's clear from Figures 6.26 and 6.28 that a large attitude maneuver takes place at approximately 24 minutes MET, while another small maneuver occurs at roughly 25.5 minutes MET; as the

simulation ends and the vehicle lands, several attitude correction maneuvers are also seen. With the beginning of the powered descent phase, the vehicle begins a burn that lasts until the vehicle has landed, as seen in Figure 6.27.

The IMU gyroscope and accelerometer measurements are modeled to be consistent with the error statistics for a Northrop Grumman LN-200S, with specifications given in Table 6.1, and are modeled as described in Section 4.3. Measurement error sources of white noise, bias, scale factor, misalignment and nonorthogonality are included for both the gyro and accelerometer measurements. Each error is sampled from a zero-mean Gaussian distribution defined by the statistics in Table 6.1; the bias, scale factor, misalignment, and nonorthogonality sources are modeled to be constant throughout a given trial.

6.2.1. Nominal Simulation. The nominal state propagation considers the case in which the state is propagated at the rate of the IMU measurements, 40 Hz. Processing a single measurement is generally the desired approach for the navigation system, though it is often desirable to process high-frequency IMU data to detect underlying vibrations. Unfortunately, significant computational resources may be spent to maintain an estimate and its uncertainty at the frequencies that modern inertial sensors are capable of, even when considering state-of-the-art computing systems. The dynamics given in Equations (4.33) govern the propagation of the vehicle's position, velocity, and attitude in this case, which gives a baseline performance for the navigation system's state and covariance propagation as it exemplifies the most common method of inertial navigation.

6.2.2. Coning, Sculling, and Scrolling Simulation. An architecture employing the coning, sculling, and scrolling algorithms presented in Section 4, and using an error propagation derived within Section 5, can also be used to propagate the mean and covariance of the vehicle. For the simulation, these algorithms operate at a frequency of 10 Hz, while the measurements are simulated at 40 Hz. Therefore, a batch of measurements obtained between t_{k-1} and t_k are used to propagate the state and uncertainty of the vehicle by utilizing the coning, sculling, and scrolling algorithms.
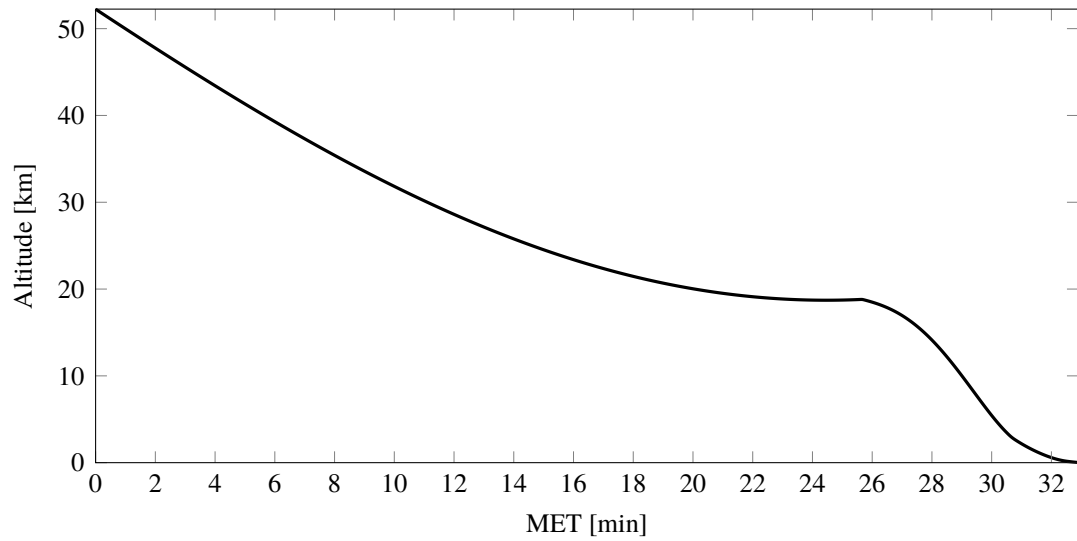
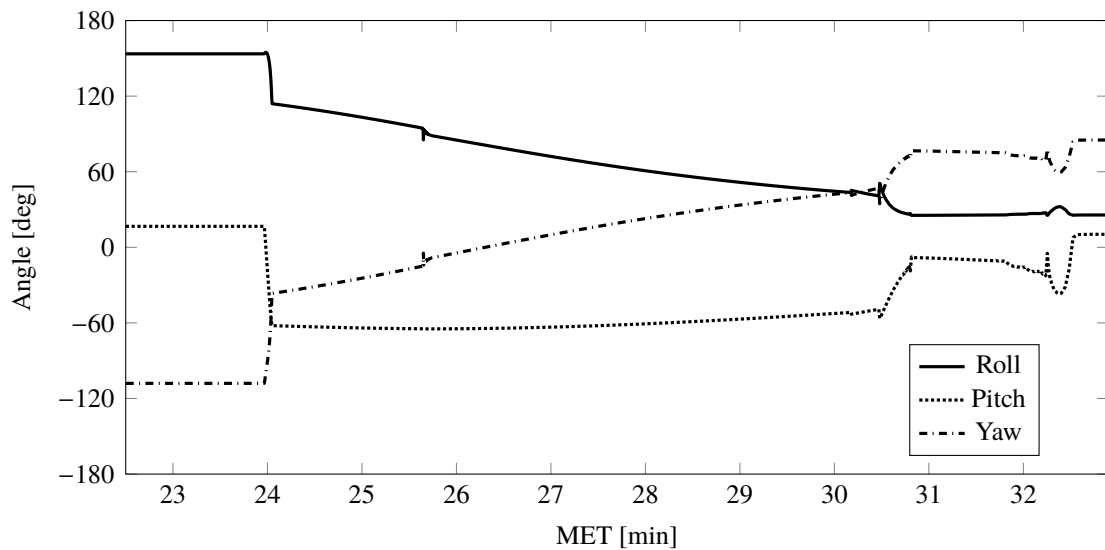Figure 6.25. Vehicle altitude during terminal descent

Figure 6.26. Vehicle attitude (Euler angles) during terminal descent
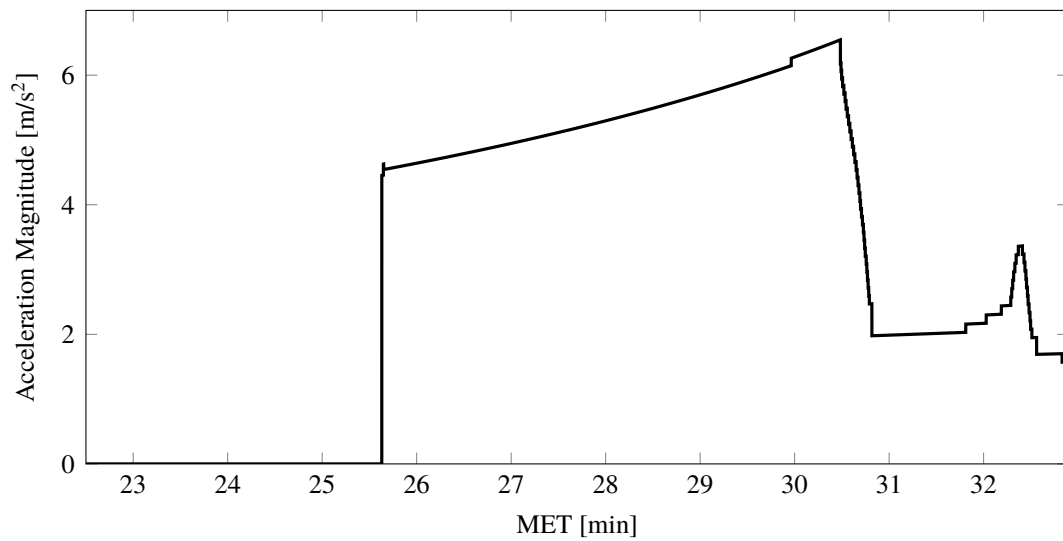
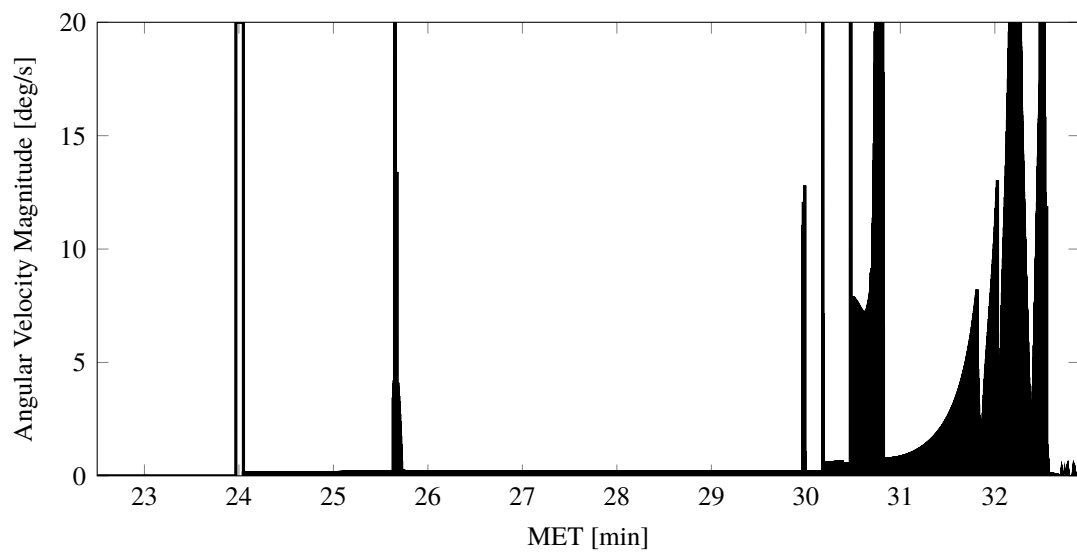Figure 6.27. Non-gravitational acceleration magnitude during terminal descent

Figure 6.28. Vehicle angular velocity magnitude during terminal descent

6.2.3. Comparison of Results. The Monte Carlo sample and averaged filter co-variance are examined for each configuration to determine statistical consistency, while comparisons between the two methods are made by directly comparing the filter predicted and observed uncertainties. In Figures 6.29–6.34, results for the position, velocity, and attitude estimation errors obtained from the nominal simulation are shown. Figures 6.29–6.31 show the mean estimation error, alongside the averaged filter and Monte Carlo sample covariance 3–σ intervals for position, velocity, and attitude, whereas Figures 6.32–6.34 show the RSS values. Additionally, Figures 6.35–6.40 show similar results for the application of CSS algorithms. From these figures, it is clear that both configurations appear to be consistent with the Monte Carlo statistics, despite the presence of a bias in the mean error.

Within Figures 6.41–6.49, a direct comparison of each method is made. Examining Figures 6.32–6.34 closely, it can be observed that the mean estimation error is slightly reduced by application of the CSS algorithms, while no noticeable differences exist for the predicted uncertainty. Figures 6.44–6.46 show the ANEES for position, velocity, and attitude, allowing the declaration that each estimator has the same level of credibility for the estimation of those states. While no significant difference manifests, notice the slight deviation in the ANEES for the position – the CSS formulation is slightly more conservative than that of the traditional methods. Figures 6.47–6.49 compare the ratio of standard deviations (RSSs) for the CSS configuration's Monte Carlo sample and averaged filter to those of the traditional methods. Even though the differences are small, a few concessions can be made. First, notice that the ratio of the Monte Carlo sample standard deviations is less than zero for the velocity and position distributions – this allows the recognition that the CSS algorithms are reducing the mean error present in the system. The same trend is followed by the averaged filter ratio until approximately 24 minutes MET, when the attitude maneuver that occurs. After the attitude maneuver, a burn is performed to decelerate the vehicle – the continued divergence between the ratios is observed in this case. It's therefore clear that the introduction of these algorithms allows for a slightly more

Table 6.4. Mean run-time for 500 Monte Carlo trials

Configuration	Run-Time
Traditional (40 Hz)	66.8
CSS (10 Hz)	61.8

conservative representation of the uncertainty during maneuvers. A caveat to the analysis is that the sample size of 500 Monte Carlo trials is likely somewhat undersampled and the significance of the presumptions made by examining the ratios are difficult to justify as the differences are relatively small.

A comparison of the run-time requirements are provided in Table 6.4. The required runtime to process the same measurements and provide the state and covariance at a downsampled frequency yielded computational savings. Unfortunately, the time savings do not seem to be as large as was shown in Section 6.1. It should, however, be noted that the difference in operational frequencies is relatively small in this case and, if higher frequency measurements were available, the reduction would likely be much more significant. Finally, it should be noted that an attempt at streamlining the implementation may also yield additional run-time reduction.
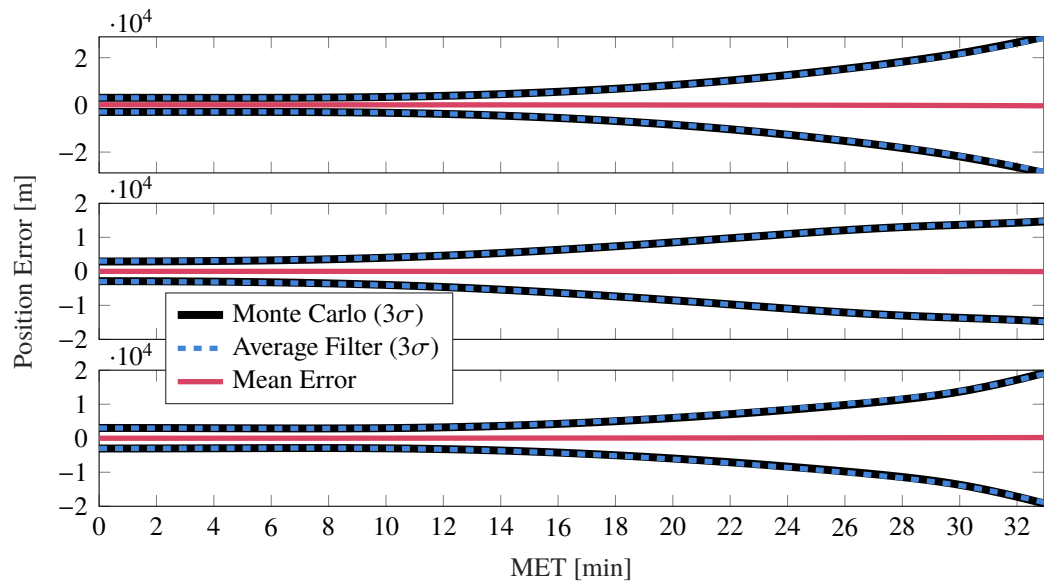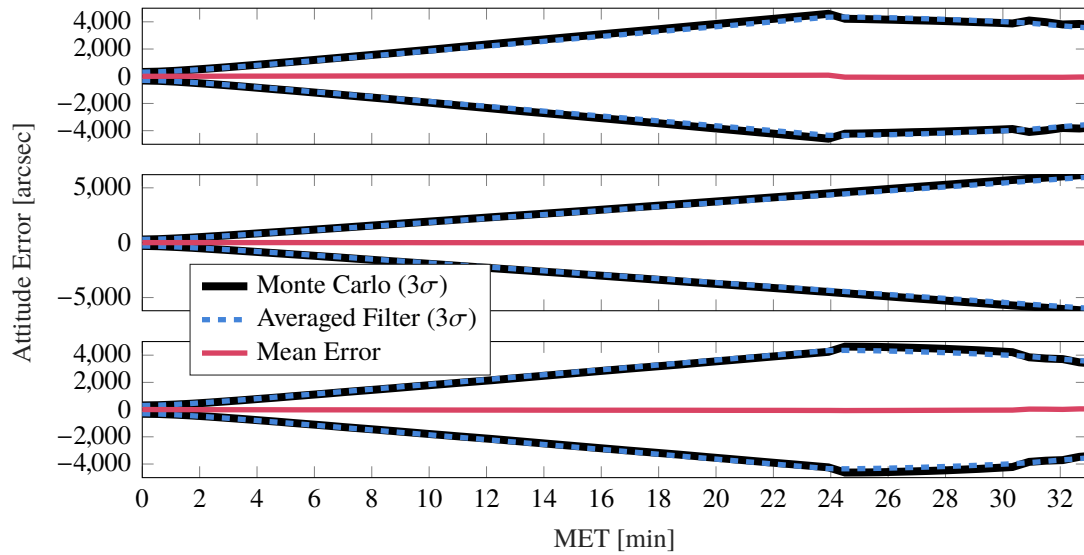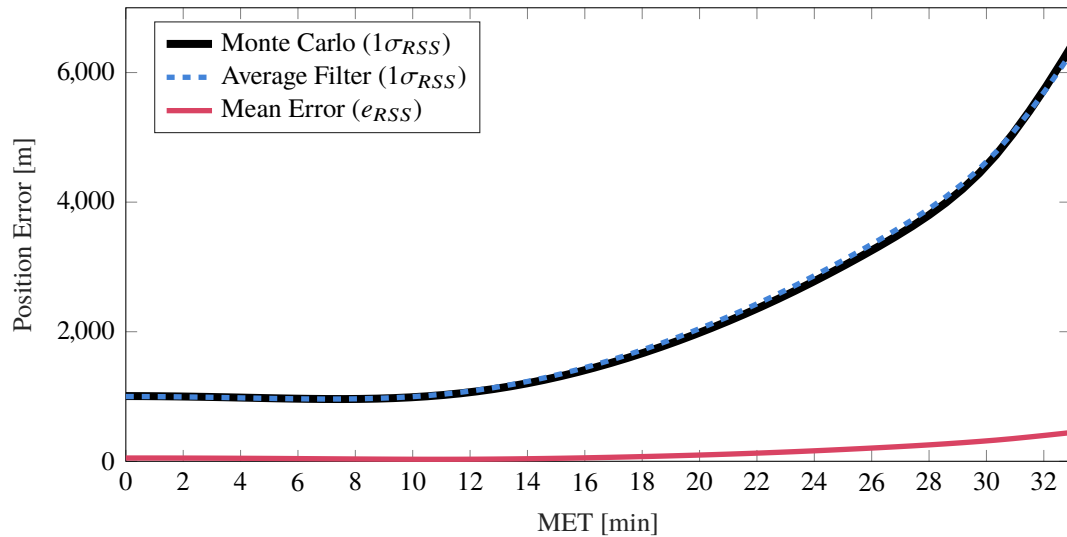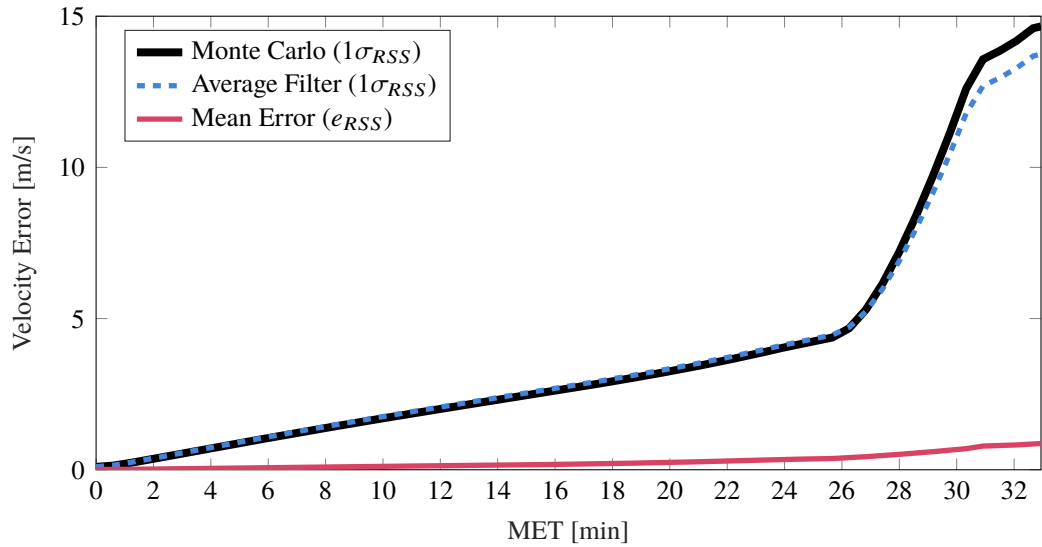
Figure 6.29. Monte Carlo simulation results from 500 trials using traditional methods of inertial navigation in the descent-to-landing simulation; mean position error, averaged filter covariance (3σ), and Monte Carlo sample covariance (3σ)
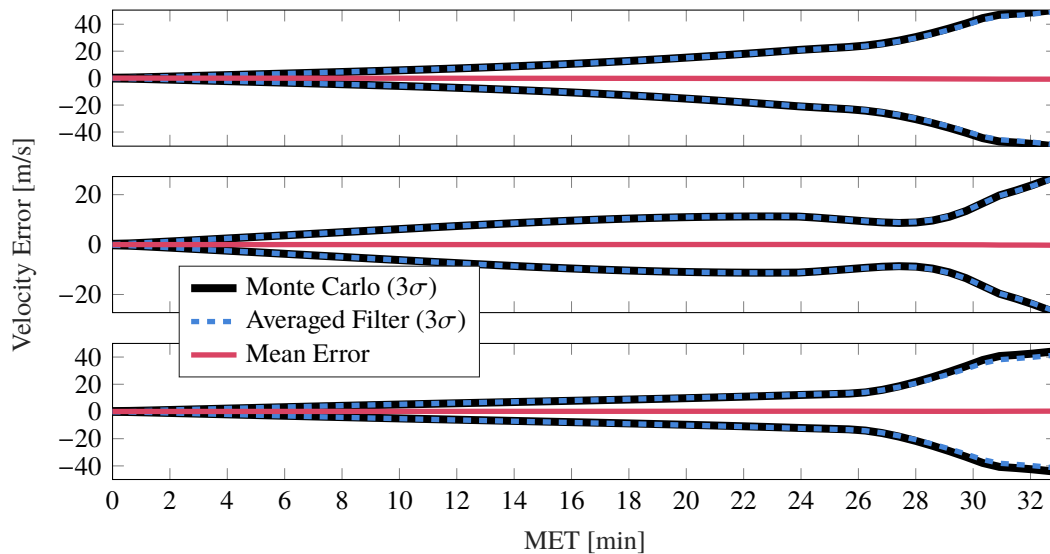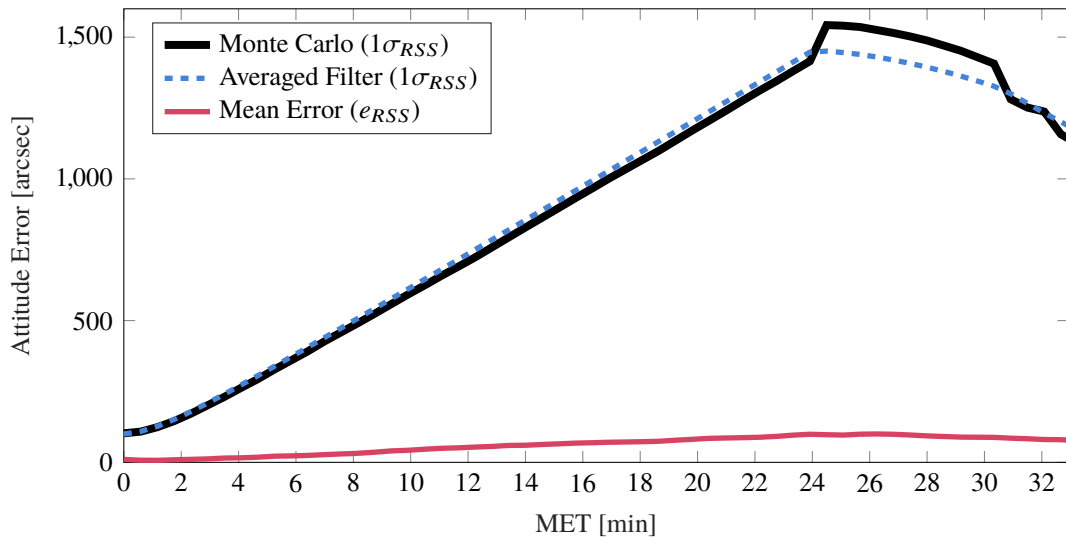

Figure 6.30. Monte Carlo simulation results from 500 trials using traditional methods of inertial navigation in the descent-to-landing simulation; mean velocity error, averaged filter covariance (3σ), and Monte Carlo sample covariance (3σ)

Figure 6.31. Monte Carlo simulation results from 500 trials using traditional methods of inertial navigation in the descent-to-landing simulation; mean attitude error, averaged filter covariance (3σ), and Monte Carlo sample covariance (3σ)

Figure 6.32. Monte Carlo simulation results from 500 trials using traditional methods of inertial navigation in the descent-to-landing simulation; mean position error (RSS), averaged filter covariance ($1\sigma_{RSS}$), and Monte Carlo sample covariance ($1\sigma_{RSS}$)
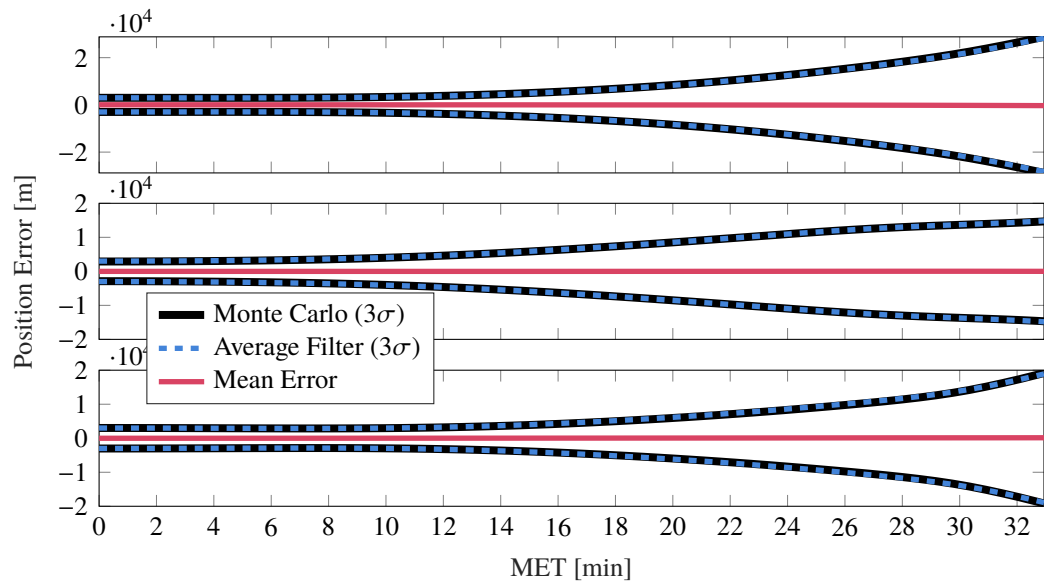
Figure 6.33. Monte Carlo simulation results from 500 trials using traditional methods of inertial navigation in the descent-to-landing simulation; mean velocity error (RSS), averaged filter covariance ($1\sigma_{RSS}$), and Monte Carlo sample covariance ($1\sigma_{RSS}$)

Figure 6.34. Monte Carlo simulation results from 500 trials using traditional methods of inertial navigation in the descent-to-landing simulation; mean attitude error (RSS), averaged filter covariance ($1\sigma_{RSS}$), and Monte Carlo sample covariance ($1\sigma_{RSS}$)
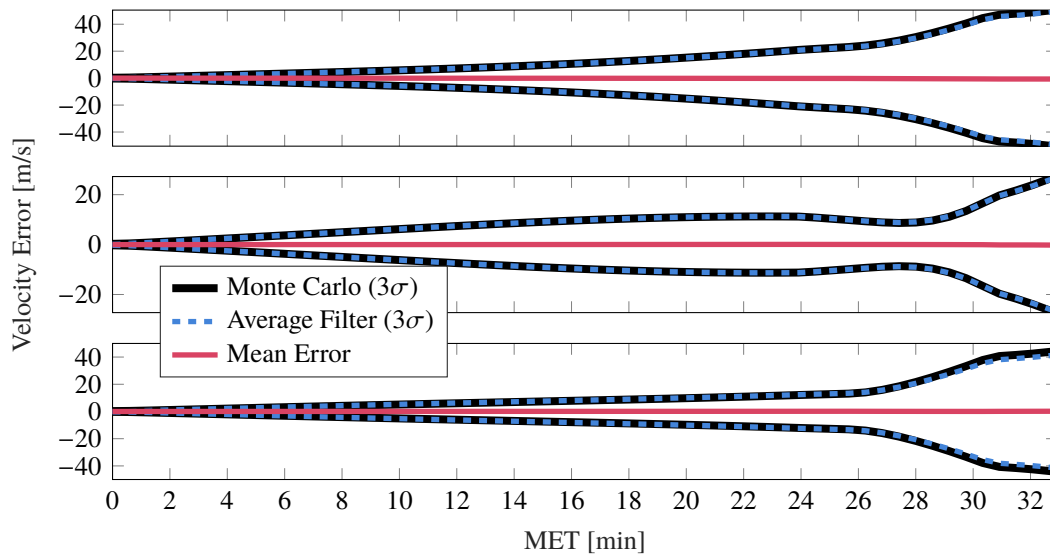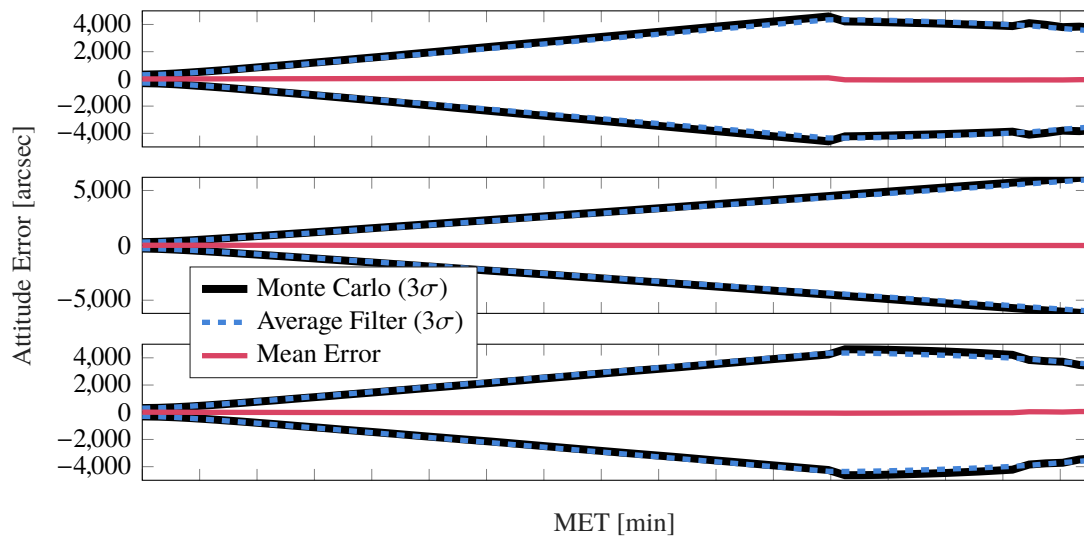
Figure 6.35. Monte Carlo simulation results from 500 trials using CSS corrections for inertial navigation in the descent-to-landing simulation; mean position error, averaged filter covariance (3σ), and Monte Carlo sample covariance (3σ)
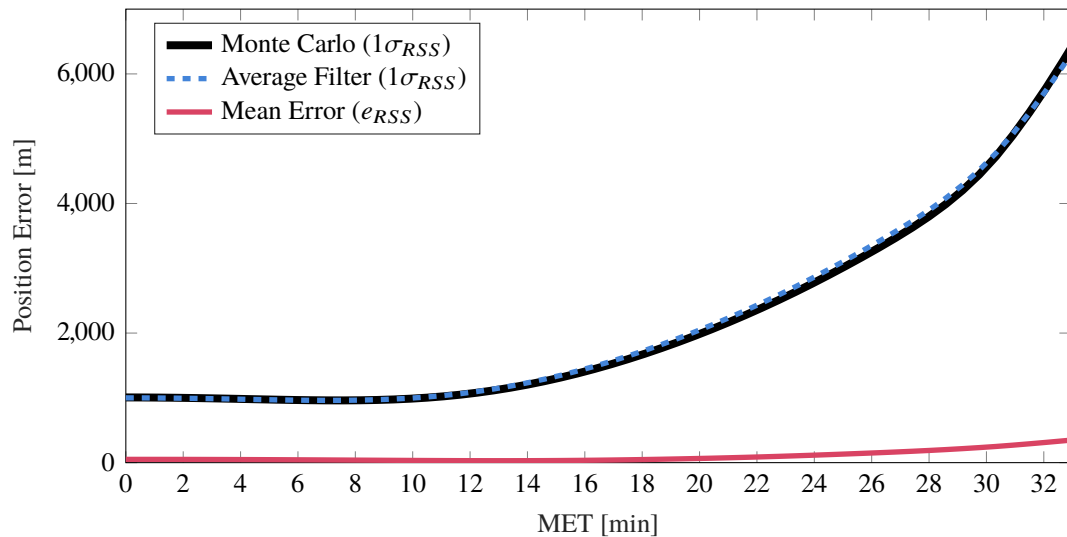

Figure 6.36. Monte Carlo simulation results from 500 trials using CSS corrections for inertial navigation in the descent-to-landing simulation; mean velocity error, averaged filter covariance (3σ), and Monte Carlo sample covariance (3σ)

Figure 6.37. Monte Carlo simulation results from 500 trials using CSS corrections for inertial navigation in the descent-to-landing simulation; mean attitude error, averaged filter covariance (3σ), and Monte Carlo sample covariance (3σ)

Figure 6.38. Monte Carlo simulation results from 500 trials using CSS corrections for inertial navigation in the descent-to-landing simulation; mean position error (RSS), averaged filter covariance ($1\sigma_{RSS}$), and Monte Carlo sample covariance ($1\sigma_{RSS}$)
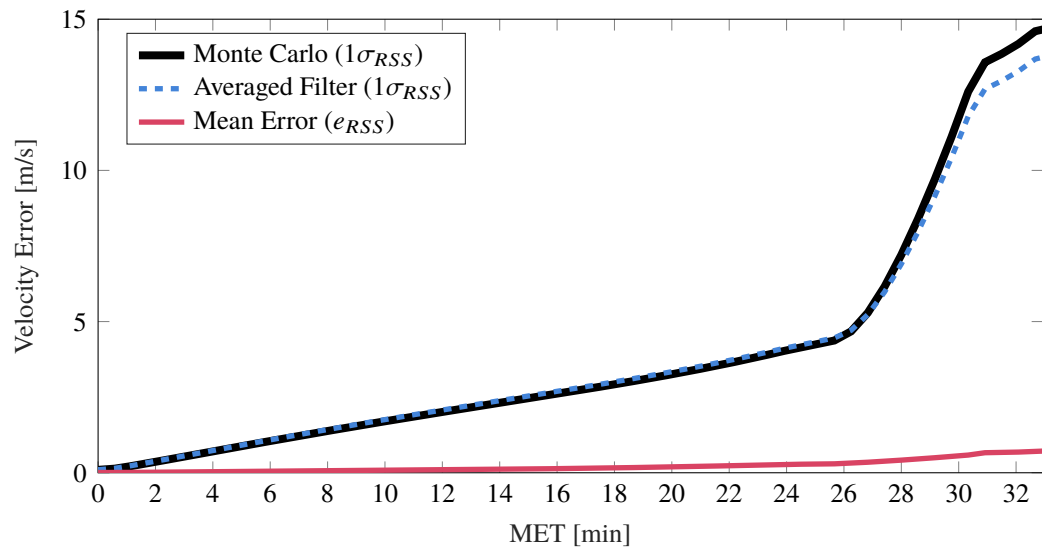
Figure 6.39. Monte Carlo simulation results from 500 trials using CSS corrections for inertial navigation in the descent-to-landing simulation; mean velocity error (RSS), averaged filter covariance ($1\sigma_{RSS}$), and Monte Carlo sample covariance ($1\sigma_{RSS}$)
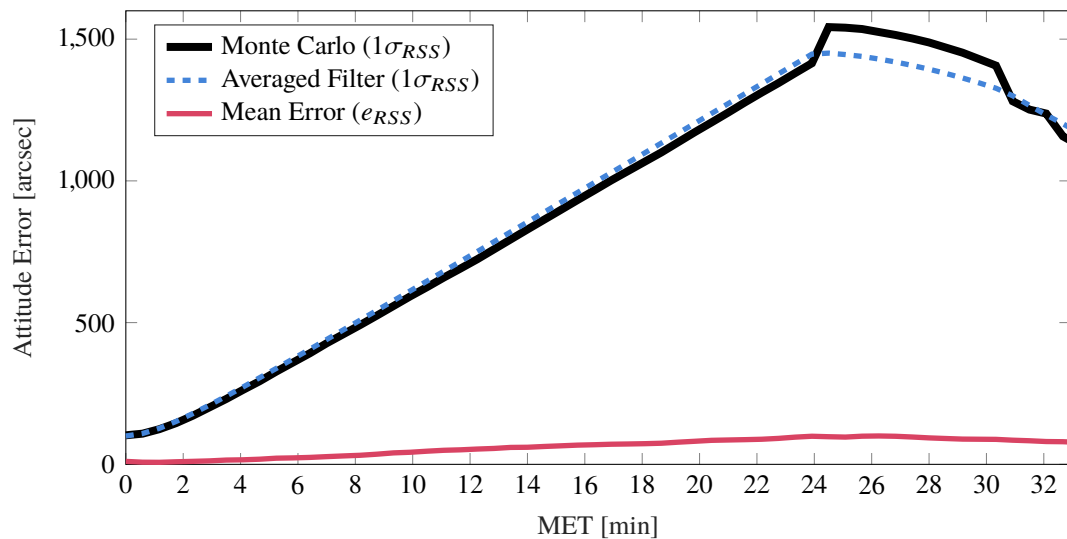

Figure 6.40. Monte Carlo simulation results from 500 trials using CSS corrections for inertial navigation in the descent-to-landing simulation; mean attitude error (RSS), averaged filter covariance ($1\sigma_{RSS}$), and Monte Carlo sample covariance ($1\sigma_{RSS}$)
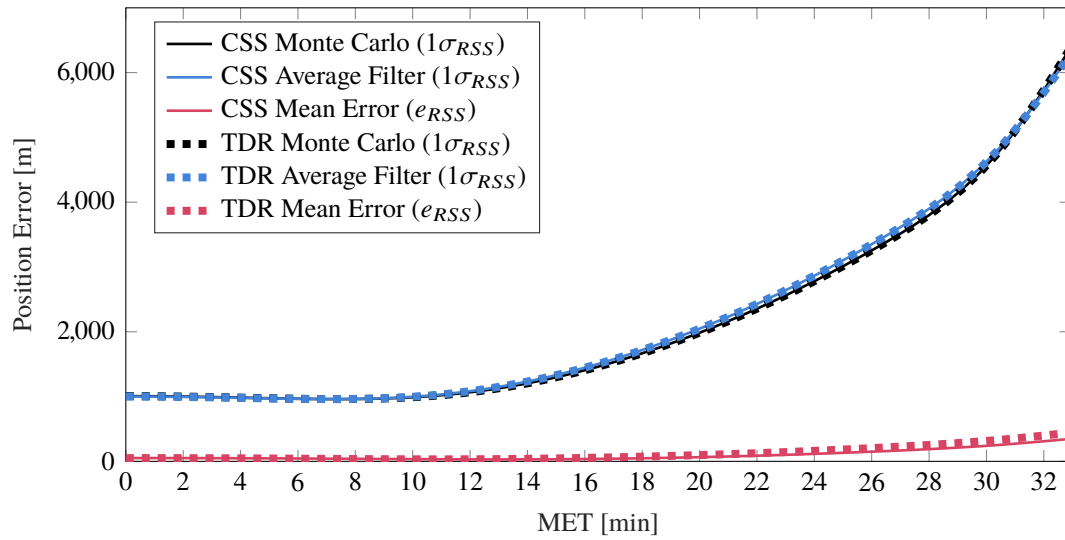
Figure 6.41. Monte Carlo results comparison between CSS and traditional methods for inertial navigation; mean position error (RSS), averaged filter covariance ($1\sigma_{RSS}$), and Monte Carlo sample covariance ($1\sigma_{RSS}$)
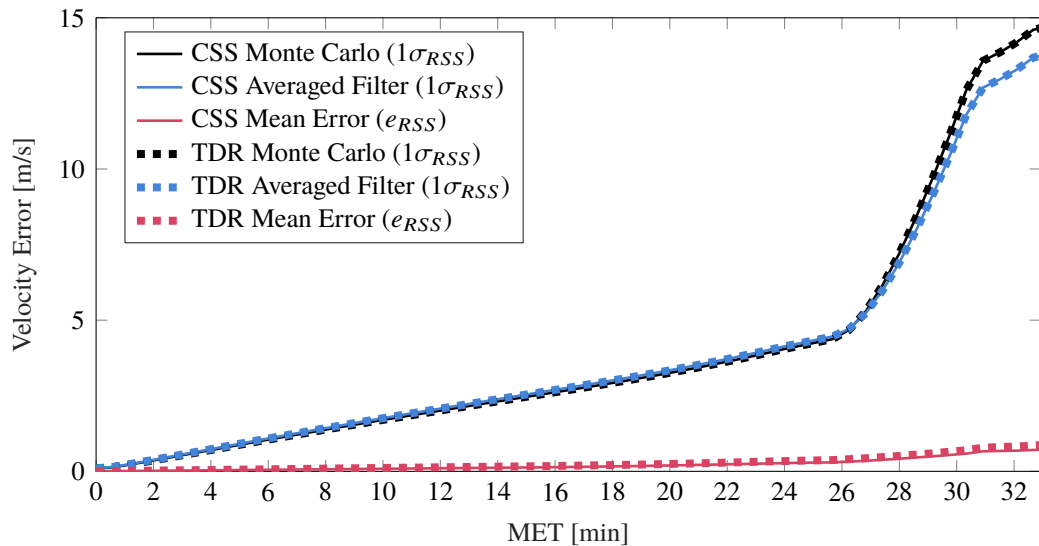

Figure 6.42. Monte Carlo results comparison between CSS and traditional methods for inertial navigation; mean velocity error (RSS), averaged filter covariance ($1\sigma_{RSS}$), and Monte Carlo sample covariance ($1\sigma_{RSS}$)
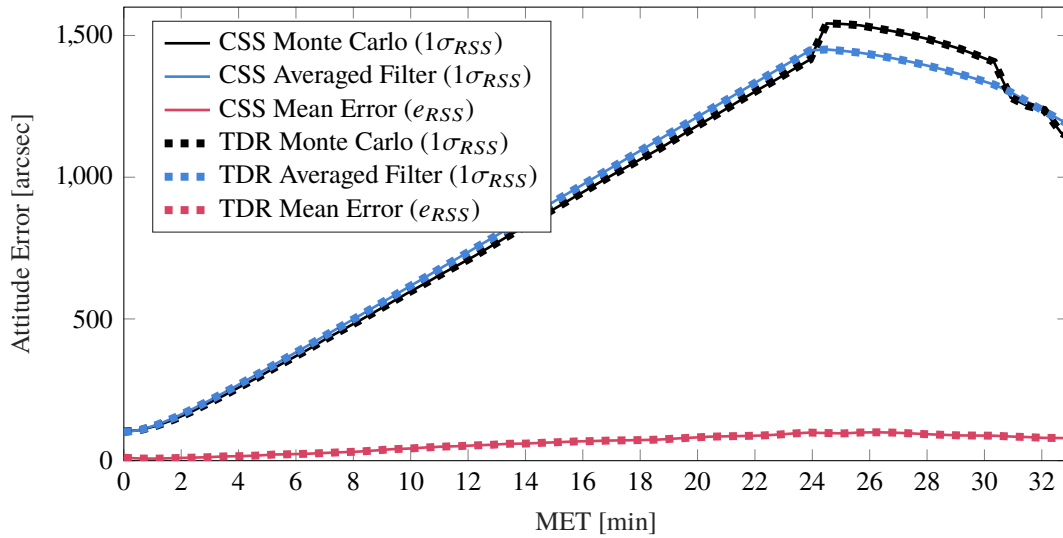
Figure 6.43. Monte Carlo results comparison between CSS and traditional methods for inertial navigation; mean attitude error (RSS), averaged filter covariance ($1\sigma_{RSS}$), and Monte Carlo sample covariance ($1\sigma_{RSS}$)
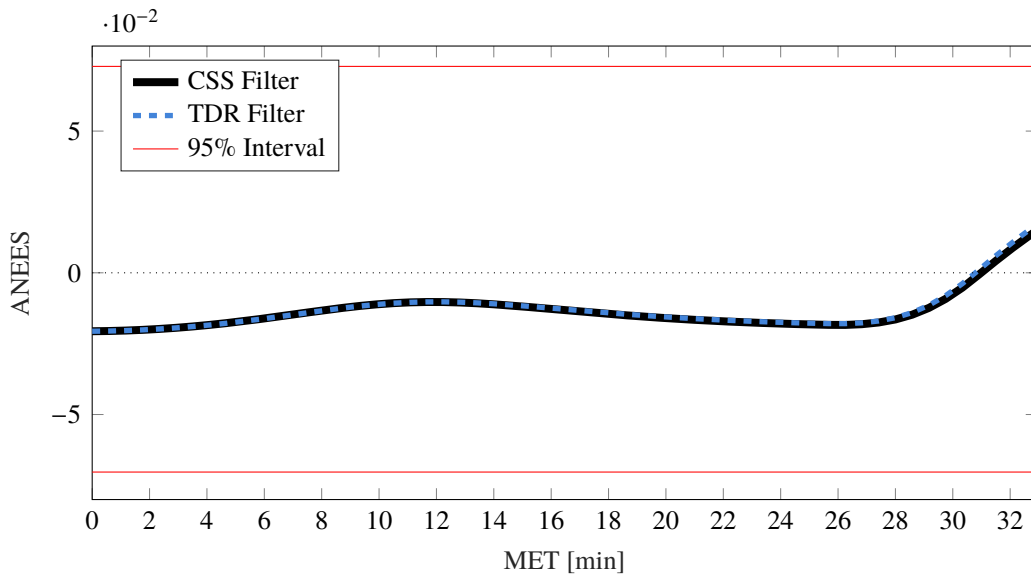

Figure 6.44. ANEES comparison for Monte Carlo position errors generated by CSS and traditional inertial navigation strategies
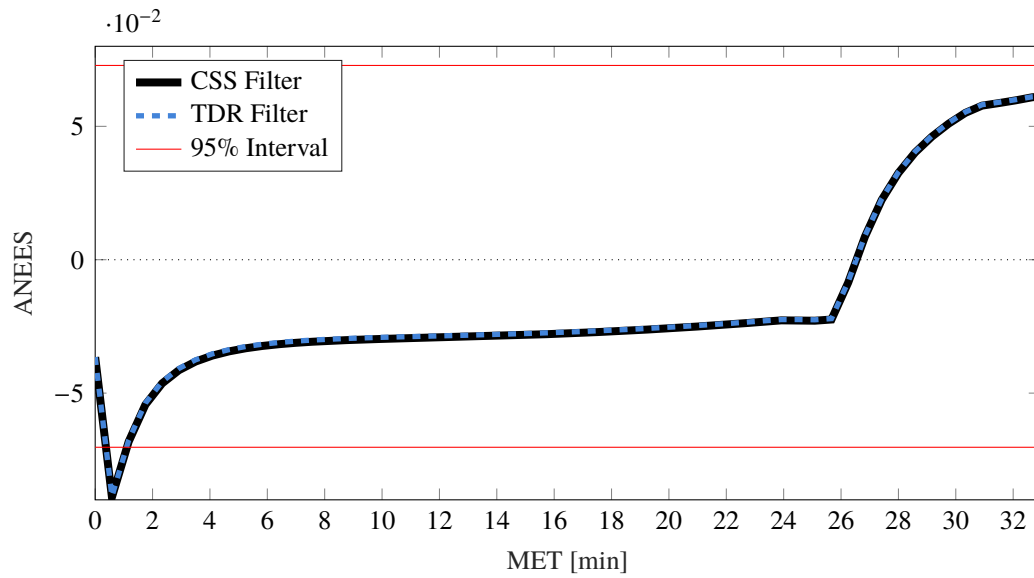
Figure 6.45. ANEES comparison for Monte Carlo velocity errors generated by CSS and traditional inertial navigation strategies
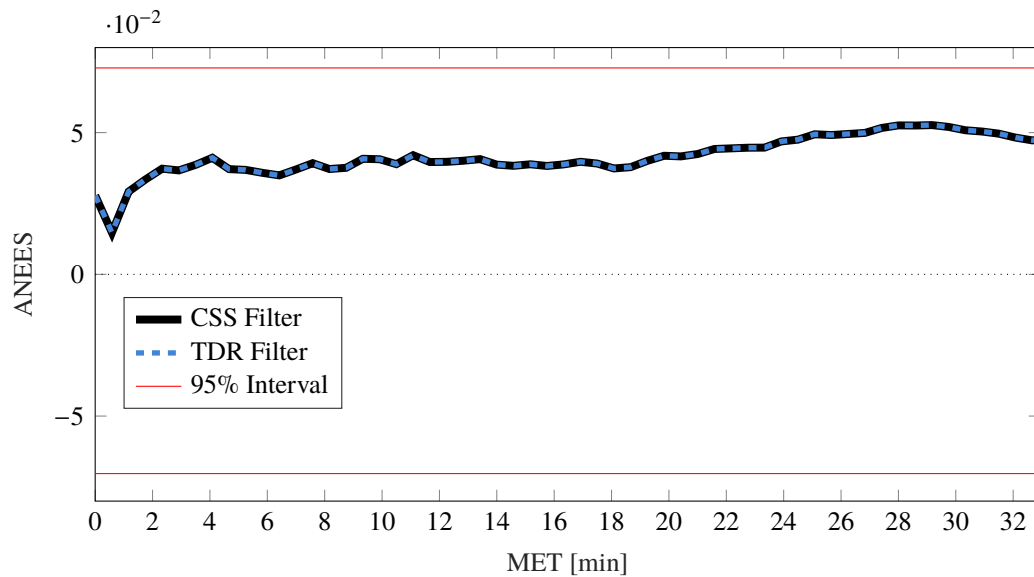
Figure 6.46. ANEES comparison for Monte Carlo attitude errors generated by CSS and traditional inertial navigation strategies

Figure 6.47. Normalized RSS standard deviation error between CSS and high-frequency traditional dead-reckoning averaged filter and Monte Carlo sample covariances for position

Figure 6.48. Normalized RSS standard deviation error between CSS and traditional dead-reckoning averaged filter and Monte Carlo sample covariances for velocity
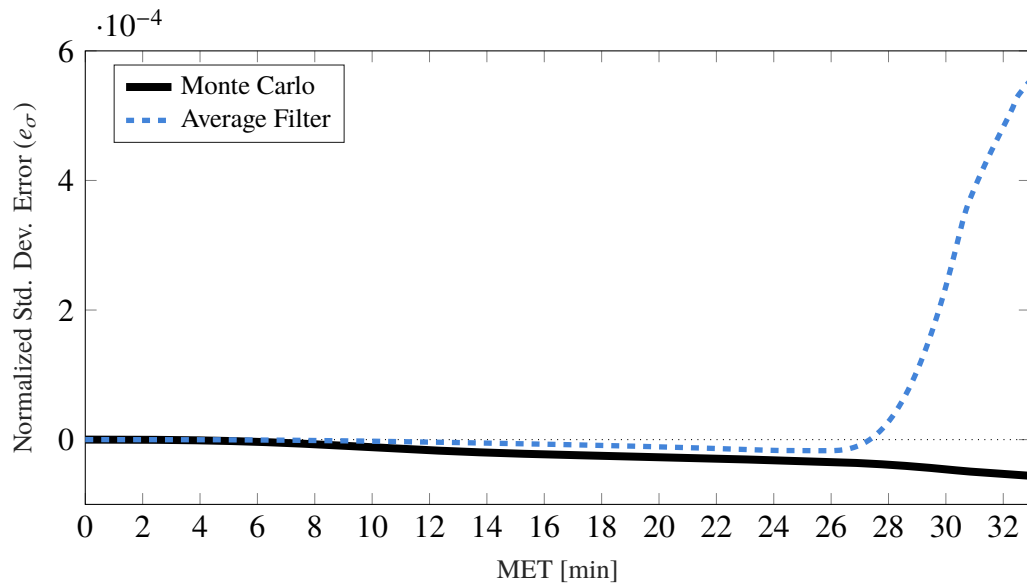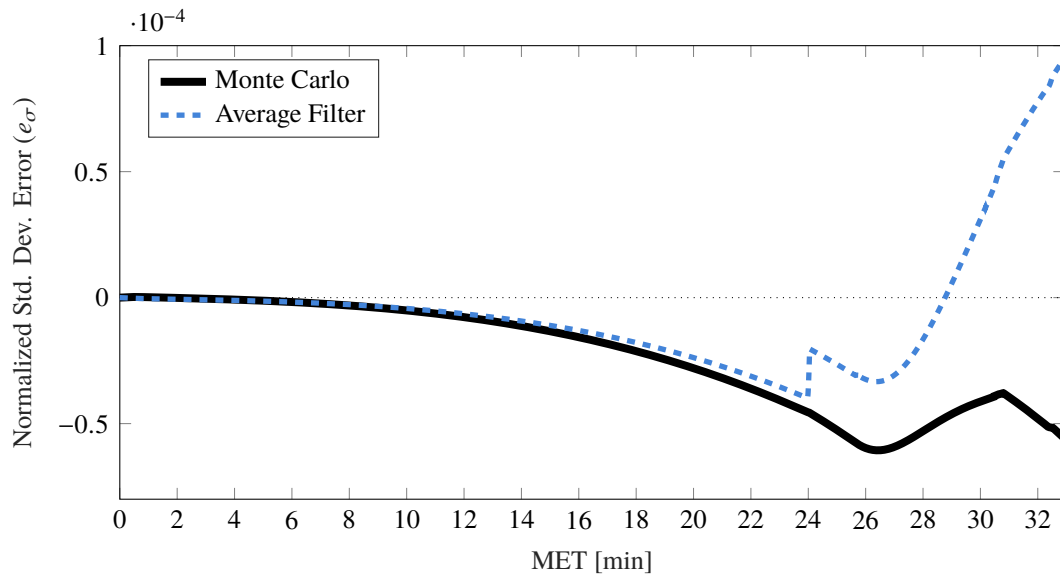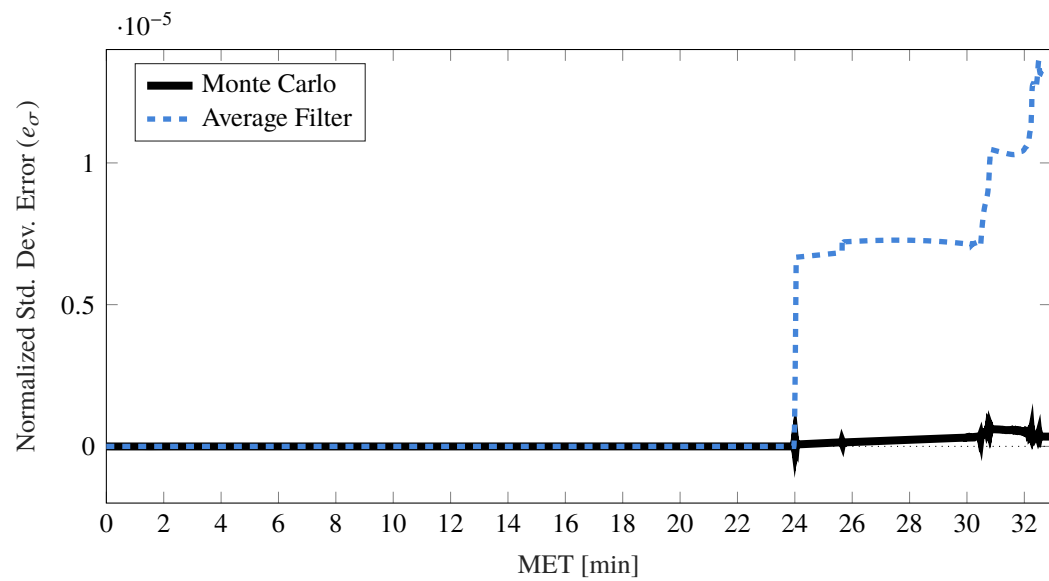
Figure 6.49. Normalized RSS standard deviation error between CSS and traditional dead-reckoning averaged filter and Monte Carlo sample covariances for attitude

7. CONCLUSION

To enable the development of autonomous systems seeking evermore ambitious capabilities, improved precision navigation systems are needed. Typical navigation system design often relies upon inertial navigation techniques to partially describe their state and uncertainty propagation. When navigating within an ideal environment, it is preferred to propagate the state and covariance at the operational frequency of the inertial sensors. However, when in an environment where the vehicle's angular velocity and non-gravitational acceleration exhibit significant nonlinear behavior, an accumulation of error will often occur in the state estimates. By processing extremely high-frequency data from inertial sensors, this error growth can be mitigated. However, as the frequency of measurements increases, the computational complexity of the covariance propagation becomes an issue. To combat the trade-off between computational efficiency and accurate state estimation, high-frequency measurements can be down-sampled in a variety of methods prior to processing, including the application of coning, sculling, and scrolling corrections. Within this thesis, the error dynamics for coning, sculling, and scrolling algorithms commonly integrated within inertial navigation systems have been developed for integration into an extended Kalman filter based navigation system. The developed error dynamics provide a mapping of gyro and accelerometer measurement and parametric estimation errors through coning, sculling, and scrolling algorithms into the estimation of position, velocity, and attitude aided by strapdown inertial sensors.

To examine the effects of the presented error propagation, two separate simulations are developed and analyzed. In the first, the presence of coning motion on attitude estimation and the filter predicted uncertainty are observed where underlying coning motion is introduced. It is found that the application of the coning algorithm provides no significant benefit when the angular velocity vector is constant in time, though it outperforms the rest

when coning motion is introduced. Additionally, the uncertainty predicted by each method is comparable, while the coning algorithms predict a minimally reduced uncertainty as underlying coning increases. An alternative method that predicts the attitude based upon a summation of measurements obtained between state estimates is found to have reduced reliability as coning motion increases and is deemed non-credible to a level of 95% when undergoing 200 Hz coning motion, based upon the ANEES consistency test. However, when applying the coning algorithm to the same batch of data and utilizing the new error mapping for covariance propagation, the consistency of coned dead-reckoning is comparable to other methods, where the estimator is accepted as consistent for each case examined.

For the second simulation, the application of coning, sculling, and scrolling corrections within a lunar descent-to-landing scenario is examined. By implementing the coning, sculling, and scrolling error dynamics within this scenario, a small but noticeable reduction in the mean estimation error for position and velocity is observed. Additionally, the developed error dynamics allow the predicted uncertainty to match this trend. However, once a significant attitude maneuver is introduced, the predicted uncertainty maintains a consistent but slightly conservative covariance prediction.

Within both simulations, it is found that the introduction of coning, sculling, and scrolling algorithms can be used to reduce the computational complexity typically incurred by using high frequency measurements to provide a down-sampled state estimate. While other methods are capable of reducing the computational complexity, the application of coning, sculling, and scrolling algorithms, paired with the developed error propagation, comparatively provides a moderate reduction in computational complexity. However, due to the increased efficiency, the reduction in the mean error, and the consistency between the predicted and observed levels of uncertainty, future systems should look to leverage coning, sculling, and scrolling corrections for inertial navigation.

To better understand the limitations and identify any shortcomings of the developed error dynamics, a higher-fidelity trajectory is desired. The best inspection of these developments would occur given a modular trajectory that can have coning, sculling, and scrolling motion superimposed on the vehicle dynamics, and can also produce variable frequency inertial measurements. While the current trajectory does not allow for an in-depth analysis of the fully integrated coning, sculling, and scrolling system, it does provide a useful examination of its implementation within a realistic scenario.

Significant future development is possible for the future of coning, sculling, and scrolling algorithms for inertial navigation systems when considering their application within real systems. First, the extension of the methods applied within this thesis to optimal coning, sculling, and scrolling algorithms may prove fruitful as the algorithms examined here are are not derived for optimality. Second, an examination of further configurations is a logical next step. Within this thesis, a comparison of several potential configurations for inertial navigation systems are made in which the impact of including the error propagation for the coning, sculling, and scrolling corrections appears to be relatively low. Leveraging what has been observed, it may be useful to inspect configurations in which the mean is propagated using coning, sculling, and scrolling corrections, while the covariance is propagated using simpler methods such as summing the measurements.

Finally, it would be a useful exercise to examine whether or not it is beneficial to perform the inertial navigation corrections in the presence of external measurements. It is likely that the benefits of including the corrections for coning, sculling, and scrolling motion would be insignificant in comparison to the information gained by incorporating external measurements. That being said, the algorithms are likely well suited to a scenario in which external measurements are not available for a long period of time. It may then be worthwhile to instead determine how often external measurements need to be processed in order to maintain minimal estimation error in the presence of underlying coning, sculling, and scrolling motion, allowing for a more simple navigation system design.

REFERENCES

[1] Archinal, B. A. and et. al., 'Report of the IAU working group on cartographic coordinates and rotational elements: 2015,' Celestial Mechanics and Dynamical Astronomy, 2018, **130**(3), p. 22, doi:10.1007/s10569-017-9805-5.

[2] Bar-Shalom, Y. and Birmiwal, K., 'Consistency and robustness of PDAF for target tracking in cluttered environments,' Automatica, 1983, **19**(4), pp. 431–437, doi: 10.1016/0005-1098(83)90059-6.

[3] Bortz, J. E., 'A new mathematical formulation for strapdown inertial navigation,' IEEE Transactions on Aerospace and Electronic Systems, 1971, **AES-7**(21), pp. 61–66, doi: 10.1109/TAES.1971.310252.

[4] Carson, J. M. and et. al., 'The SPLICE project: Continuing NASA development of GN&C technologies for safe and precise landing,' in 'AIAA SciTech 2019 Forum,' 2019 doi:10.2514/6.2019-0660.

[5] Crassidis, J. L. and Junkins, J. L., *Optimal Estimation of Dynamic Systems*, Chapman and Hall/CRC, 2004.

[6] DeMars, K. J., *Precision Navigation for Lunar Descent and Landing*, Master's thesis, The University of Texas at Austin, 2007.

[7] Edwards, Jr., A., 'The state of strapdown inertial guidance and navigation,' Navigation, 1971, **18**(4), pp. 386–401, doi:10.1002/j.2161-4296.1971.tb00110.x.

[8] Golub, G. H. and Van Loan, C. F., *Matrix Computations*, The Johns Hopkins University Press, 3rd edition, 1996.

[9] Holley, M. D., Swingle, W. L., Bachman, S. L., LeBlanc, C. J., Howard, H. T., and Biggs, H. M., 'Apollo experience report - guidance and control systems: Primary guidance, navigation, and control system development,' Technical Report TN-D-8227, NASA, May 1976.

[10] Ignagni, M. B., 'Optimal strapdown attitude integration algorithms,' Journal of Guidance, Control and Dynamics, 1990, **13**(2), pp. 363–369, doi:10.2514/3.20558.

[11] Ignagni, M. B., 'Efficient class of optimized coning compensation algorithms,' Journal of Guidance, Control and Dynamics, 1996, **19**(2), pp. 424–429, doi:10.2514/3.21635.

[12] Jordan, J. W., 'An accurate strapdown direction cosine algorithm,' Technical Report TN-D-5384, NASA, September 1969.

[13] Kalman, R. E., 'A new approach to linear filtering and prediction problems,' Journal of Basic Engineering, 1960, **82**, pp. 35–45.

[14] Kalman, R. E. and Bucy, R. S., 'New results in linear filtering and prediction theory,' Journal of Basic Engineering, 1961, pp. 95–108.

[15] Lefferts, E. J., Markley, F. L., and Shuster, M. D., 'Kalman filtering for spacecraft attitude estimation,' Journal of Guidance, Control and Dynamics, 1982, **5**(45), pp. 417–429, doi:10.2514/3.56190.

[16] Li, X. R., Zhao, Z., and Jilkov, V. P., 'Practical measures and test for credibility of an estimator,' in 'Proc. Workshop on Estimation, Tracking, and Fusion – A Tribute to Yaakov Bar-Shalom,' 2001 pp. 481–495.

[17] Li, X. R., Zhao, Z., and Li, X.-B., 'Evaluation of estimation algorithms–credibility tests,' IEEE Transactions on Aerospace and Electronic Systems, 2012, **42**(1), pp. 147–163, doi:10.1109/TSMCA.2011.2158095.

[18] Markley, F. L. and Crassidis, J. L., *Fundamentals of Spacecraft Attitude Determination and Control*, Springer, 2014.

[19] McKern, R. A., *A Study of Transformation Algorithms for use in a Digital Computer*, Master's thesis, Massachusetts Institute of Technology, 1968.

[20] Miller, R. B., 'A new strapdown attitude algorithm,' Journal of Guidance, Control and Dynamics, 1983, **6**(4), pp. 287–291, doi:10.2514/3.19831.

[21] Mission Evaluation Team, 'Apollo 11 mission report,' Technical Report MSC-00171, NASA, November 1969.

[22] Savage, P. G., 'A new second-order solution for strapped-down attitude computation,' in 'Proc. of AIAA/JACC Guidance and Control Conference,' 1966 pp. 60–71, doi: 10.2514/6.1966-1805.

[23] Savage, P. G., 'Coning algorithm design by explicit frequency shaping,' Journal of Guidance, Control, and Dynamics, 1998, **33**(4), pp. 1123–1132, doi:10.2514/1.47337.

[24] Savage, P. G., 'Strapdown inertial navigation integration algorithm design part 1: Attitude algorithms,' Journal of Guidance, Control, and Dynamics, 1998, **21**(1), pp. 19–28, doi:10.2514/2.4228.

[25] Savage, P. G., 'Strapdown inertial navigation integration algorithm design part 2: Velocity and position algorithms,' Journal of Guidance, Control, and Dynamics, 1998, **21**(2), pp. 208–221, doi:10.2514/2.4242.

[26] Savage, P. G., *Strapdown Analytics, Parts 1 and 2*, Strapdown Associates, Inc., 2000.

[27] Savage, P. G., 'Blazing gyros: The evolution of strapdown inertial navigation technology for aircraft,' Journal of Guidance, Control, and Dynamics, 2013, **36**(3), pp. 637–655, doi:10.2514/1.60211.

[28] Shuster, M. D., 'A survey of attitude representations,' Journal of the Astronautical Sciences, 1993, **41**(4), pp. 439–517.

[29] Wang, H. G. and Williams, T. C., 'Strategic inertial navigation systems: High-accuracy inertially stabilized platforms for hostile environments,' IEEE Control Systems Magazine, 2008, **28**(1), pp. 65–85, doi:10.1109/MCS.2007.910206.

[30] Ward, K. C., Fritsch, G. S., Helmuth, J. C., and DeMars, K. J., 'Design and analysis of descent-to-landing navigation incorporating terrain effects,' Journal of Spacecraft and Rockets, 2020.

[31] Ward, K. C., Helmuth, J. C., Fritsch, G. S., and DeMars, K. J., 'Fusion of multiple terrain-based sensors for descent-to-landing navigation,' in 'AIAA Scitech 2019 Forum,' San Diego, CA, 2019 doi:10.2514/6.2019-0922.

[32] Zanetti, R., *Advanced Navigation Algorithms for Precision Landing*, Ph.D. thesis, The University of Texas at Austin, 2007.

[33] Zanetti, R. and Bishop, R. H., 'Kalman filters with uncompensated biases,' Journal of Guidance, Control, and Dynamics, 2012, **35**(1), pp. 327–330, doi:10.2514/1.55120.

VITA

James Daniel Alan Brouk studied aerospace engineering at Missouri S&T beginning in the fall of 2014. Throughout this period, he began to work with the Missouri S&T satellite research team, where he gained interest in the fields of astrodynamics and estimation. In December of 2017, he graduated Summa Cum Laude with a Bachelor of Science in Aerospace Engineering from Missouri S&T, deciding to continue his education in the pursuit of a graduate degree under the advising of Dr. Kyle DeMars.

As a graduate student, he began work on a lunar lander navigation system with other members of the AREUS lab. In August of 2019, he presented a conference paper at the 2019 Astrodynamics Specialist Conference in Portland, Maine, and was selected as a recipient of the John V. Breakwell Student Travel Award. He obtained a Master of Science in Aerospace Engineering from Missouri S&T in December of 2019.